

University of New Hampshire

University of New Hampshire Scholars' Repository

Master's Theses and Capstones

Student Scholarship

Spring 2012

Comparison of methods for on-line calibration of cutting force models in end milling

Yong Zhao

University of New Hampshire, Durham

Follow this and additional works at: <https://scholars.unh.edu/thesis>

Recommended Citation

Zhao, Yong, "Comparison of methods for on-line calibration of cutting force models in end milling" (2012). *Master's Theses and Capstones*. 703.
<https://scholars.unh.edu/thesis/703>

This Thesis is brought to you for free and open access by the Student Scholarship at University of New Hampshire Scholars' Repository. It has been accepted for inclusion in Master's Theses and Capstones by an authorized administrator of University of New Hampshire Scholars' Repository. For more information, please contact Scholarly.Communication@unh.edu.

**COMPARISON OF METHODS FOR ON-LINE CALIBRATION OF CUTTING
FORCE MODELS IN END MILLING**

by

Yong Zhao

B.S., Huazhong University of Science and Technology, 2010

THESIS

Submitted to the University of New Hampshire
in Partial Fulfillment of the Requirements for the Degree of

Master of Science
in
Mechanical Engineering

May, 2012

UMI Number: 1518008

All rights reserved

INFORMATION TO ALL USERS

The quality of this reproduction is dependent upon the quality of the copy submitted.

In the unlikely event that the author did not send a complete manuscript and there are missing pages, these will be noted. Also, if material had to be removed, a note will indicate the deletion.

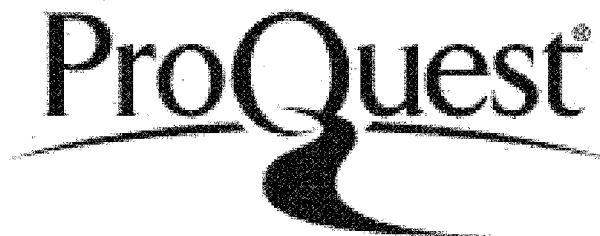


UMI 1518008

Published by ProQuest LLC 2012. Copyright in the Dissertation held by the Author.

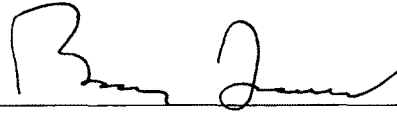
Microform Edition © ProQuest LLC.

All rights reserved. This work is protected against unauthorized copying under Title 17, United States Code.

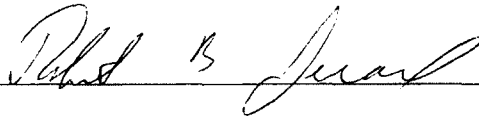


ProQuest LLC
789 East Eisenhower Parkway
P.O. Box 1346
Ann Arbor, MI 48106-1346

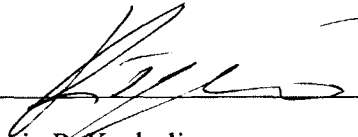
This thesis has been examined and approved.



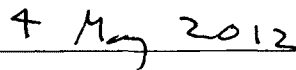
Thesis Director, Dr. Barry K. Fussell
Professor of Mechanical Engineering



Thesis Co-Director, Dr. Robert B. Jerard
Professor of Mechanical Engineering



Dr. Yannis P. Korkolis
Assistant Professor of Mechanical Engineering



Date

ACKNOWLEDGEMENTS

I would like to thank Prof. Jerard and Prof. Fussell for their continual encouragement, support and guidance throughout my graduate study. I feel myself extremely lucky to be a part of the research group at the Design and Manufacturing Lab and work with them. I believe that I have learnt a lot from this special and precious experience.

I would also like to thank Prof. Korkolis for his thorough review of this thesis and many constructive suggestions.

I feel the utmost gratitude for Prof. Rong. Without his help and recommendation, I might not have the chance to study at UNH. I also thank him for his longtime support and friendship.

I greatly appreciate all of my lab partners for their support and friendship. I would like to thank Firat, Saman, Minhyong, Andrew, Anthony, Kyle and Chris for all their help and making the lab a enjoyable place to work.

Special thanks go to Donald Esterling for providing the magnetic brake and torque sensor system needed for the experiment described in Chapter 3.

The support of the National Science Foundation under grant CMMI 0928602 and the Department of Mechanical Engineering are greatly acknowledged.

Finally, I would like to thank my family. I felt their love and support at every moment during my graduate study. Special thanks to my uncle Chunhua Zhao, without his support, I would not have the chance to study in the United States.

TABLE OF CONTENTS

ACKNOWLEDGEMENTS	iii
LIST OF TABLES	vii
LIST OF FIGURES	xii
LIST OF SYMBOLS	xv
ABSTRACT.....	xvii

CHAPTER	PAGE
1. INTRODUCTION.....	1
1.1 Introduction.....	1
1.2 Thesis Overview	3
2. BACKGROUND	4
2.1 Introduction.....	4
2.2 Force Model	4
2.3 Sensor Introduction.....	7
2.3.1 LCI Power Sensor	7
2.3.2 Kistler Dynamometer.....	8
2.3.3 Smart Tool	9
2.4 Summary	10
3. SPINDLE MOTOR POWER SENSOR SYSTEM CALIBRATION	11
3.1 Introduction.....	11

3.2	Experiment Purpose	11
3.3	Experiment Setup.....	12
3.4	Experiment Results and Discussion.....	13
3.5	Summary	23
4.	CUTTING TEST DESIGN	24
4.1	Introduction.....	24
4.2	Cutting Test Design	24
4.3	Summary	28
5.	FORCE MODEL CALIBRATION METHODS	29
5.1	Introduction.....	29
5.2	Spindle Motor Power	29
5.3	Kistler Reaction Force	31
5.3.1	Force Profile Method	31
5.3.2	Average Force Method	40
5.4	Smart Tool Tangential and Radial Force	41
5.4.1	Force Profile Method	41
5.4.2	Average Force Method	47
5.5	Summary	48
6.	CALIBRATION AND SIMULATION RESULTS AND COMPARISON OF METHODS	49
6.1	Introduction.....	49
6.2	Calibration Results.....	50
6.3	Simulation Results	58

6.4 Comparison of Methods.....	66
6.5 Summary.....	70
7. CONCLUSIONS AND FUTURE WORK.....	71
7.1 Introduction.....	71
7.2 Conclusions.....	71
7.3 Future Work.....	74
 REFERENCES	 76
APPENDIX A: EXPERIMENT PROCEDURES FOR SPINDLE MOTOR POWER	
SENSOR SYSTEM CALIBRATION	78
APPENDIX B: SPINDLE MOTOR POWER SENSOR SYSTEM CALIBRATION	
RESULTS	81
APPENDIX C: CUTTING COEFFICIENTS CALIBRATION RESULTS	87
APPENDIX D: SIMULATION RESULTS.....	99
APPENDIX E: MATLAB PROGRAMS	104

LIST OF TABLES

Table 3.1 - Motor-Sensor System Sensitivity (K_s) versus Spindle Speed (ω)	17
Table 4.1 - Feedrate Design for 600 rpm Cutting Test.....	26
Table 4.2 - Feedrate Design for 3000 rpm Cutting Test.....	26
Table 6.1 - Mean of K_{rc}/K_{tc} and K_{re}/K_{te}	56
Table 6.2 - Cost of Different Sensors.....	66
Table B.1 - Spindle Motor Power Sensor System Calibration Results.....	81
Table C.1 - Average Force and Spindle Motor Power Based Cutting Coefficients for 600 rpm Quarter Immersion (T)	87
Table C.2 - Kistler Force Profile Based Cutting Coefficients for 600 rpm Quarter Immersion (T).....	87
Table C.3 - Smart Tool Force Profile Based Cutting Coefficients for 600 rpm Quarter Immersion (T).....	87
Table C.4 - Average Force and Spindle Motor Power Based Cutting Coefficients for 600 rpm Quarter Immersion (R)	88
Table C.5 - Kistler Force Profile Based Cutting Coefficients for 600 rpm Quarter Immersion (R).....	88
Table C.6 - Smart Tool Force Profile Based Cutting Coefficients for 600 rpm Quarter Immersion (R).....	88
Table C.7 - Average Force and Spindle Motor Power Based Cutting Coefficients for 600 rpm Half Immersion (T).....	89

Table C.8 - Kistler Force Profile Based Cutting Coefficients for 600 rpm Half Immersion (T)	89
Table C.9 - Smart Tool Force Profile Based Cutting Coefficients for 600 rpm Half Immersion (T)	89
Table C.10 - Average Force and Spindle Motor Power Based Cutting Coefficients for 600 rpm Half Immersion (R)	90
Table C.11 - Kistler Force Profile Based Cutting Coefficients for 600 rpm Half Immersion (R)	90
Table C.12 - Smart Tool Force Profile Based Cutting Coefficients for 600 rpm Half Immersion (R)	90
Table C.13 - Average Force and Spindle Motor Power Based Cutting Coefficients for 600 rpm Three Quarter Immersion (T)	91
Table C.14 - Kistler Force Profile Based Cutting Coefficients for 600 rpm Three Quarter Immersion (T)	91
Table C.15 - Smart Tool Force Profile Based Cutting Coefficients for 600 rpm Three Quarter Immersion (T)	91
Table C.16 - Average Force and Spindle Motor Power Based Cutting Coefficients for 600 rpm Three Quarter Immersion (R)	92
Table C.17 - Kistler Force Profile Based Cutting Coefficients for 600 rpm Three Quarter Immersion (R)	92
Table C.18 - Smart Tool Profile Based Cutting Coefficients for 600 rpm Three Quarter Immersion (R)	92

Table C.19 - Average Force and Spindle Motor Power Based Cutting Coefficients for 3000 rpm Quarter Immersion (T)	93
Table C.20 - Kistler Force Profile Based Cutting Coefficients for 3000 rpm Quarter Immersion (T)	93
Table C.21 - Smart Tool Force Profile Based Cutting Coefficients for 3000 rpm Quarter Immersion (T)	93
Table C.22 - Average Force and Spindle Motor Power Based Cutting Coefficients for 3000 rpm Quarter Immersion (R)	94
Table C.23 - Kistler Force Profile Based Cutting Coefficients for 3000 rpm Quarter Immersion (R)	94
Table C.24 - Smart Tool Force Profile Based Cutting Coefficients for 3000 rpm Quarter Immersion (R)	94
Table C.25 - Average Force and Spindle Motor Power Based Cutting Coefficients for 3000 rpm Half Immersion (T)	95
Table C.26 - Kistler Force Profile Based Cutting Coefficients for 3000 rpm Half Immersion (T)	95
Table C.27 - Smart Tool Force Profile Based Cutting Coefficients for 3000 rpm Half Immersion (T)	95
Table C.28 - Average Force and Spindle Motor Power Based Cutting Coefficients for 3000 rpm Half Immersion (R)	96
Table C.29 - Kistler Force Profile Based Cutting Coefficients for 3000 rpm Half Immersion (R)	96

Table C.30 - Smart Tool Force Profile Based Cutting Coefficients for 3000 rpm Half Immersion (R).....	96
Table C.31 - Average Force and Spindle Motor Power Based Cutting Coefficients for 3000 rpm Three Quarter Immersion (T).....	97
Table C.32 - Kistler Force Profile Based Cutting Coefficients for 3000 rpm Three Quarter Immersion (T).....	97
Table C.33 - Smart Tool Force Profile Based Cutting Coefficients for 3000 rpm Three Quarter Immersion (T).....	97
Table C.34 - Average Force and Spindle Motor Power Based Cutting Coefficients for 3000 rpm Three Quarter Immersion (R).....	98
Table C.35 - Kistler Force Profile Based Cutting Coefficients for 3000 rpm Three Quarter Immersion (R).....	98
Table C.36 - Smart Tool Profile Based Cutting Coefficients for 3000 rpm Three Quarter Immersion (R).....	98
Table D.1 - REp for 600 rpm Quarter Immersion (T).....	99
Table D.2 - REp for 600 rpm Quarter Immersion (R).....	99
Table D.3 - REp for 600 rpm Half Immersion (T).....	100
Table D.4 - REp for 600 rpm Half Immersion (R).....	100
Table D.5 - REp for 600 rpm Three Quarter Immersion (T).....	101
Table D.6 - REp for 600 rpm Three Quarter Immersion (R).....	101
Table D.7 - REp for 3000 rpm Quarter Immersion (T).....	102
Table D.8 - REp for 3000 rpm Quarter Immersion (R).....	102
Table D.9 - REp for 3000 rpm Half Immersion (T).....	102

Table D.10 - REp for 3000 rpm Half Immersion (R) 103
Table D.11 - REp for 3000 rpm Three Quarter Immersion (T) 103
Table D.12 - REp for 3000 rpm Three Quarter Immersion (R) 103

LIST OF FIGURES

Figure 2.1 - End Milling Cutting Geometry	4
Figure 2.2 - LCI Power Sensor	7
Figure 2.3 - Kistler Dynamometer	8
Figure 2.4 - Typical Frequency Response Curve of Kistler	9
Figure 2.5 - Smart Tool.....	9
Figure 3.1 - Motor Characterization Experiment Setup.....	12
Figure 3.2 - Available Cutting Power vs LCI Sensor Voltage Output at 1500 rpm	15
Figure 3.3 - Available Cutting Power vs LCI Sensor Voltage Output at 3600 rpm	16
Figure 3.4 - Motor-Sensor System Sensitivity Plot	18
Figure 3.5 - Motor-Sensor System Sensitivity Curve for Low Range Speeds	18
Figure 3.6 - Motor-Sensor System Sensitivity Curve for High Range Speeds.....	19
Figure 3.7 - Residual Plot of Motor-Sensor System Sensitivity for Low Range Speeds .	20
Figure 3.8 - Residual Plot of Motor-Sensor System Sensitivity for High Range Speeds.	20
Figure 3.9 - Confidence and Prediction Interval for the Polynomial Fit of Motor-Sensor System Sensitivity for Low Range Speeds	21
Figure 3.10 - Confidence and Prediction Interval for the Linear Fit of Motor-Sensor System Sensitivity for High Range Speeds	22
Figure 4.1 - Cutting Test Design.....	27
Figure 5.1 - 20 Cycles of F_x , 600 rpm, Quarter Immersion and Feedrate 1 (T).....	33
Figure 5.2 - 20 Cycles of F_y , 600 rpm, Quarter Immersion and Feedrate 1 (T).....	34
Figure 5.3 - FFT of F_x , 600 rpm, Quarter Immersion and Feedrate 1 (T).....	34

Figure 5.4 - FFT of Fy, 600 rpm, Quarter Immersion and Feedrate 1 (T).....	35
Figure 5.5 - Averaged One Cycle of Fx, 600 rpm, Quarter Immersion and Feedrate 1 (T)	36
Figure 5.6 - Averaged One Cycle of Fy, 600 rpm, Quarter Immersion and Feedrate 1 (T)	36
Figure 5.7 - Unshifted Fx, 600 rpm, Quarter Immersion and Feedrate 1 (T).....	37
Figure 5.8 - Unshifted Fy, 600 rpm, Quarter Immersion and Feedrate 1 (T).....	37
Figure 5.9 - Shifted Fx, 600 rpm, Quarter Immersion and Feedrate 1 (T).....	38
Figure 5.10 - Shifted Fy, 600 rpm, Quarter Immersion and Feedrate 1 (T).....	38
Figure 5.11 - Cutting Force Profile and Tick Signal, 600 rpm, Quarter Immersion and Feedrate 1 (T).....	40
Figure 5.12 - 20 Cycles of Ft, 600 rpm, Quarter Immersion and Feedrate 1.....	43
Figure 5.13 - FFT of Ft, 600 rpm, Quarter Immersion and Feedrate 1.....	43
Figure 5.14 - Unshifted Ft, 600 rpm, Quarter Immersion and Feedrate 1.....	44
Figure 5.15 - Shifted Ft, 600 rpm, Quarter Immersion and Feedrate 1.....	44
Figure 5.16 - Averaged One Cycle of Ft, 600 rpm, Quarter Immersion and Feedrate 1 ..	45
Figure 5.17 - Ft/a vs Instantaneous Chip Thickness, 600 rpm, Quarter Immersion and Feedrate 1.....	46
Figure 6.1 - Average Force and Spindle Motor Power Based Calibration Results for 600 rpm Cutting Tests.....	50
Figure 6.2 - Kistler Force Profile Based Calibration Results for 600 rpm Cutting Tests	51
Figure 6.3 - Smart Tool Force Profile Based Calibration Results for 600 rpm Cutting Tests.....	52

Figure 6.4 - Average Force and Spindle Motor Power Based Calibration Results for 3000 rpm Cutting Tests..... 53

Figure 6.5 - Kistler Force Profile Based Calibration Results for 3000 rpm Cutting Tests... .. 54

Figure 6.6 - Smart Tool Force Profile Based Calibration Results for 3000 rpm Cutting Tests 55

Figure 6.7 - Resultant Force Simulation for 600 rpm, Quarter Immersion and Feedrate 1 (T) 59

Figure 6.8 - Resultant Force Simulation for 600 rpm, Half Immersion and Feedrate 2 (T) 60

Figure 6.9 - Resultant Force Simulation for 600 rpm, Three Quarter Immersion and Feedrate 3 (T)..... 60

Figure 6.10 - Resultant Force Simulation for 3000 rpm, Quarter Immersion and Feedrate 1 (T) 61

Figure 6.11 - Resultant Force Simulation for 3000 rpm, Half Immersion and Feedrate 2 (T) 61

Figure 6.12 - Resultant Force Simulation for 3000 rpm, Three Quarter Immersion and Feedrate 3 (T)..... 62

Figure 6.13 - REp for 600 rpm Cutting Tests 63

Figure 6.14 - REp for 3000 rpm Cutting Tests 64

LIST OF SYMBOLS

- ϕ = edge locating angle of cutting tool, (rad)
- h = chip thickness, (mm)
- c = feed per tooth, (mm)
- ψ = lag angle, (rad)
- β = helix angle of cutting tool, (rad)
- D = tool diameter, (mm)
- ω_n = natural frequency, (Hz)
- ω = spindle speed, (rpm)
- P_c = available cutting power, (watt)
- P_e = electrical power input into the spindle motor, (watt)
- η_e = motor efficiency
- P_f = frictional power, (watt)
- E_o = output voltage from the LCI power sensor, (volt)
- K_p = the sensitivity of the LCI sensor, (watt/volt)
- K_s = the motor-sensor system sensitivity, (watt/volt)
- E_t = tare power voltage, (volt)
- h_a = average chip thickness, (mm)
- ϕ_s = angle at which tooth enters material, (rad)
- ϕ_{ex} = angle at which tooth exits material, (rad)

- \dot{Q} = volumetric removal rate, (mm³/s)
 \dot{A}_c = contact area rate, (mm²/s)
 G = geometry matrix related to the cut geometry
 N = number of teeth on the cutting tool
 a = axial depth of cut, (mm)
 K_{rc} = model coefficient for radial shearing force component, (N/mm²)
 K_{re} = model coefficient for radial friction force component, (N/mm)
 K_{tc} = model coefficient for tangential shearing force component, (N/mm²)
 K_{te} = model coefficient for tangential friction force component, (N/mm)
 F_r = radial force on the tool, (N)
 F_t = tangential force on the tool, (N)
 F_{res} = resultant force on the tool, (N)
 F_x = force on the tool in the x-direction, (N)
 $\overline{F_x}$ = average force in the x-direction, (N)
 F_y = force on the tool in the y-direction, (N)
 $\overline{F_y}$ = average force in the y-direction, (N)
 \overline{F} = vector of average forces in x and y direction
 K = force model coefficient vector
 RE_p = relative error of the peak force

ABSTRACT

COMPARISON OF METHODS FOR ON-LINE CALIBRATION OF CUTTING FORCE MODELS IN END MILLING

by

Yong Zhao

University of New Hampshire, May 2012

Accurate estimation of cutting coefficients is extremely important in end milling process modeling, and it forms the basis of a smart machining system that can be used for process planning and monitoring. Specific applications include feedrate selection based on force constraints and monitoring of tool wear [1, 2].

This thesis investigates five different methods to calibrate the cutting force model coefficients in end milling processes and compares them in terms of cost, efficiency, compliance, accuracy, repeatability and applicability. The five methods are based on: 1. spindle motor power, 2. Kistler average force, 3. Kistler force profile, 4. Smart Tool average force and 5. Smart Tool force profile. Three different sensors are used in the calibration processes: 1. a spindle motor power sensor purchased from Load Control Inc, 2. a Kistler dynamometer which measures the workpiece reaction force in the X and Y directions and 3. a wireless Smart Tool which measures tangential and radial cutting forces on the tool. For the power sensor, only average power is available to calibrate the

cutting coefficients, while for the Kistler dynamometer and the Smart Tool, both average force and force profiles are used to calibrate the cutting coefficients.

Applicability and limitations of each calibration method are discussed, and general conclusions are made for on-line calibration.

CHAPTER 1

INTRODUCTION

1.1 Introduction

Accurate estimation of cutting coefficients is extremely important in end milling process modeling, and it forms the basis of a smart machining system that can be used for process planning and monitoring. Specific applications include feedrate selection based on force constraints and monitoring of tool wear [1, 2].

There are various methods to calibrate cutting coefficients. Budak et al. presented a unified mechanistic model for estimating the cutting coefficients for cylindrical helical end mills [3]. It is shown that the cutting coefficients for all force components and cutter geometries can be predicted from an orthogonal cutting database and a generic oblique cutting analysis. Lee et al. further extended the approach to helical ball end mills [4]. The distribution of cutting force on the helical ball end mill flutes is accurately predicted by the proposed method. However, some cutting tools may have complex geometry, and the evaluation of cutting constants by creating a time-consuming orthogonal cutting database may not be practical.

The model coefficients can also be identified through an empirical curve fit to measured average milling power, average forces, or instantaneous forces. The least squares fit method is widely used in force model calibration by trying to either fit the average power or force for a number of cuts, or the instantaneous cutting force of one

specific cut [5-9]. Although power sensors are cheap, easy to implement and noninvasive, only tangential cutting coefficients can be obtained from the average power method [5]. To use average power or average force based calibration method [5, 6], typically, a set of milling experiments are conducted at different feedrates with constant spindle speed, radial immersion and axial depth of cut to provide different average chip thicknesses. However, there is a major limitation with this calibration process. Since average power or force is used to calibrate the cutting coefficients, there need to be at least two different cutting conditions to generate two different average chip thicknesses to realize the calibration. Thus, one cannot get the cutting coefficients from any cutting test having the same cutting condition, which limits its practicality.

Other researchers used the instantaneous force profile measured from a single cutting test to predict the cutting coefficients, but their methods are based on a much more complicated model that requires significant knowledge of the tool geometry and synchronization of the measured and simulated cutting forces, making their calibration methods somewhat limited for on-line calibration [7-9]. By investigating milling forces in the frequency domain, Zhang et al. provided an improved method to calibrate the cutting coefficients [10]. The validity of the method is confirmed based on a series of experiments and numerical simulations.

In this thesis, five different calibration methods are introduced and compared. They are based on: 1. spindle motor power, 2. Kistler average force, 3. Kistler force

profile, 4. Smart Tool average force and 5. Smart Tool force profile. Each calibration method is described in details in Chapter 5.

1.2 Thesis Overview

Chapter 1 is an introduction to force model calibration. Chapter 2 introduces the cutting force model used in this research as well as the three different sensors used for force model calibration: LCI power sensor, Kistler dynamometer and wireless Smart Tool.

Chapter 3 describes the spindle motor characterization experiment to determine the motor-sensor system sensitivity at each spindle speed, information necessary to estimate cutting power from the measured spindle motor power. Experimental setup and discussion of experiment results are included in this chapter.

Chapter 4 introduces the cutting test design. Low spindle speed of 600 rpm and high spindle speed of 3000 rpm cutting tests are designed and conducted in this research. Chapter 5 describes the aforementioned five calibration methods in detail.

In Chapter 6, cutting coefficient calibration results of the five different methods are shown and compared. The simulated cutting force using the calibrated coefficients from each method is compared to the force measured by the Kistler dynamometer. The comparison of the five different calibration methods in terms of cost, efficiency, compliance, accuracy, repeatability and applicability is also included. Chapter 7 summarizes the outcomes of this research and offers suggestions for future work.

CHAPTER 2

BACKGROUND

2.1 Introduction

In this chapter, the milling force model used in this research is introduced. The three different sensors used for force model calibration are also introduced. They are the LCI power sensor, Kistler dynamometer and Smart Tool respectively.

2.2 Force Model

The mechanistic milling force model used in this research is described by Altintas [11]. The tangential and radial force consists of a shearing component and a rubbing, ploughing or friction component. Compared to other more complicated models [12], this linear model is simple to calibrate and extensive testing in our facility has demonstrated good accuracy and repeatability as long as the model is calibrated correctly [6]. Figure 2.1 defines a general cutting geometry for end milling.

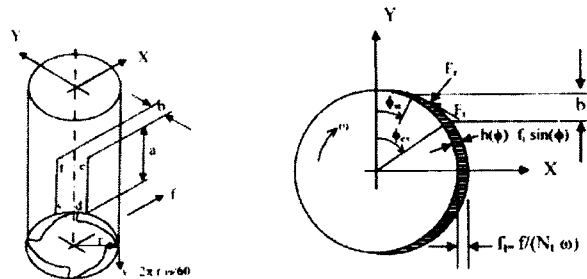


Figure 2.1 - End Milling Cutting Geometry [13]

For simplicity, only flat-end milling cutters with a single cutting tooth are considered in this thesis, and the force component in the axial or Z direction is ignored. Although the calibration method relies on the use of a single tooth cutter, the cutting coefficients obtained by the process can be applied to multi-tooth cutters. Tangential (dF_t) and radial (dF_r) forces acting on a differential tooth element with height dz are expressed as [11]:

$$dF_t(\phi, z) = [K_{tc} h(\phi(z)) + K_{te}] dz \quad (2.1)$$

$$dF_r(\phi, z) = [K_{rc} h(\phi(z)) + K_{re}] dz \quad (2.2)$$

where K_{tc} and K_{te} are tangential cutting coefficients, K_{rc} and K_{re} are radial cutting coefficients, $\phi(z)$ is the edge locating angle, and the chip thickness is:

$$h(\phi(z)) = c \sin \phi(z) \quad (2.3)$$

where c is the feed per tooth (mm/tooth). Assuming that the bottom of the tooth is designated as the reference locating angle ϕ_1 , at an axial depth of cut z the lag angle is

$\psi = k_\beta z$, where $k_\beta = 2 \frac{\tan \beta}{D}$, β is the helix angle, and D is the diameter of the cutting

tool. The locating immersion angle for the tooth at the axial depth of cut z is:

$$\phi(z) = \phi_1 - k_\beta \cdot z \quad (2.4)$$

The elemental forces are resolved into feed (x) and normal (y) directions using the transformation:

$$dF_x(\phi(z)) = -dF_t \cos \phi(z) - dF_r \sin \phi(z) \quad (2.5)$$

$$dF_y(\phi(z)) = +dF_t \sin \phi(z) - dF_r \cos \phi(z) \quad (2.6)$$

Substituting the differential forces (Equations 2.1 and 2.2) and chip thickness (Equation 2.3) into Equations 2.5 and 2.6 leads to:

$$dF_x(\phi(z)) = \left\{ \begin{array}{l} \frac{c}{2} [-K_{tc} \sin 2\phi(z) - K_{rc} (1 - \cos 2\phi(z))] \\ + [-K_{tc} \cos \phi(z) - K_{rc} \sin \phi(z)] \end{array} \right\} dz \quad (2.7)$$

$$dF_y(\phi(z)) = \left\{ \begin{array}{l} \frac{c}{2} [K_{tc} (1 - \cos 2\phi(z)) - K_{rc} \sin 2\phi(z)] \\ + [K_{tc} \sin \phi(z) - K_{rc} \cos \phi(z)] \end{array} \right\} dz \quad (2.8)$$

The differential cutting forces are integrated analytically along the in-cut portion of the tooth in order to obtain the total cutting force acting on the tooth:

$$F_q(\phi(z)) = \int_{z_1}^{z_2} dF_q(\phi(z)), \quad q = x, y \quad (2.9)$$

where $z_1(\phi(z))$ and $z_2(\phi(z))$ are the lower and upper axial engagement limits of the in-cut portion of the tooth. The integrations are carried out by noting $\phi(z) = \phi_1 - k_\beta z$,

$d\phi(z) = -k_\beta dz$. Thus:

$$F_x = \left\{ \frac{c}{4k_\beta} (-K_{tc} \cos 2\phi) + \frac{1}{k_\beta} K_{rc} \sin \phi + \frac{c}{4k_\beta} [K_{rc} (2\phi - \sin 2\phi)] + \frac{1}{k_\beta} (-K_{rc} \cos \phi) \right\}_{z_1(\phi(z))}^{z_2(\phi(z))}$$

(2.10)

$$F_y = \left\{ \frac{c}{4k_\beta} [-K_{tc} (2\phi - \sin 2\phi)] + \frac{1}{k_\beta} K_{tc} \cos \phi + \frac{c}{4k_\beta} [-K_{rc} \cos 2\phi] + \frac{1}{k_\beta} (K_{rc} \sin \phi) \right\}_{z_1(\phi(z))}^{z_2(\phi(z))}$$

(2.11)

2.3 Sensor Introduction

Three different sensors have been used in this research. They are the LCI power sensor, the Kistler dynamometer and the Smart Tool respectively. Each sensor is briefly introduced as below.

2.3.1 LCI Power Sensor

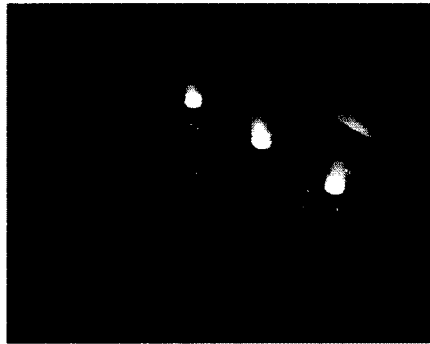


Figure 2.2 - LCI Power Sensor

Model UPC from Load Control Incorporated (LCI) has been used to measure the electrical power input into the spindle motor. The LCI power sensor provides an analog output of 0-10 volts proportional to the spindle motor power with an accuracy of 0.5% full scale [14]. The LCI power sensor is non-invasive and easy to install. The low cost (\$650) and non-invasive nature of the sensor make it ideal for the shop floor environment. The time constant is about 25 ms which was evaluated by measuring the power signal of a step input [15]. With known LCI sensor sensitivity and CNC spindle motor efficiency, good force model coefficients estimation is possible [1, 2, 5, 15]. For our model calibration in this research, we treat the spindle motor efficiency and LCI sensitivity

together, as an overall spindle motor power sensor system sensitivity. The calibration of this system and its use is described in Chapter 3.

2.3.2 Kistler Dynamometer

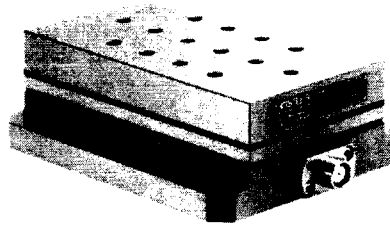


Figure 2.3 - Kistler Dynamometer

The Kistler dynamometer used in this research is model number 9257B. It is a three-component dynamometer for measuring three orthogonal components of a force and has great rigidity (stiffness $>10^9$ N/m in the X and Y direction) and consequently a high natural frequency (2.3 KHz in the X and Y direction if it is mounted on its flanges). Its high resolution enables the smallest dynamic changes in large forces to be measured. It has a range of -5 kN to +5 kN for all the three force components with a linearity of 1% full scale [16].

If a workpiece is mounted on the top plate of the dynamometer, then according to

$\omega_n = \sqrt{k/m}$, its natural frequency will be decreased. By doing tap tests in both X and

Y directions of the dynamometer with the workpiece attached, we find its natural frequency around 1000 Hz in both directions.

Figure 2.4 shows a typical frequency response curve of the Kistler dynamometer. As shown, a 5% amplitude rise can be expected at approximately 1/5 of the resonant frequency [16]. Of course it is also noted that some phase delay will occur if the signal measured by the dynamometer has frequency components near its natural frequency. Therefore in our case, the Kistler dynamometer can work well in a frequency range up to approximately 200 Hz. Overall, the Kistler is a high quality sensor and has been widely used in academic research in machining for many years. It is not a practical choice for use in industry due to its high cost (~\$35K) and invasive nature.

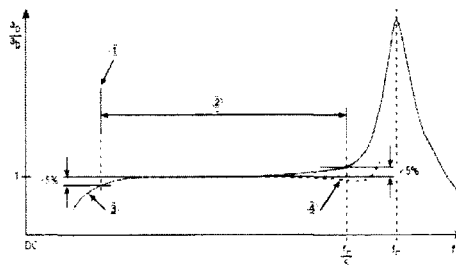


Figure 2.4 - Typical Frequency Response Curve of Kistler [16]

2.3.3 Smart Tool

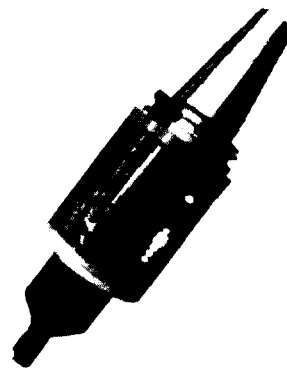


Figure 2.5 - Smart Tool

The Smart Tool is a custom-designed wireless sensor that is used to measure tangential and radial forces. Semi-conductor strain gages mounted on the tool holder shank produce a signal proportional to cutting force when measured statically. It is statically calibrated to measure tangential and radial forces up to 1334.5 N (300 lb) with an accuracy of 5% full scale. The Smart Tool has a natural frequency of approximately 650 Hz, a stiffness of $5 \cdot 10^6$ N/m, and a static sensitivity of 23.5 bits/N for a 16-bit A/D chip [17]. One of the important goals of this research is to determine if the Smart Tool can provide “Kistler like” information at a cost and convenience that is closer to that of the LCI power sensor.

2.4 Summary

In Chapter 2, the milling force model used in this research is introduced. The three different sensors used for force model calibration are also briefly introduced. They are the LCI power sensor, the Kistler dynamometer and the Smart Tool respectively.

CHAPTER 3

SPINDLE MOTOR POWER SENSOR SYSTEM CALIBRATION

3.1 Introduction

Accurate cutting power is the most critical factor for obtaining good force model coefficients using the power model calibration method [15]. In order to get accurate cutting power, an experiment was designed to characterize the relationship between the cutting power and the signal from the Load Control Inc (LCI) power sensor. This chapter describes the spindle motor power sensor system sensitivity calibration at each spindle speed, which can then be used to estimate the actual cutting power at the tool from the LCI sensor output. The LCI sensor output is proportional to the electrical input power to the motor and the system sensitivity will be different at each spindle speed since the spindle motor efficiency changes with spindle speed.

3.2 Experiment Purpose

A magnetic brake and torque sensor system was used to characterize the FADAL EMC CNC milling machine and get an accurate estimation of cutting power based on spindle speed and the electrical power input into the spindle motor. A similar experiment has been done before [15], but because of the limitations of the previous experiment equipment, only spindle speeds less than 1800 RPM have been tested. To check whether the CNC machine performance has changed for the low range speeds (less than 2500

RPM) and explore its performance for the high range speeds (over 2500 RPM), new equipment and experiment procedures are needed.

3.3 Experiment Setup

The setup is shown in Figure 3.1. The magnetic brake, an AHB-6 from Magtrol, provides resistance torque that is proportional to the applied current. Torque sensor T22/20NM from HBM is used to measure the exact load torque provided by the magnetic brake while the spindle rotates at a specified speed. The LCI power sensor produces a signal which is proportional to the electrical input power P_e to the spindle motor.

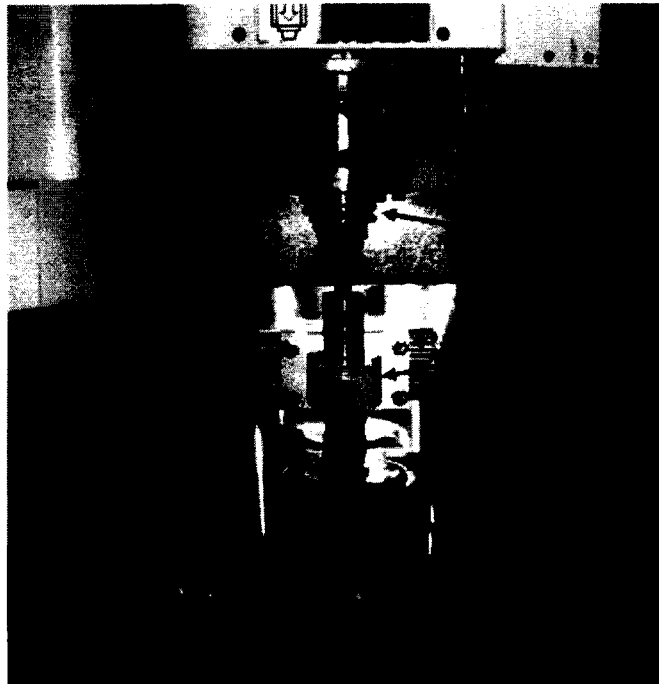


Figure 3.1 - Motor Characterization Experiment Setup

The experiment was performed at different spindle speeds, every 50 rpm from 200 to 700 rpm, then every 100 rpm from 800 to 2000 rpm and 2200, 2400 and 2500 rpm

for the low range. For the high range speeds, data was taken every 200 rpm from 2600 to 4000 rpm, including 3500 rpm. To prevent the brake from overheating, the input current was limited to a maximum of 1 amp for the low range speeds and 0.6 amps for the high range speeds. Readings were taken at evenly spaced current intervals, every 0.2 amps for the low range speeds and every 0.1 amps for the high range speeds. Readings were taken at 0 amps before and after each test sequence to assess mechanical friction and measuring system hysteresis. For each condition, actual torque provided by the brake and electrical power input to the motor are measured. Experiment procedures are described in Appendix A.

3.4 Experiment Results and Discussion

The results are shown in tabular form in Appendix B. The first four columns are spindle speed, current output from the BK power supply to the magnetic brake, voltage output from the torque sensor and measured torque respectively. The fifth column is the output mechanical power calculated from the measured torque and the spindle speed. The last column is the voltage output from the LCI power sensor.

Repeated test data is marked with an R in the table. For each spindle speed, data for zero input current was used to measure hysteresis and was not used to determine the power curve. Thus there are five data points used to calculate the spindle motor power sensor system sensitivity for each spindle speed in the low range and six data points for the high range.

At a given spindle speed, the relationship between the available cutting power and the electrical power input into the spindle motor in a cutting process is [15]:

$$P_c = P_e * \eta_e - P_f \quad (3.1)$$

where P_c is the available cutting power which is actually used to machine the part, P_e is the electrical power input into the spindle motor, η_e is the motor efficiency and P_f is the power to overcome the mechanical friction in the motor and drive system. $P_c + P_f$ can be regarded as the total mechanical power. η_e and P_f are assumed to be constant for a given spindle speed [15].

P_e can be expressed as:

$$P_e = E_o * K_p \quad (3.2)$$

where E_o is output voltage from the LCI power sensor and K_p is the sensitivity of the LCI sensor in watt/volt.

Unfortunately, the sensitivity of the LCI power sensor K_p is not accurately known, which means the electrical power input to the spindle motor P_e is unknown. We substitute Equation 3.2 into Equation 3.1 and get:

$$P_c = E_o * K_p * \eta_e - P_f = E_o * K_s - P_f \quad (3.3)$$

where K_s equals $K_p * \eta_c$, which is regarded as the spindle motor power sensor system sensitivity, or simply the motor-sensor system sensitivity.

For each spindle speed, a curve can be generated by plotting the available cutting power P_c vs the LCI sensor voltage output E_o . We can see the curve is quite linear at every spindle speed. Figures 3.2 and 3.3 are the curves at 1500 and 3600 rpm respectively.

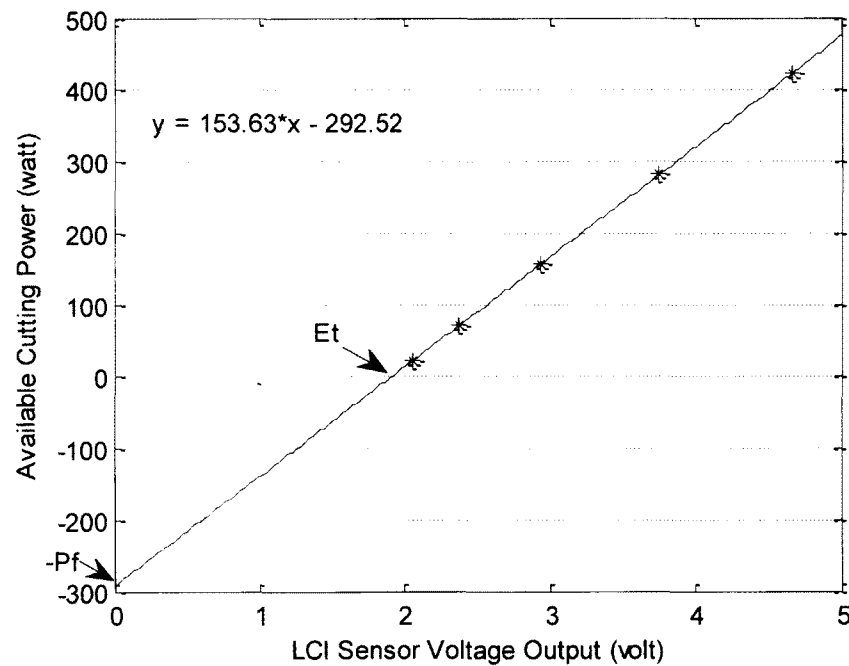


Figure 3.2 - Available Cutting Power vs LCI Sensor Voltage Output at 1500 rpm

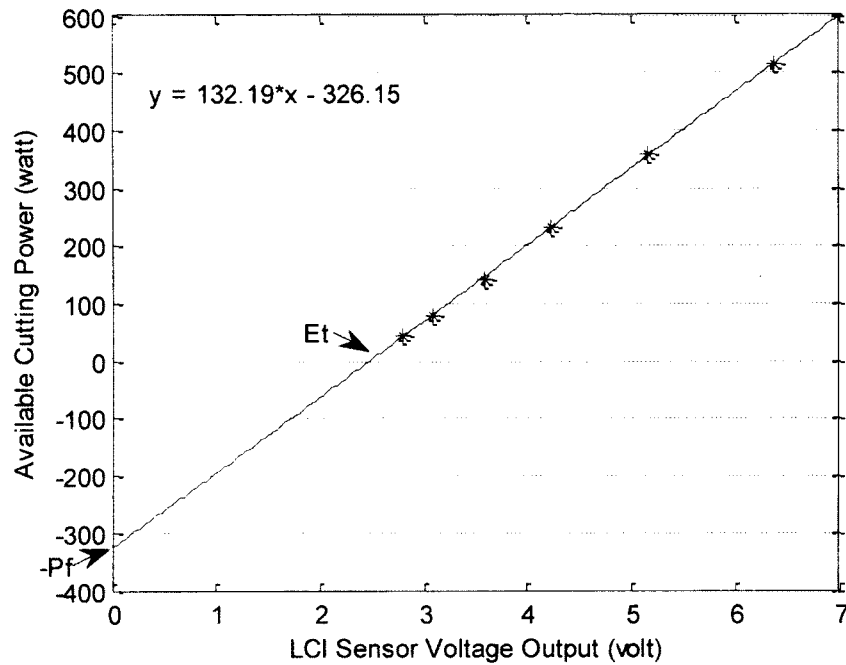


Figure 3.3 - Available Cutting Power vs LCI Sensor Voltage Output at 3600 rpm

From Equation 3.3, assuming the frictional losses are constant for a given spindle speed, we can see the plot of P_c vs E_o should be a line, and the slope of this line is K_s . Figures 3.2 and 3.3 confirm this. Based on Equation 3.3, when E_o is zero, P_c equals $-P_f$, which corresponds to the intercept between the line and y axis in Figure 3.2 and 3.3. When the spindle motor runs at a constant speed without cutting any material, P_c equals zero, the LCI sensor voltage output is called tare power voltage notified by E_t . From Equation 3.3, when P_c equals zero, E_o equals to P_f / K_s , which corresponds to the intercept between the line and x axis. After plotting figures similar to Figure 3.2 and 3.3 for all the different spindle speeds, we can get the slope of each line, which is the motor-

sensor system sensitivity at each spindle speed. Since the tests for spindle speed at 2500, 3000, 3500 and 4000 rpm are repeated once each, the sensitivity at these four different spindle speeds is gained through averaging. Table 3.1 shows the motor-sensor system sensitivity for each spindle speed. We can then plot the sensitivity versus the spindle speed as shown in Figure 3.4.

We find that the motor-sensor system sensitivity for the low range and the high range speeds seems to have different behavior, observable in Figure 3.4. That is because the CNC machine changes the transmission gears from the low range speeds to the high range speeds at a transition speed of 2500 rpm, resulting in the different trends of the motor-sensor system sensitivity for the low range and the high range speeds. Therefore different curves are needed to fit the sensitivity for the two speed ranges to better represent their behavior, which can be seen in Figure 3.5 and 3.6.

Table 3.1 - Motor-Sensor System Sensitivity (K_s) versus Spindle Speed (ω)

ω (rpm)	200	250	300	350	400	450	500	550	600	650
K_s (watt/volt)	144	145	143	145	146	149	150	147	147	150
ω (rpm)	700	750	800	900	1000	1100	1200	1300	1400	1500
K_s (watt/volt)	149	148	150	148	153	153	153	152	151	154
ω (rpm)	1600	1700	1800	1900	2000	2200	2400	2500	2600	2800
K_s (watt/volt)	152	152	151	152	152	151	149	147	139	139
ω (rpm)	3000	3200	3400	3500	3600	3800	4000			
K_s (watt/volt)	137	136	133	132	132	131	129			

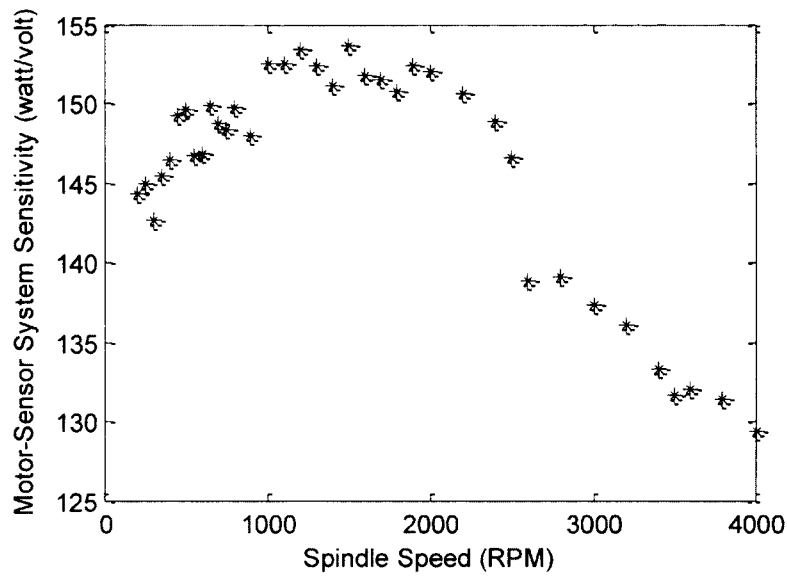


Figure 3.4 - Motor-Sensor System Sensitivity Plot

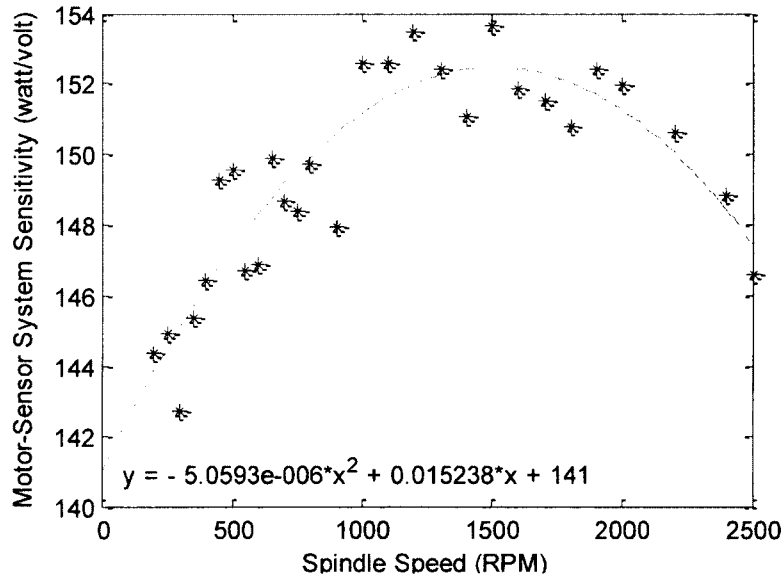


Figure 3.5 - Motor-Sensor System Sensitivity Curve for Low Range Speeds

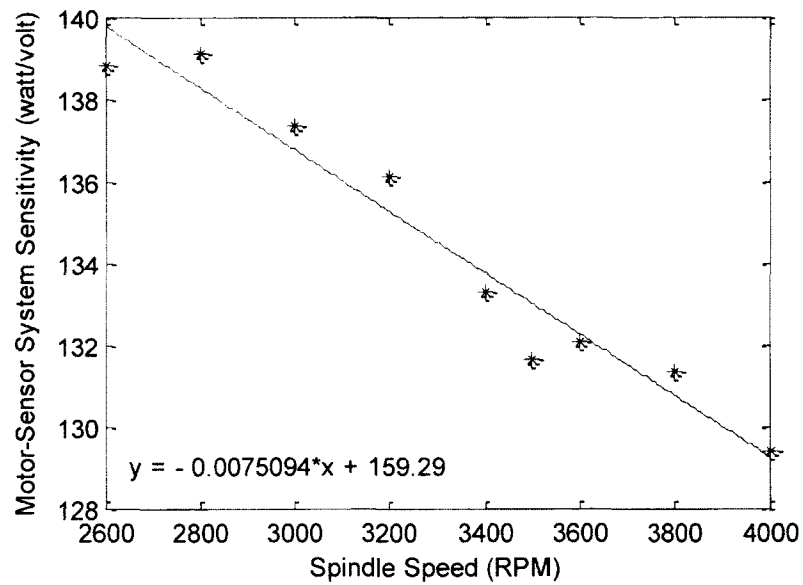


Figure 3.6 - Motor-Sensor System Sensitivity Curve for High Range Speeds

Figure 3.7 and 3.8 are the residual plots for the fit of motor-sensor system sensitivity for the low range and high range speeds respectively. As we can see, the residuals are within 3 and 1.5 for each fit, which confirms that the quadratic curve and linear line fit the low range and high range data quite well respectively. Therefore the motor-sensor system sensitivity at any spindle speed from 200 to 4000 rpm can be estimated from the above curve fits.

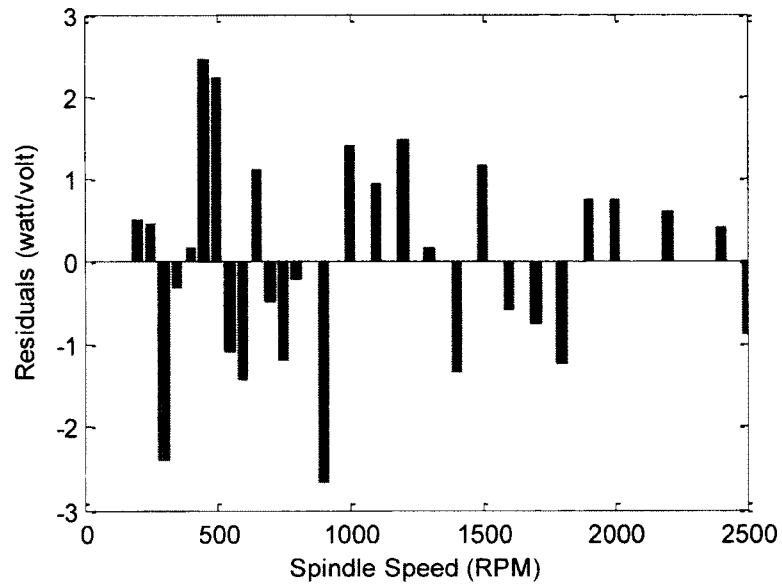


Figure 3.7 - Residual Plot of Motor-Sensor System Sensitivity for Low Range Speeds

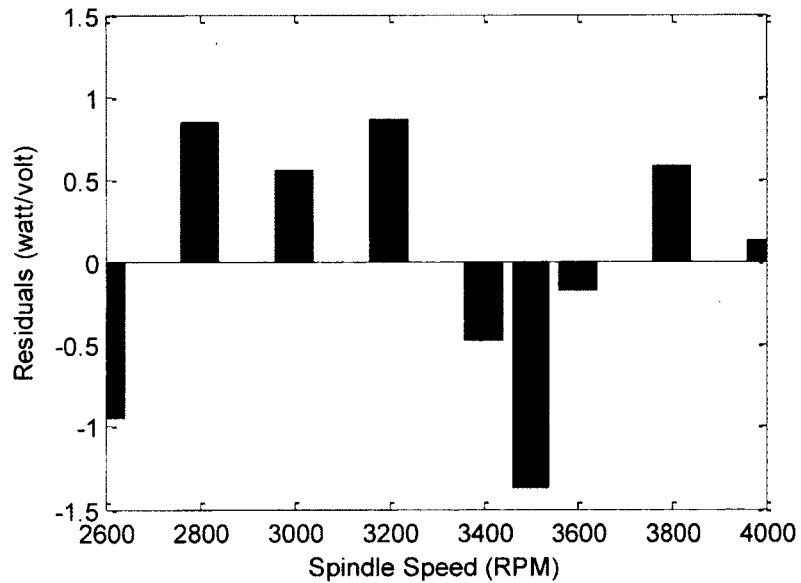


Figure 3.8 - Residual Plot of Motor-Sensor System Sensitivity for High Range Speeds

Since there are residuals which can be regarded as the estimation error for the fit of motor-sensor system sensitivity, it is better to quantify how much the estimation error

would be, which can be found from the confidence interval and prediction interval of the fit in Figure 3.9 and 3.10 for the low range and high range speeds respectively.

The 95% confidence interval of the fit tells us the uncertainty in determining the mean of the motor-sensor system sensitivity for each spindle speed, while the 95% prediction interval of the fit tells us the distribution of the motor-sensor system sensitivity for each spindle speed. Thus we can quantify how much the variation would be using the corresponding fit to estimate the motor-sensor system sensitivity for each spindle speed.

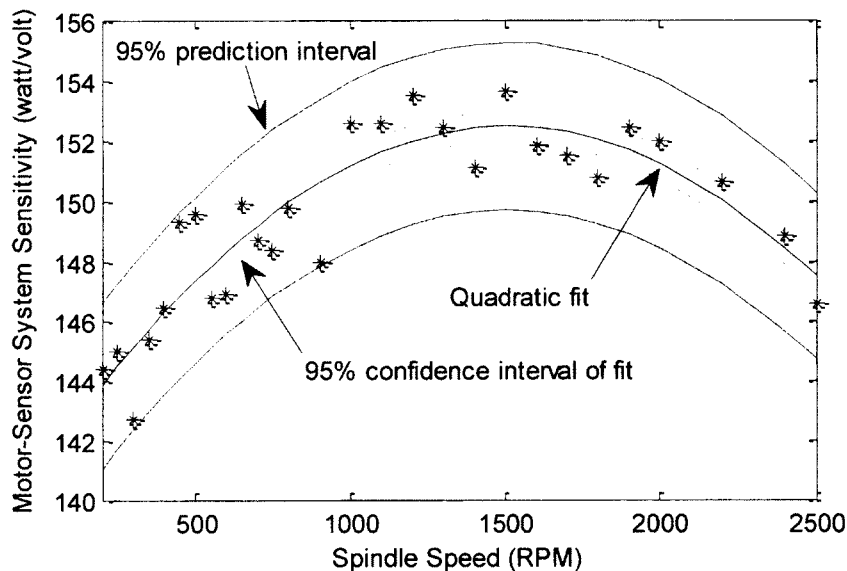


Figure 3.9 - Confidence and Prediction Interval for the Polynomial Fit of Motor-Sensor System Sensitivity for Low Range Speeds

For low range spindle speeds, the quadratic curve fit is:

$$K_s = -5.0593 * 10^{-6} * \omega^2 + 1.5238 * 10^{-2} * \omega + 141 \quad (3.4)$$

where ω is the spindle speed (rpm).

The 95% confidence interval of the fit is $K_s \pm 0.5155$ while the 95% prediction interval of the fit is $K_s \pm 2.7761$.

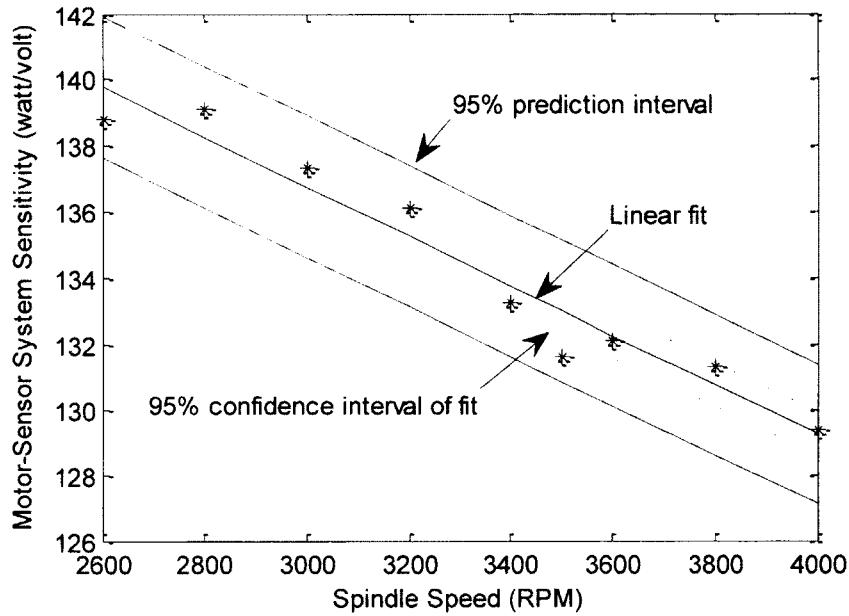


Figure 3.10 - Confidence and Prediction Interval for the Linear Fit of Motor-Sensor System Sensitivity for High Range Speeds

For high range spindle speeds, the linear fit is:

$$K_s = -7.5094 * 10^{-3} * \omega + 159.29 \quad (3.5)$$

The 95% confidence interval of the fit is $K_s \pm 0.6781$ while the 95% prediction interval of the fit is $K_s \pm 2.1445$.

From Equation 3.3, at a given spindle speed, the change in P_c is proportional to the change in E_o , which can be represented by Equation 3.6.

$$\Delta P_c = \Delta E_o * K_s \quad (3.6)$$

where ΔP_c and ΔE_o are the change in P_c and E_o respectively. Now that we have the motor-sensor system sensitivity K_s , for any spindle speed, ΔP_c can be simply calculated with Equation 3.6. During the actual cutting test, the tare power voltage E_t is measured when P_c is zero. After measuring the LCI sensor voltage output E_o for any case which is machining material, the actual cutting power can then be calculated using Equation 3.7.

$$P_c = (E_o - E_t) * K_s \quad (3.7)$$

3.5 Summary

This chapter describes the spindle motor characterization experiment to calibrate the motor-sensor system sensitivity at each spindle speed. As can be seen, the motor-sensor system sensitivity is different at each spindle speed since the spindle motor efficiency changes with spindle speed. The obtained sensitivity can then be used to estimate the cutting power for milling force model calibration.

CHAPTER 4

CUTTING TEST DESIGN

4.1 Introduction

This chapter introduces the cutting test design for force model calibration. The choices of cutting process variables such as spindle speed, radial immersion, axial depth of cut, tool geometry and workpiece material are included. The data recording system is briefly introduced as well.

To minimize the dynamic effects of both the Kistler dynamometer and the Smart Tool on force measurements and tool vibration, we designed cutting tests at a relatively low spindle speed of 600 rpm. We also designed cutting tests at a high spindle speed of 3000 rpm for comparison.

4.2 Cutting Test Design

As mentioned in Chapter 2, the dynamic effects of the Kistler force dynamometer limit its frequency range to around 200 Hz. The Smart Tool frequency response is unknown, but it is found to have a natural frequency of approximately 650 Hz.

In order to minimize the dynamic effects of both sensors on force measurement, we designed cutting tests at a relatively low spindle speed of 600 rpm. For a one tooth cutter, this gives a periodic signal with a fundamental frequency of 10 Hz, well below the

bandwidth of both dynamometers. We also designed and conducted cutting tests at a high spindle speed of 3000 rpm for comparison.

Currently, the Smart Tool is only capable of measuring either tangential force or radial force at a given time, thus each experiment had to be performed twice in order to collect both radial and tangential components for calibration. For the results of this calibration to be accurate, it is required that cut-to-cut variability remains small. In the rest of this thesis, (T) denotes the experiment that was conducted with the Smart Tool measuring tangential force while (R) denotes the experiment that was conducted with the Smart Tool measuring radial force.

Up milling cutting tests are performed and repeated once at both 600 and 3000 rpm using a single tooth cutter to eliminate the effect of tool runout and to lower the tooth passing frequency to 10 and 50 Hz respectively. The diameter of the cutting tool is 19.05 mm and the helix angle is 14.73 degrees. The insert of the cutting tool is a Sandvik R390-11 T3 08E-NL H13A. The workpiece material is aluminum 6061. The axial depth of cut is 3.175 mm (0.125 inch). Table 4.1 and 4.2 show the feedrates for the cutting tests at 600 and 3000 rpm respectively. The four feedrates for each radial immersion are chosen to make the average chip thickness 0.0254, 0.0508, 0.0762 and 0.1016 mm (0.001, 0.002, 0.003 and 0.004 inches) respectively.

Table 4.1 - Feedrate Design for 600 rpm Cutting Test

Feedrate (mm/sec)	Quarter Immersion	Half Immersion	Three Quarter Immersion
Feedrate 1	0.5321	0.3988	0.3548
Feedrate 2	1.0638	0.7980	0.7095
Feedrate 3	1.5960	1.1968	1.0638
Feedrate 4	2.1281	1.5960	1.4186

Table 4.2 - Feedrate Design for 3000 rpm Cutting Test

Feedrate (mm/sec)	Quarter Immersion	Half Immersion	Three Quarter Immersion
Feedrate 1	2.6598	1.9947	1.7733
Feedrate 2	5.3196	3.9899	3.5467
Feedrate 3	7.9798	5.9857	5.3196
Feedrate 4	10.6396	7.9798	7.0930

The average chip thickness for up milling can be expressed as [11]:

$$h_a = -c \frac{\cos \phi_{ex} - \cos \phi_{st}}{\phi_{ex} - \phi_{st}} \quad (4.1)$$

For each radial immersion cutting test, the feedrate changes in steps from feedrate 1 to feedrate 4 as the cutting tool moves in the feed direction, as shown in Figure 4.1.

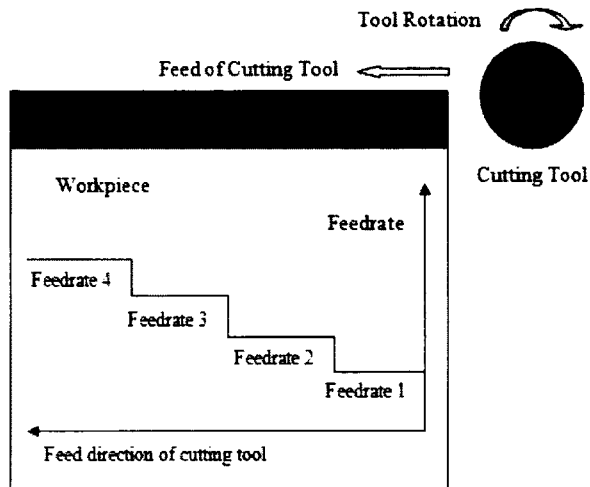


Figure 4.1 - Cutting Test Design

During the cutting processes, the instantaneous cutting forces F_x and F_y are measured by the Kistler dynamometer having an anti-aliasing filter with a cut-off frequency at 2.2 KHz and recorded by a computer through a data acquisition board with the sampling frequency of 7200 Hz and 18000 Hz for the 600 rpm and 3000 rpm cutting tests respectively. For cutting tests at 600 rpm, 720 samples are taken for each tool revolution while for cutting tests at 3000 rpm, 360 samples are taken for each tool revolution. Data measured by the LCI power sensor is recorded by the same board at the same sampling rate as the Kistler dynamometer data.

The Smart Tool has a fixed sampling frequency of 10.24 kHz for all cutting tests and has an anti-aliasing filter with a cut-off frequency at 2.84 kHz. Instantaneous tangential or radial forces measured by the Smart Tool are transmitted through Bluetooth and recorded by a separate computer.

4.3 Summary

In this chapter, the cutting test design for force model calibration is presented. The choices of spindle speed, radial immersion, axial depth of cut, tool geometry and workpiece material are given and a brief introduction of the data recording system is included.

In order to minimize the dynamic effects of both sensors on force measurement, cutting tests are performed at a relatively low spindle speed of 600 rpm. For a one tooth cutter, this gives a periodic signal with a fundamental frequency of 10 Hz, well below the bandwidth of both dynamometers. We also designed cutting tests at a high spindle speed of 3000 rpm for comparison.

CHAPTER 5

FORCE MODEL CALIBRATION METHODS

5.1 Introduction

As mentioned in Chapter 2, five different calibration methods are introduced and compared in this research. They are based on spindle motor power, Kistler average force and force profile, and Smart Tool average force and force profile. This chapter describes each calibration method in detail.

5.2 Spindle Motor Power

Based on previous research, we have the following relationship between the average cutting power and the cutting geometry [14]:

$$P_c = K_{tc} * \dot{Q} + K_{te} * \dot{A}_c \quad (5.1)$$

where P_c , \dot{Q} and \dot{A}_c are average cutting power, volumetric removal rate and contact area rate respectively.

The cutting power is related to the spindle motor power through:

$$P_c = (E_o - E_t) * K_s \quad (5.2)$$

Please refer to Chapter 3 for detailed derivation of Equation 5.2 which was presented as Equation 3.7 in Section 3.4.

Usually, we rotate the spindle at a desired speed for about 10 – 15 minutes before measuring tare power voltage E_t . E_o and E_t can be easily measured from the LCI power sensor. As long as we have the motor-sensor system sensitivity K_s , which can be found through the experiments described in Chapter 3, we can get P_c from Equation 5.2. The volumetric removal rate and contact area rate for each cutting test can be found from the cutting geometry [5]. Equation 5.1 is written once for each test and then combined in matrix form:

$$[P_c] = \begin{bmatrix} \dot{Q} & \dot{A}_c \end{bmatrix} \begin{bmatrix} K_{tc} \\ K_{rc} \end{bmatrix} = [G][K_t] \quad (5.3)$$

where the G matrix is defined by the cutting geometry.

Least square regression can be applied to the above equation to obtain the tangential cutting coefficients.

$$K_t = (G^T G)^{-1} G^T P_c \quad (5.4)$$

After we get the tangential cutting coefficients, a ratio method can be applied to get the radial cutting coefficients K_{rt} and K_{rc} [17]. Specifically, the ratios of radial to tangential cutting coefficients can be found from the four cutting coefficients calibrated from the Kistler average force based method. Then those ratios can be applied to the tangential coefficients calibrated from the spindle motor power to get the radial coefficients.

5.3 Kistler Reaction Force

The Kistler dynamometer 9257B is used in this research to measure the reaction force between the workpiece and the cutting tool in both X and Y directions.

5.3.1 Force Profile Method

Based on the force model described in Chapter 2, a number of F_x and F_y forces, with known cutting geometry values and unknown edge locating angle at each instant the forces are measured, can be combined in the following matrix form:

$$[F] = [M][K] \quad (5.5)$$

$$\text{where } [F] = \begin{bmatrix} F_{x1} \\ F_{x2} \\ \vdots \\ F_{y1} \\ F_{y2} \\ \vdots \end{bmatrix}, [K] = \begin{bmatrix} K_{tc} \\ K_{te} \\ K_{rc} \\ K_{re} \end{bmatrix}, [M] \text{ is the geometric matrix consisting of the remaining}$$

terms in Equation 2.7 with the four cutting coefficients removed. An example M matrix is:

$$[M] = \begin{bmatrix} -\frac{c}{4k_\beta} \cos 2\phi_{\phi_1}^{\phi_2} & \frac{1}{k_\beta} \sin \phi_{\phi_1}^{\phi_2} & \frac{c}{4k_\beta} (2\phi - \sin 2\phi)_{\phi_1}^{\phi_2} & -\frac{1}{k_\beta} \cos \phi_{\phi_1}^{\phi_2} \\ \vdots & \vdots & \vdots & \vdots \\ -\frac{c}{4k_\beta} (2\phi - \sin 2\phi)_{\phi_1}^{\phi_2} & \frac{1}{k_\beta} \cos \phi_{\phi_1}^{\phi_2} & -\frac{c}{4k_\beta} \cos 2\phi_{\phi_1}^{\phi_2} & \frac{1}{k_\beta} \sin \phi_{\phi_1}^{\phi_2} \\ \vdots & \vdots & \vdots & \vdots \end{bmatrix} \quad (5.6)$$

where c is the feed per tooth (mm/tooth), ϕ_1 and ϕ_2 are the edge locating angle for the lower and upper axial engagement limits of the in-cut portion of the flute and they have the following relationship:

$$\phi_2 = \phi_1 - k_\beta \cdot a \quad (5.7)$$

where a is the axial depth of cut. Please refer to Section 2.1 for the definition of k_β .

A least squares estimation can be applied to Equation 5.5 to calculate the cutting coefficients K_{tc} , K_{te} , K_{rc} and K_{re} :

$$\begin{bmatrix} K_{tc} \\ K_{te} \\ K_{rc} \\ K_{re} \end{bmatrix} = (M^T M)^{-1} M^T F \quad (5.8)$$

To use a cutting force profile and least squares regression to calibrate the cutting coefficients, we need to average a number of cycles of cutting force to get one average profile, with less noise, to form the force matrix F in Equation 5.8. We also need to know the geometric matrix M , consisting of the known feed per tooth, the diameter and helix angle of the cutting tool, and the unknown edge locating angles. These angles are for the lower and upper limit of the in-cut portion of the flute at each instant the force is measured.

To get the edge locating angles, we use a Hall element sensor mounted on the housing of the spindle of our CNC machine. The sensor outputs a pulse when the spindle just reaches its home position. This provides a once per revolution “tick signal” that can be used to determine edge locating angles. As long as we can get one clean cycle of

cutting force and the corresponding geometric matrix, then we can easily implement the least squares regression (Equation 5.8) to get the cutting coefficients.

Aligning and Averaging Different Cycles of Force

Figures 5.1 and 5.2 show the profile of 20 cycles of instantaneous force F_x and F_y measured by the Kistler dynamometer for one cutting case (600 rpm, quarter immersion, feedrate 1 (T)) respectively. We find both F_x and F_y vary some in amplitude and have noticeable noise.

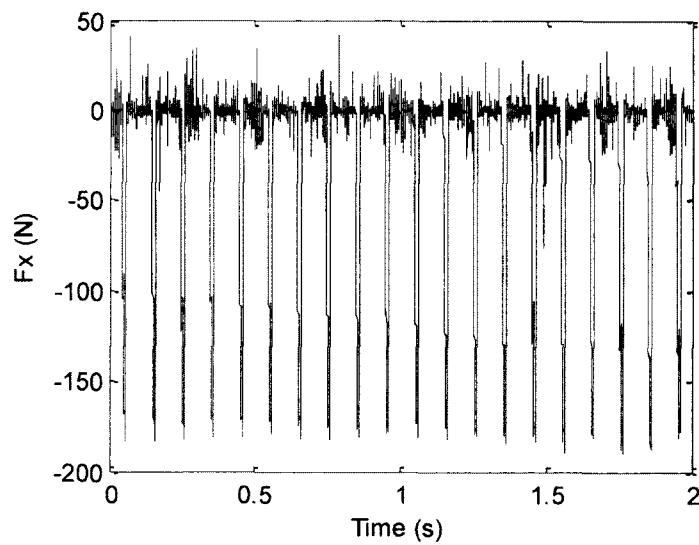


Figure 5.1 - 20 Cycles of F_x , 600 rpm, Quarter Immersion and Feedrate 1 (T)

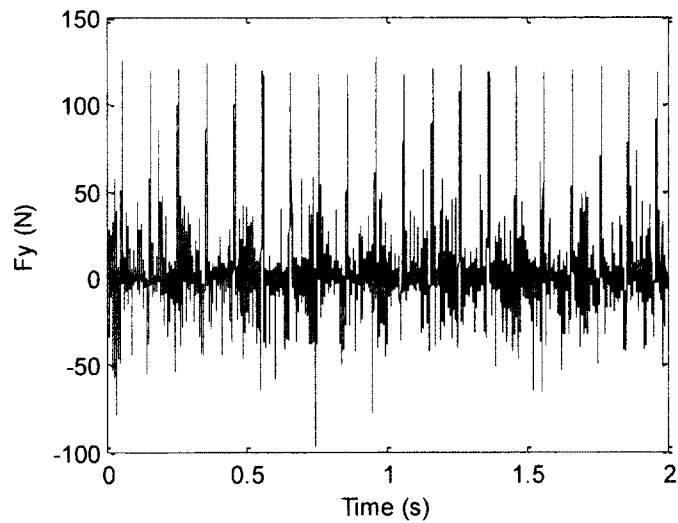


Figure 5.2 - 20 Cycles of F_y , 600 rpm, Quarter Immersion and Feedrate 1 (T)

Figures 5.3 and 5.4 show the FFT results of the cutting force presented in Figures 5.1 and 5.2 respectively. The FFT results confirm that most frequency components of the cutting force lie within the working bandwidth of the Kistler and it is possible to use the force data directly without any filtering.

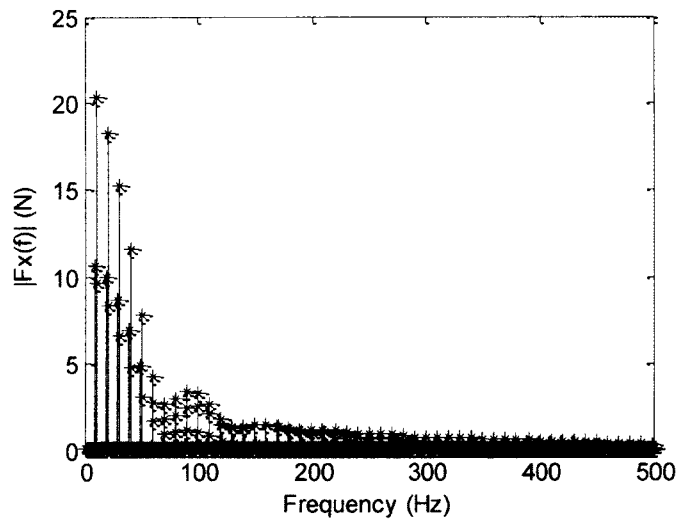


Figure 5.3 - FFT of F_x , 600 rpm, Quarter Immersion and Feedrate 1 (T)

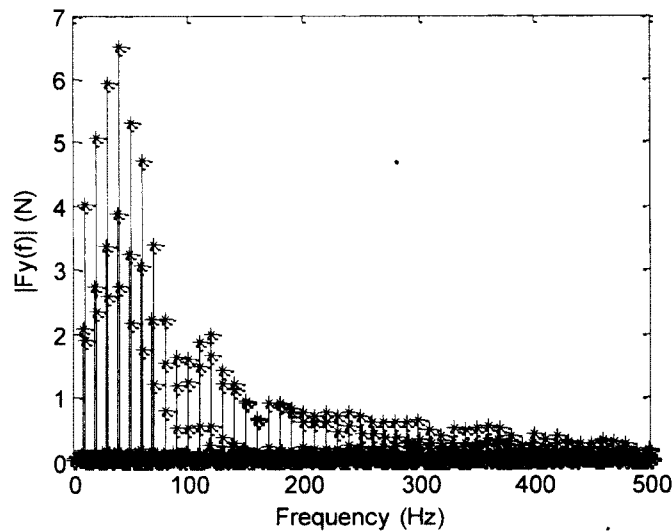


Figure 5.4 - FFT of F_y , 600 rpm, Quarter Immersion and Feedrate 1 (T)

In order to get a clean force profile which can be used in the calibration of the cutting coefficients, we align 20 selected cycles of F_x and F_y and average them to get one cycle of F_x and F_y . Figures 5.5 and 5.6 show the unshifted 20 cycles of F_x and F_y . Because of the stochastic nature of cutting and the fact that the spindle speed of the CNC machine may vary during the cutting test (open-loop induction motor), the unshifted 20 cycles of F_x and F_y are not perfectly aligned with each other. To correctly align the 20 cycles of force, the first cycle is selected as the reference and each one of the remaining cycles is compared to the first cycle and shifted back and forth based on the cross-correlation between itself and the first cycle. Figures 5.7 and 5.8 show the shifted 20 cycles of F_x and F_y . After being aligned, the 20 cycles of force are then averaged to get one cycle of force, as shown in Figures 5.9 and 5.10.

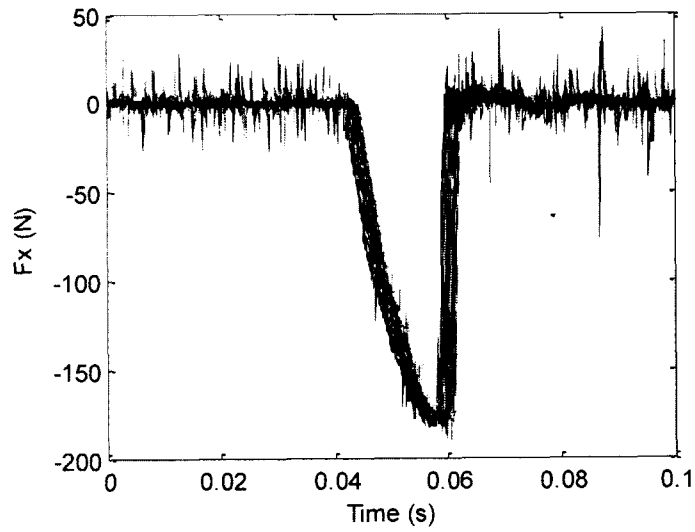


Figure 5.5 - Unshifted F_x , 600 rpm, Quarter Immersion and Feedrate 1 (T)

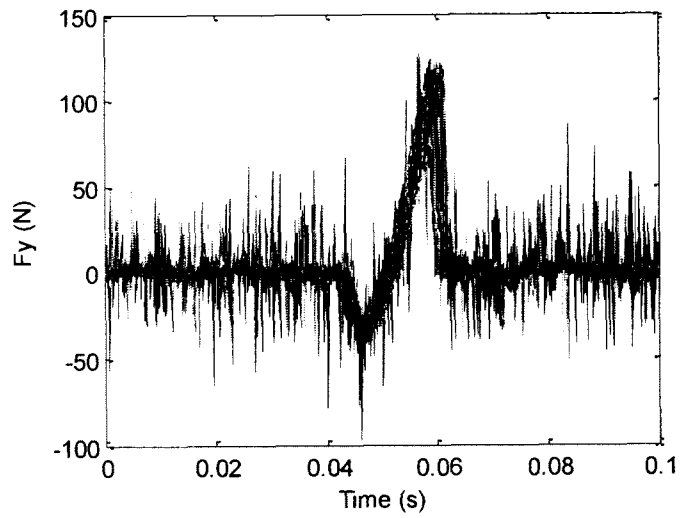


Figure 5.6 - Unshifted F_y , 600 rpm, Quarter Immersion and Feedrate 1 (T)

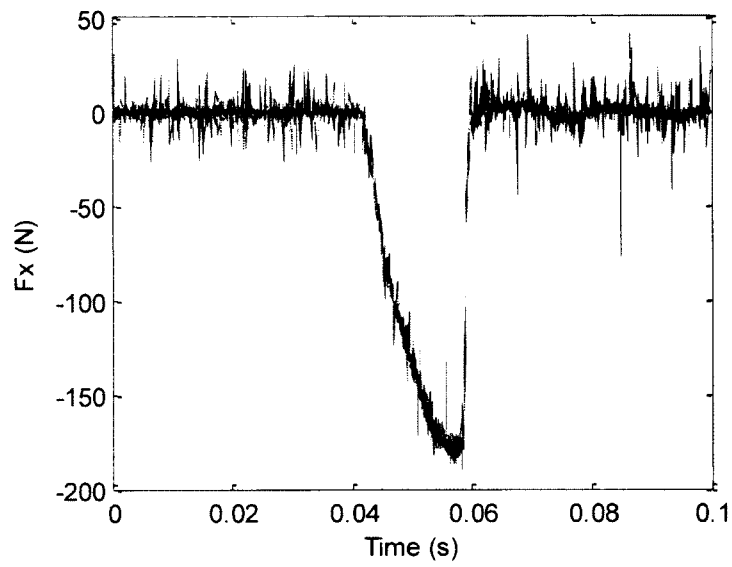


Figure 5.7 - Shifted F_x , 600 rpm, Quarter Immersion and Feedrate 1 (T)

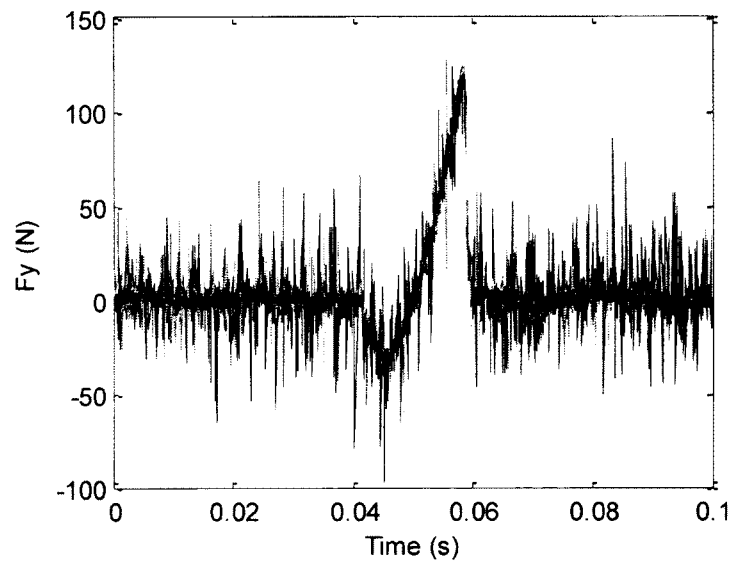


Figure 5.8 - Shifted F_y , 600 rpm, Quarter Immersion and Feedrate 1 (T)

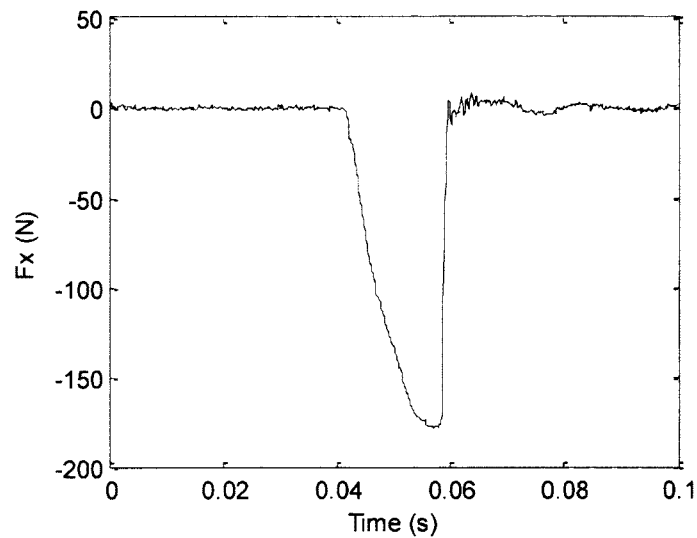


Figure 5.9 - Averaged One Cycle of F_x , 600 rpm, Quarter Immersion and Feedrate 1 (T)

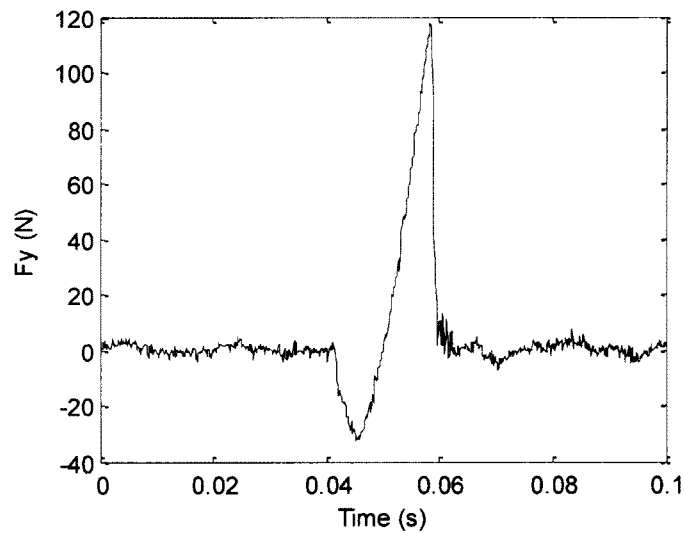


Figure 5.10 - Averaged One Cycle of F_y , 600 rpm, Quarter Immersion and Feedrate 1 (T)

Finding the Geometric Matrix for Calibration

To implement the least squares regression to get the cutting coefficients, we need to know the elements of the Geometric matrix described in Equation 5.6. The elements depend on the known feed per tooth, the helix angle and diameter of the cutting tool, and

the unknown edge locating angle of the cutting flute at each instant the cutting forces are sampled. To determine the edge locating angle of the cutting flute, we use the previously mentioned “tick signal” from the Hall effect sensor. The tick signal is sampled along with the cutting force at the same rate. The first cycle of the tick signal and the averaged cycle of F_x and F_y are shown in Figure 5.11. As mentioned in Chapter 2, the edge locating angle of the bottom of the flute ϕ_1 is designated as the reference locating angle. The tick signal drops to a low voltage when the reference locating angle is around -94 degrees for the 600 rpm cutting tests. We then know the reference locating angle at each instant the cutting forces are sampled, based on the spindle speed and the sampling frequency.

During the periods when the cutting tooth begins to enter and exit from the cutting region, the cutting tool is not fully engaged, so we do not use that force data in the calibration calculations. This section of force is represented by the circles in Figure 5.11. Typically, we use the force data for calibration when the cutting tooth is fully engaged in the desired axial depth of cut. For example, we use the range of [10 50], [10 80] and [10 110] degrees of the reference locating angle to do the calibration for quarter, half and three quarter immersion cutting tests respectively.

The procedure for calculating the coefficients starts by populating the M matrix as defined in Equations 5.5 - 5.7. With two samples per degree the M matrix will be 160x4 for the 40 degrees of interest during a 600 rpm quarter immersion cut (both x and y forces times 2 samples per degree times 40 degrees). Then we use the least squares regression expressed in Equation 5.8 to get the cutting coefficients.

The force profile based cutting coefficients for the cutting test of 600 rpm, quarter immersion and feedrate 1 (T) are: $K_{tc}=1119.3 \text{ N/mm}^2$, $K_{te}=9.9 \text{ N/mm}$, and $K_{rc}=398.0 \text{ N/mm}^2$, $K_{re}=10.3 \text{ N/mm}$.

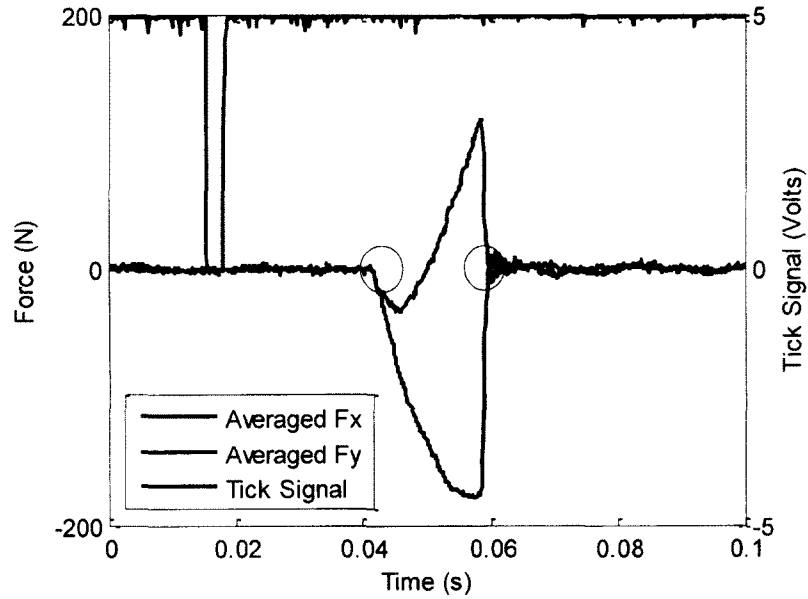


Figure 5.11 - Cutting Force Profile and Tick Signal, 600 rpm, Quarter Immersion and Feedrate 1 (T)

5.3.2 Average Force Method

Average cutting forces in the x and y direction for up milling can be expressed as Equation 5.9 and 5.10 respectively. In the equations, N is the number of teeth, a is the axial depth of cut, c is the feed per tooth, ϕ_s is the entry angle and ϕ_{ex} is the exit angle [6, 11].

$$\bar{F}_x = \left\{ \begin{array}{l} \frac{Nac}{8\pi} [K_{tc} (\cos 2\phi_{ex} - \cos 2\phi_s) - K_{te} [2\phi_{ex} - 2\phi_s - (\sin 2\phi_{ex} - \sin 2\phi_s)]] \\ + \frac{Na}{2\pi} [-K_{re} [\sin \phi_{ex} - \sin \phi_s] + K_{rc} [\cos \phi_{ex} - \cos \phi_s]] \end{array} \right\} \quad (5.9)$$

$$\bar{F}_y = \left\{ \begin{array}{l} \frac{Nac}{8\pi} [K_{tc} (2\phi_{ex} - 2\phi_s - (\sin 2\phi_{ex} - \sin 2\phi_s)) + K_{rc} [\cos 2\phi_{ex} - \cos 2\phi_s]] \\ - \frac{Na}{2\pi} [K_{tc} (\cos \phi_{ex} - \cos \phi_s) + K_{rc} (\sin \phi_{ex} - \sin \phi_s)] \end{array} \right\} \quad (5.10)$$

Equation 5.9 and 5.10 can be combined into a matrix form as seen in Equation 5.11, where K contains the model coefficients and G depends on the cutting geometry. Refer to [6] for an example of a G matrix.

$$\bar{F} = GK \quad (5.11)$$

Similarly, least squares estimation can be applied to Equation 5.11 to calculate the four cutting coefficients K_{tc} , K_{te} , K_{rc} and K_{re} , in

$$\begin{bmatrix} K_{tc} \\ K_{te} \\ K_{rc} \\ K_{re} \end{bmatrix} = (G^T G)^{-1} G^T \bar{F} \quad (5.12)$$

5.4 Smart Tool Tangential and Radial Force

The Smart Tool is used to measure tangential and radial forces during cutting. Two calibration methods using the Smart Tool, force profile and average force, are now described.

5.4.1 Force Profile Method

Due to the design of the Smart Tool [16] and the small axial depth of cut of the designed cutting tests, we ignore the 14.73 degree helix angle of the cutting tool and

assume that it has a single straight cutting flute. The instantaneous tangential and radial force at each edge locating angle ϕ can then be expressed as:

$$F_t = [K_{tc} * h(\phi) + K_{te}] * a \quad (5.13)$$

$$F_r = [K_{rc} * h(\phi) + K_{re}] * a \quad (5.14)$$

where $h(\phi)$ is the instantaneous chip thickness expressed in Equation 2.3.

Equation 5.13 can be rewritten as:

$$F_t / a = K_{tc} * h(\phi) + K_{te} \quad (5.15)$$

If we plot F_t / a against instantaneous chip thickness $h(\phi)$ for one tool rotation, we can fit a line to the data. The slope of the fitted line would be K_{tc} while the intercept between the fitting line and the Y axis would be K_{te} .

Similar to the Kistler force profile based method, we also align and average 20 cycles of tangential force to get one clean cycle to calibrate cutting coefficients. Figure 5.12 shows the chosen 20 cycles of tangential force for the cutting test of 600 rpm, quarter immersion and feedrate 1. Figure 5.13 shows the FFT result of the tangential force, which tells us that most frequency components of the tangential force lie below 200 Hz, well below the natural frequency of the Smart Tool which is around 650 Hz as mentioned in Chapter 2. Therefore it is possible to use the tangential force directly without any filtering to calibrate the tangential coefficients. Figures 5.14 and 5.15 show

the unshifted and shifted 20 cycles of the tangential force respectively. Figure 5.16 shows the averaged one cycle of the tangential force.

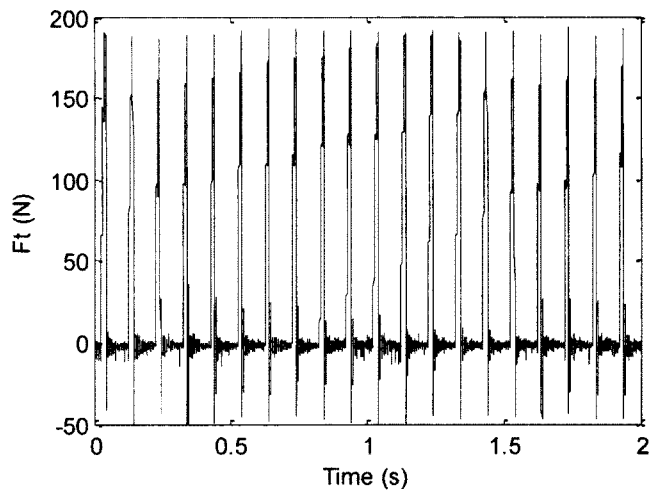


Figure 5.12 - 20 Cycles of F_t , 600 rpm, Quarter Immersion and Feedrate 1

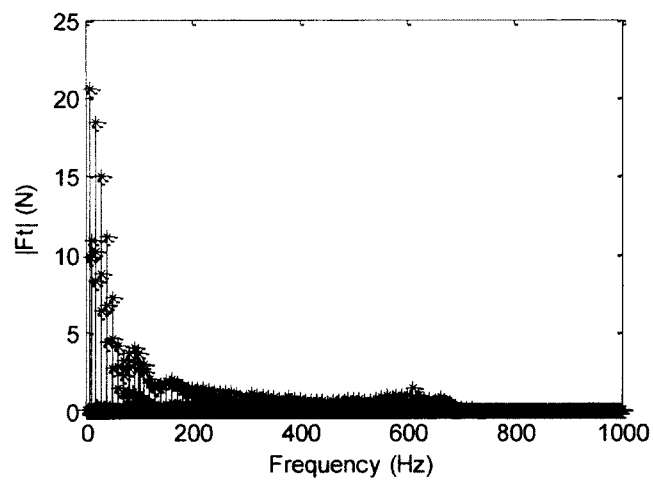


Figure 5.13 - FFT of F_t , 600 rpm, Quarter Immersion and Feedrate 1

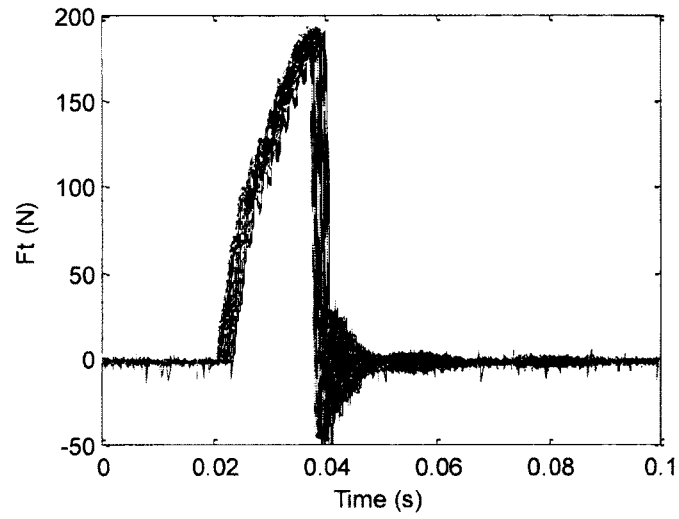


Figure 5.14 - Unshifted F_t , 600 rpm, Quarter Immersion and Feedrate 1

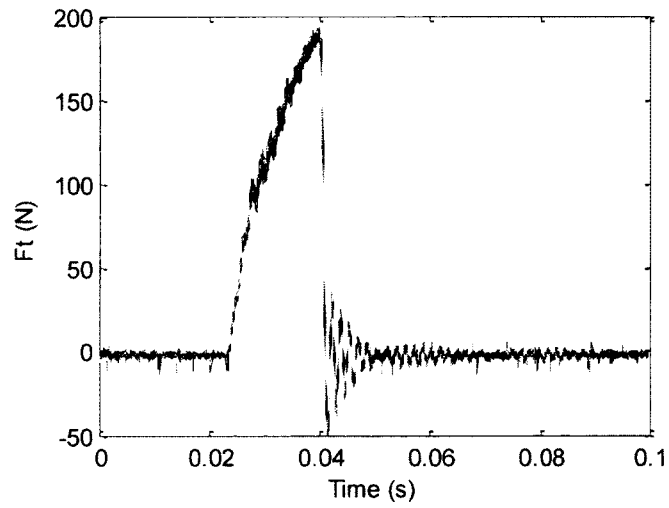


Figure 5.15 - Shifted F_t , 600 rpm, Quarter Immersion and Feedrate 1

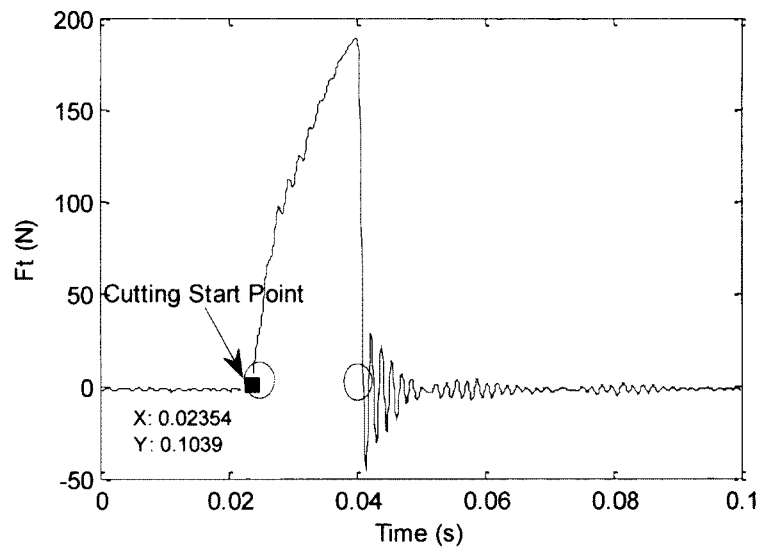


Figure 5.16 - Averaged One Cycle of F_t , 600 rpm, Quarter Immersion and Feedrate 1

Because the forces measured by the Smart Tool are recorded by a separate computer, the previously mentioned “tick signal” is not available. So we don’t really know the edge locating angles at each instant the tangential or radial forces are sampled, which means the exact instantaneous chip thickness corresponding to each force data is unknown. However, by looking at the tangential force profile shown in Figure 5.16, we can choose the data point which has a force value bigger than but closest to zero as the instant when the cutting tool just begins to engage in cutting, as noted by “Cutting Start Point” in Figure 5.16. For up milling, this start point corresponds to the edge locating angle of zero.

During periods when the cutting tooth begins to enter and exit from the cutting region, the cutting tool is not fully engaged so the force data in the very beginning or the very end of the tooth engagement is not used. This is represented by the circles in Figure 5.16. Typically, we use the force data when the cutting tooth is fully engaged in the

desired axial depth of cut to do the calibration. As mentioned in the Kistler force profile based method, we use the range of [10 50], [10 80] and [10 110] degrees of the reference locating angle to do the calibration for quarter, half and three quarter immersion cutting tests respectively.

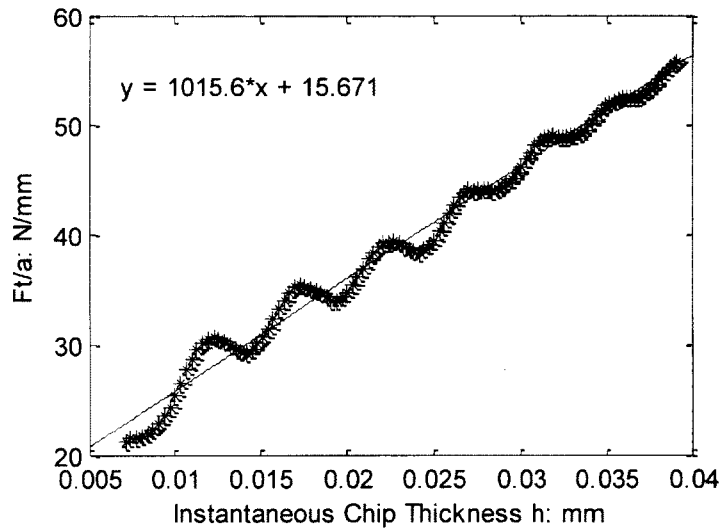


Figure 5.17 - F_t/a vs Instantaneous Chip Thickness, 600 rpm, Quarter Immersion and Feedrate 1

Figure 5.17 shows F_t/a vs instantaneous chip thickness for the cutting test of 600 rpm, quarter immersion and feedrate 1 with the tangential coefficients calibration result: $K_{tc} = 1012.4 \text{ N/mm}^2$ and $K_{te} = 16.0 \text{ N/mm}$. As can be seen, the experiment data of F_t/a vs instantaneous chip thickness is not a perfect line and there exists waviness especially when the chip thickness is small. Tool vibration occurs in the 600 rpm cutting test and this affects the instantaneous chip thickness, resulting in waviness. Because the tool vibration is small, it has less effect with increasing chip thickness. That's why the waviness fades away with increasing chip thickness.

Similarly, we can get radial coefficients from radial force data using exactly the same method. For example, we get the following radial coefficients for the cutting test of 600 rpm, quarter immersion and feedrate 1: $K_{rc} = 293.9437 \text{ N/mm}^2$ and $K_{re} = 11.3970 \text{ N/mm}$.

5.4.2 Average Force Method

We can formulate average tangential and radial forces by substituting Equations 5.13 and 5.14 into the following integrations.

$$\bar{F}_t = \frac{N}{2\pi} \int_{\phi_{st}}^{\phi_{ex}} F_t d\phi \quad (5.16)$$

$$\bar{F}_r = \frac{N}{2\pi} \int_{\phi_{st}}^{\phi_{ex}} F_r d\phi \quad (5.17)$$

where N notifies the number of cutting tooth.

The average tangential and radial forces for up milling can then be expressed as:

$$\bar{F}_t = -\frac{Nac}{2\pi} K_{tc} (\cos 2\phi_{ex} - \cos 2\phi_{st}) + \frac{Na}{2\pi} K_{te} (\phi_{ex} - \phi_{st}) \quad (5.18)$$

$$\bar{F}_r = -\frac{Nac}{2\pi} K_{rc} (\cos 2\phi_{ex} - \cos 2\phi_{st}) + \frac{Na}{2\pi} K_{re} (\phi_{ex} - \phi_{st}) \quad (5.19)$$

Similar to the Kistler average force based calibration method, the above equations can be combined into matrix form and a least squares regression can be applied to them to obtain the tangential and radial coefficients respectively.

5.5 Summary

Five different calibration methods are described in detail in this chapter. A least squares regression is applied to all the methods to calibrate the cutting coefficients. The spindle motor power based method can only provide tangential coefficients, so an assumed ratio of radial to tangential coefficients could be utilized to find the radial coefficients. As for the other four calibration methods, all the four cutting coefficients can be obtained.

CHAPTER 6

CALIBRATION AND SIMULATION RESULTS AND COMPARISON OF METHODS

6.1 Introduction

Cutting coefficients calibration results of the five different methods are shown and compared in this chapter. Then the simulated resultant cutting force using the calibrated coefficients from each method is compared to the forces as measured by the Kistler dynamometer. The Kistler is widely used in research due to its well known accuracy. Discussion and comparison of the five different calibration methods in terms of cost, efficiency, compliance, accuracy, repeatability and applicability is also presented in this chapter.

We show all the calibration and simulation results in bar plots in this chapter. The results can also be found in tabular form in Appendix C and D. As mentioned previously in Chapter 4, since the Smart Tool is only capable of measuring either tangential force or radial force at a given time, the experiments had to be performed twice in order to collect both radial and tangential components for calibration. In the rest of this thesis, (T) denotes the experiment that was conducted with the Smart Tool measuring tangential force while (R) denotes the experiment that was conducted with the Smart Tool measuring radial force.

6.2 Calibration Results

Figure 6.1 shows the average force and spindle motor power based cutting coefficients for 600 rpm cutting tests. Figures 6.2 and 6.3 show the Kistler force profile based and Smart Tool force profile based cutting coefficients for 600 rpm cutting tests respectively. Figure 6.4 shows the average force and spindle motor power based cutting coefficients for 3000 rpm cutting tests. Figures 6.5 and 6.6 show the Kistler force profile based and Smart Tool force profile based cutting coefficients for 3000 rpm cutting tests respectively.

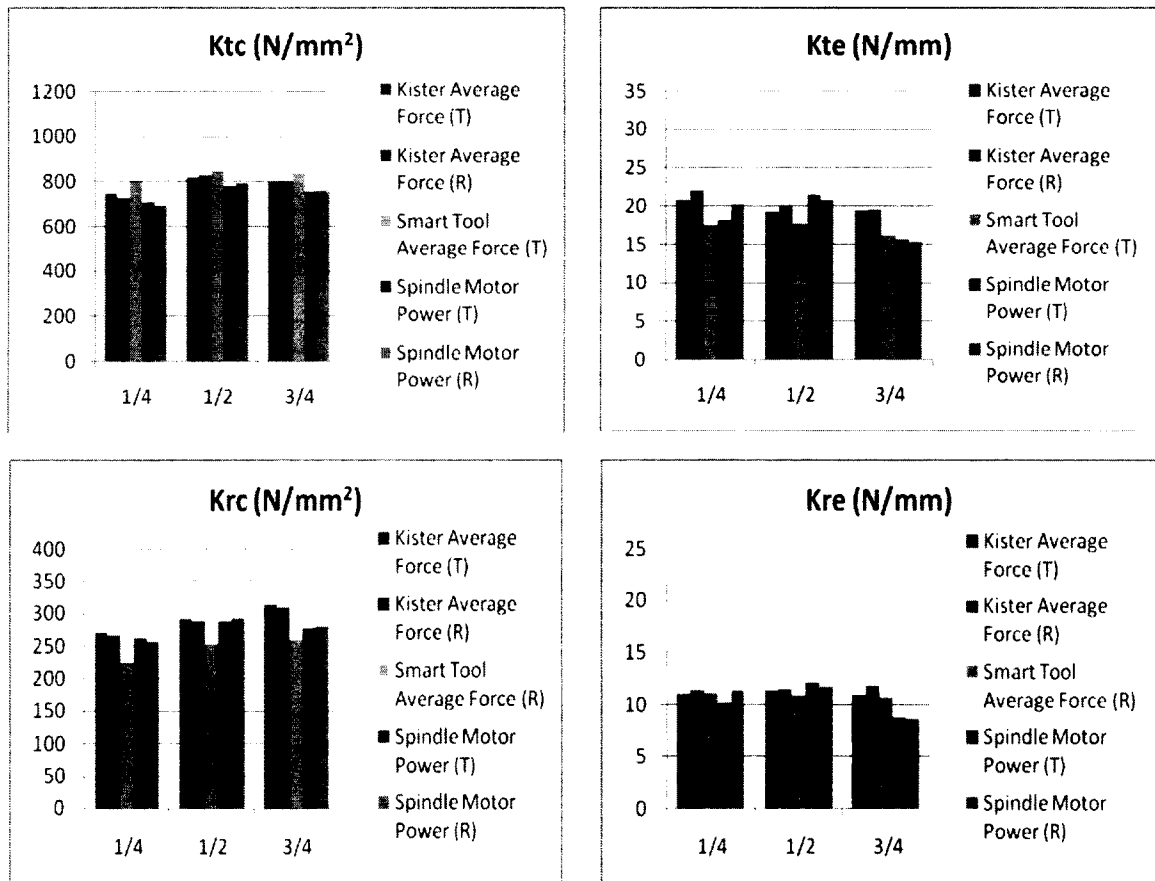


Figure 6.1 - Average Force and Spindle Motor Power Based Calibration Results for 600 rpm Cutting Tests

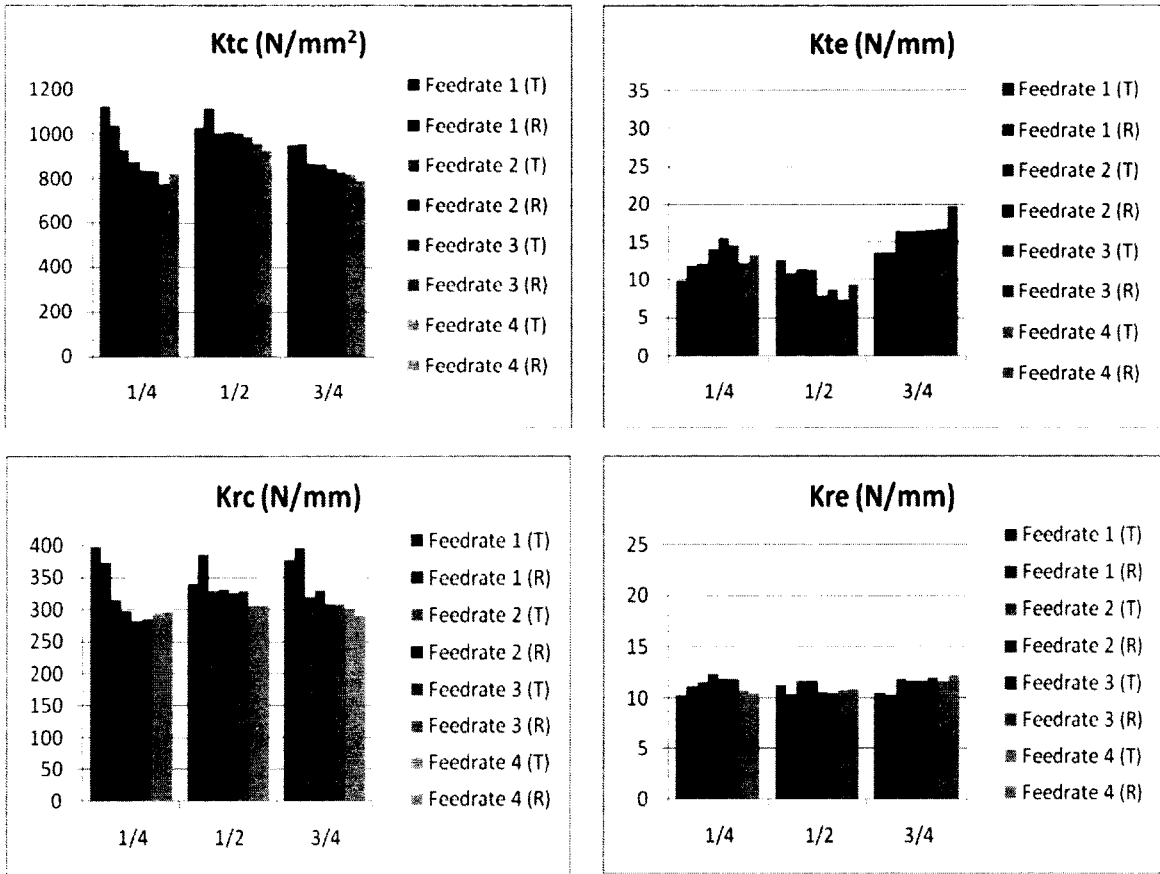


Figure 6.2 - Kistler Force Profile Based Calibration Results for 600 rpm Cutting Tests

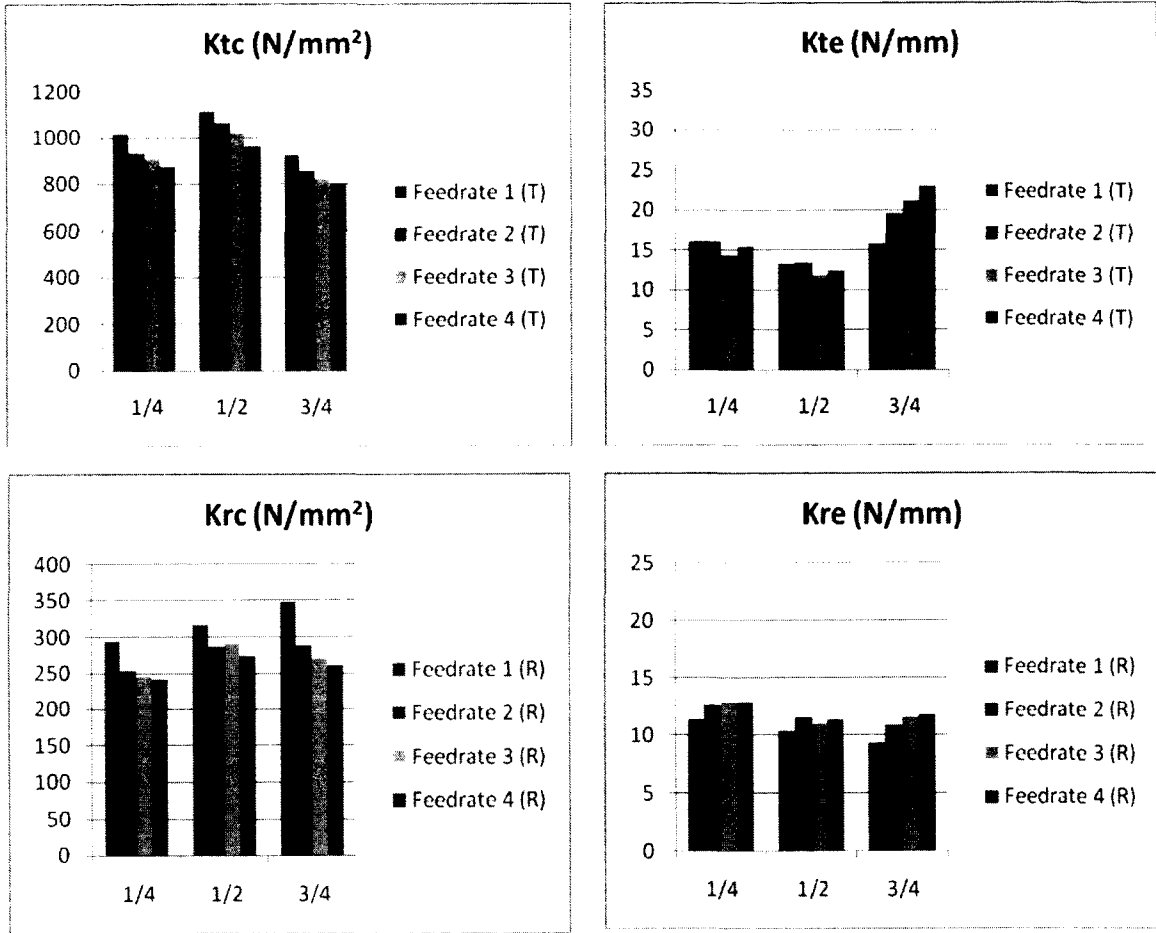


Figure 6.3 – Smart Tool Force Profile Based Calibration Results for 600 rpm Cutting Tests

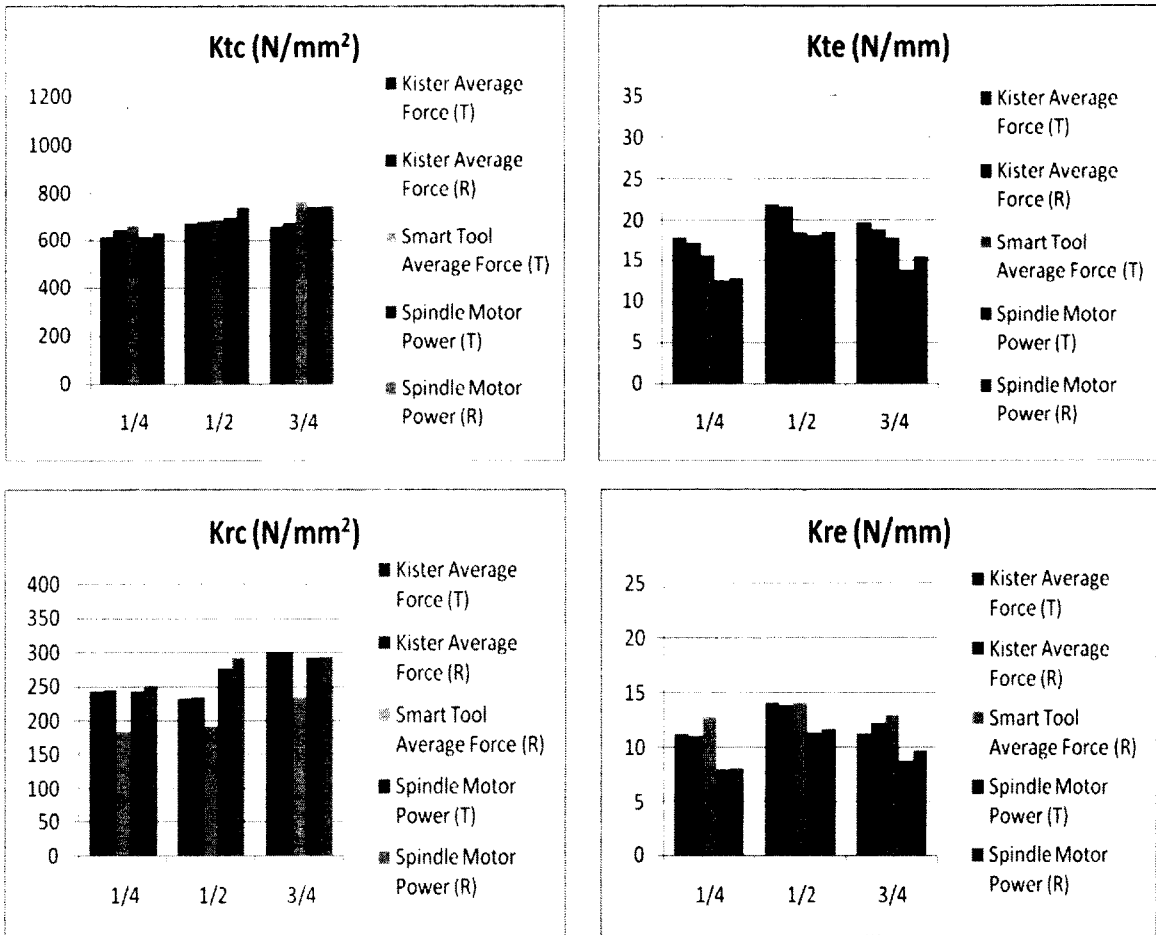


Figure 6.4 - Average Force and Spindle Motor Power Based Calibration Results for 3000 rpm Cutting Tests

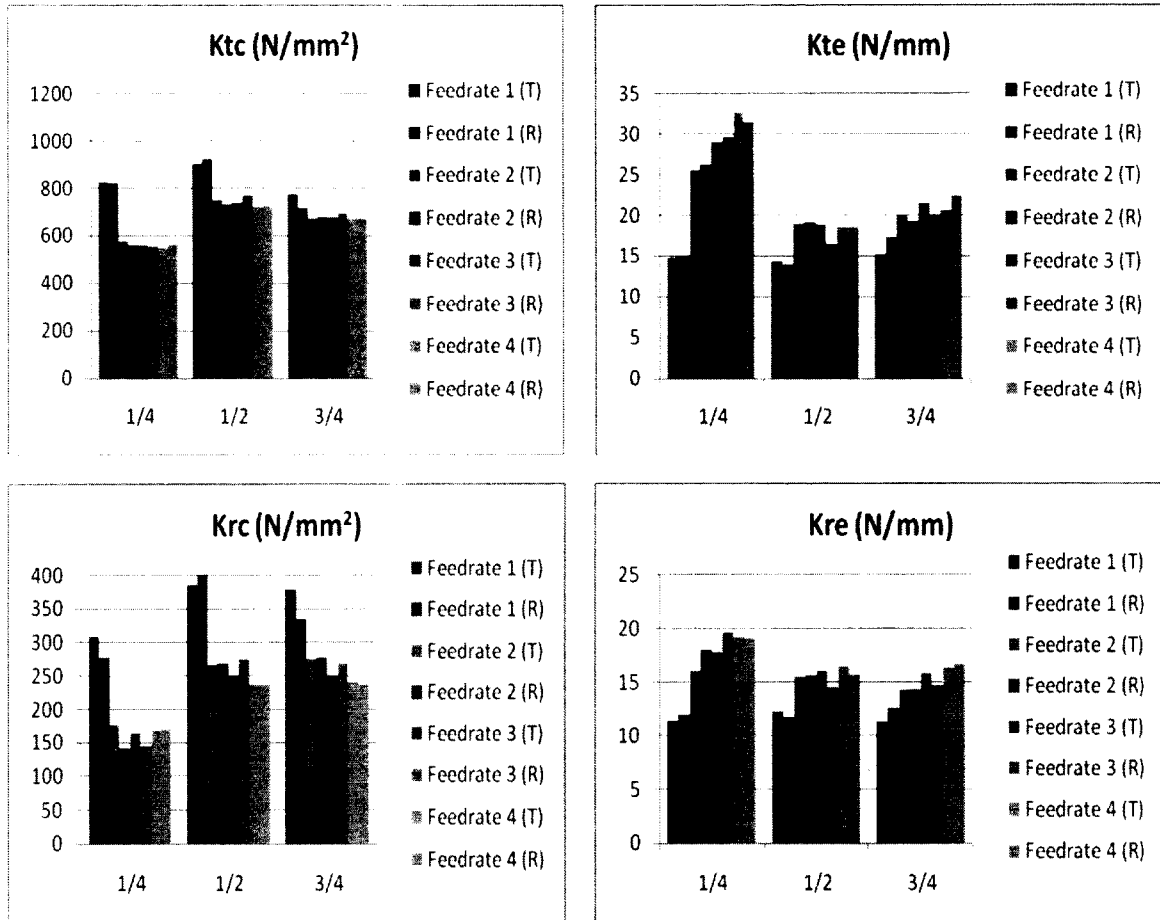


Figure 6.5 - Kistler Force Profile Based Calibration Results for 3000 rpm Cutting Tests

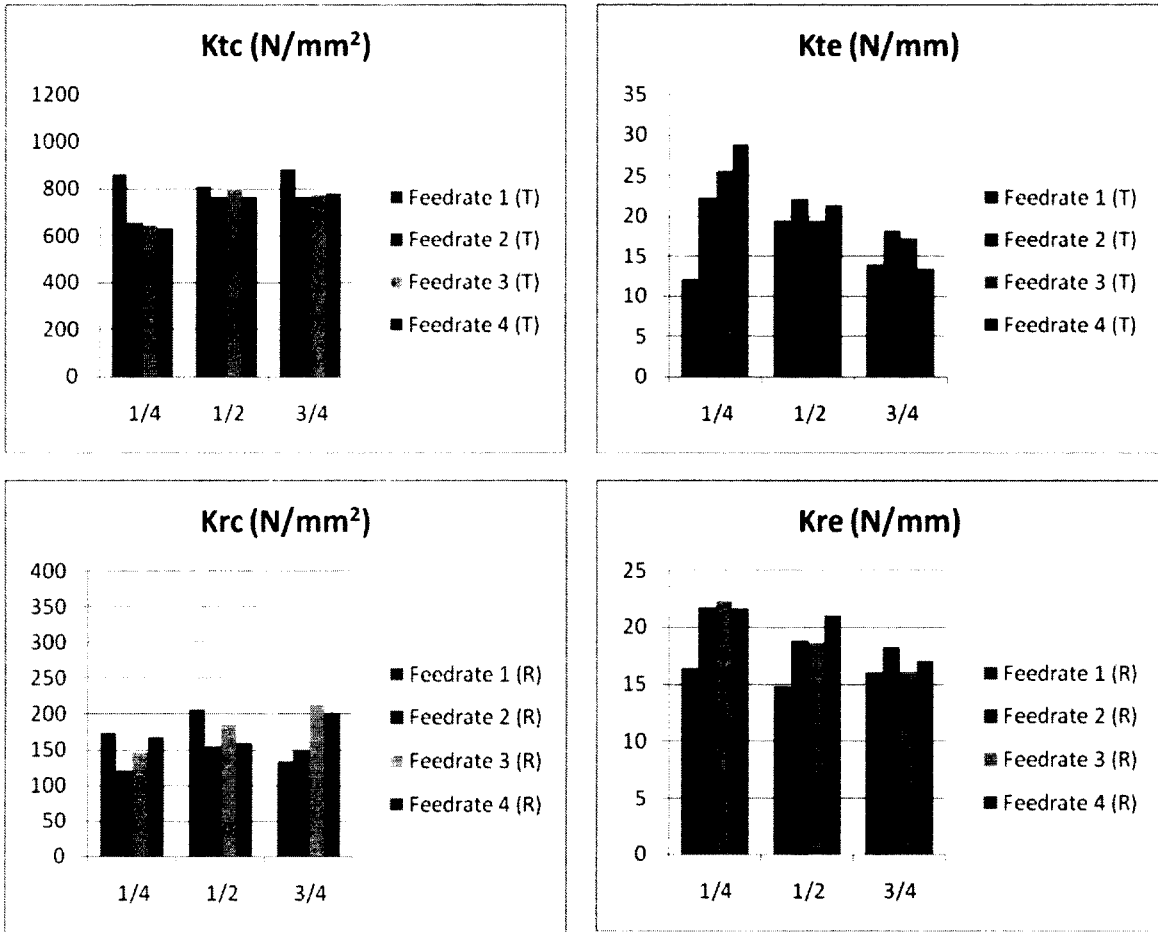


Figure 6.6 - Smart Tool Force Profile Based Calibration Results for 3000 rpm Cutting Tests

As mentioned in Chapter 5, in order to use the spindle motor power based calibration method, the ratios of radial to tangential cutting coefficients are necessary. We applied the following ratios found from the six sets of the four cutting coefficients calibrated from the Kistler average force based method to get the radial coefficients for the spindle motor power based method.

Table 6.1 - Mean of K_{rc}/K_{tc} and K_{re}/K_{te}

	Mean K_{rc}/K_{tc}	Mean K_{re}/K_{te}
600 rpm	0.3686	0.5623
3000 rpm	0.3959	0.6301

It would be better to get the ratios for each tool-workpiece pair without considering any other cutting conditions such as spindle speed, radial immersion and axial depth of cut. However, note that coolant was used in the 600 rpm cutting tests but not in the 3000 rpm cutting tests, thus it may have an effect on the ratios. Therefore we use the ratios obtained from the 600 rpm and 3000 rpm cutting tests separately.

Also note that the Smart Tool can only measure tangential or radial force at a given time, thus only tangential or radial coefficients can be obtained for both Smart Tool average force based and force profile based methods for a given cutting test.

From all the calibration results shown in Figures 6.1 – 6.6 or Tables C.1 – C.36, we can draw the following conclusions:

- The Kistler average force based calibration method shows consistent results of all the four cutting coefficients for the same cutting geometry, with typical values within 5%, which can be assessed through comparing the cutting coefficients from the Kistler Average Force (T) and (R) from Figures 6.1 and 6.4. We can draw the same conclusion for the Kistler force profile based and spindle motor power based calibration methods. This indicates that these three calibration

methods can provide repeatable and consistent calibration results. We are not as certain about the consistency of results obtained using the Smart Tool average force and force profile based calibration methods due to the limited experiments we have conducted. This should be investigated in the future.

- The Kistler average force based, the Smart Tool average force based and the spindle motor power based methods provide similar results for K_{tc} for the same cutting geometry, with an error within 10%, which can be assessed from Figures 6.1 and 6.4.
- The “see-saw effect”, which means higher (or lower) shearing coefficients (K_{tc} or K_{rc}) are offset by lower (or higher) edge coefficients (K_{te} or K_{re}), has been found consistently among almost all the calibration results. This can be verified by comparing the cutting coefficients obtained from different methods but for the same cutting condition, or from the same force profile based method but for different feedrates. We believe the “see-saw effect” to be an artifact of the regression being applied to the cutting coefficients which are highly cross correlated [6].
- The Kistler force profile based calibration method provides quite different sets of cutting coefficients between feedrate 1 and other feedrates for all the three different radial immersion cutting tests, especially for quarter and half immersion cutting tests, indicating that chip thicknesses of small value used in calibration will have an effect on estimating cutting coefficients. The same conclusion can be

drawn for the Smart Tool force profile based calibration method. It tells us that we need to be careful about choosing which range of chip thickness is used for force profile based calibration. This is a topic for future investigation.

6.3 Simulation Results

Accurate estimation of the peak resultant cutting force is very important in process planning in order to avoid tool breakage and excessive deflection. We evaluate the accuracy by comparing the estimated peak resultant cutting forces to those measured from the Kistler dynamometer. The resultant cutting force is easily calculated from the X and Y components:

$$F_{res} = \sqrt{F_x^2 + F_y^2} \quad (6.1)$$

The cutting coefficients obtained from each method can be used to simulate the resultant cutting force. Considering the effect of helix angle of the cutting tool, we need to divide the in-cut portion of the cutting flute into small slices and add up all the cutting forces contributed from each differential slices using Equations 2.7 – 2.11 described in Chapter 2.

The simulated resultant cutting force is compared to the averaged measured force profile for one tool revolution. Figures 6.7, 6.8 and 6.9 show the comparison between the simulated resultant cutting forces and the measured ones for cases of 600 rpm, quarter immersion and feedrate 1 (T), half immersion and feedrate 2 (T) and three quarter immersion and feedrate 3 (T) respectively. Figures 6.10, 6.11 and 6.12 show the comparison between the simulated and measured resultant cutting forces for cases of

3000 rpm, quarter immersion and feedrate 1 (T), half immersion and feedrate 2 (T) and three quarter immersion and feedrate 3 (T) respectively. In all these figures, Simulated 1, 2, 3, 4 and 5 denote simulation using the corresponding cutting coefficients obtained from the methods based on: 1. Kistler average force, 2. Smart Tool average force, 3. spindle motor power, 4. Kistler force profile and 5. Smart Tool force profile.

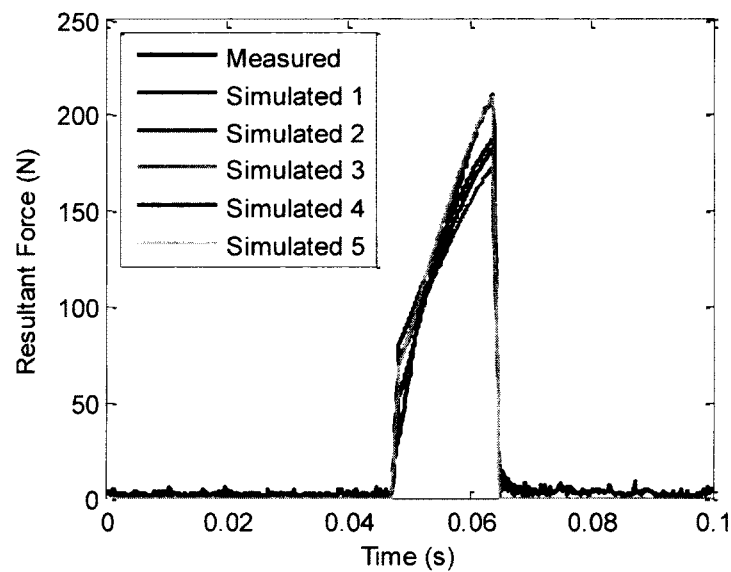


Figure 6.7 - Resultant Force Simulation for 600 rpm, Quarter Immersion and Feedrate 1 (T)

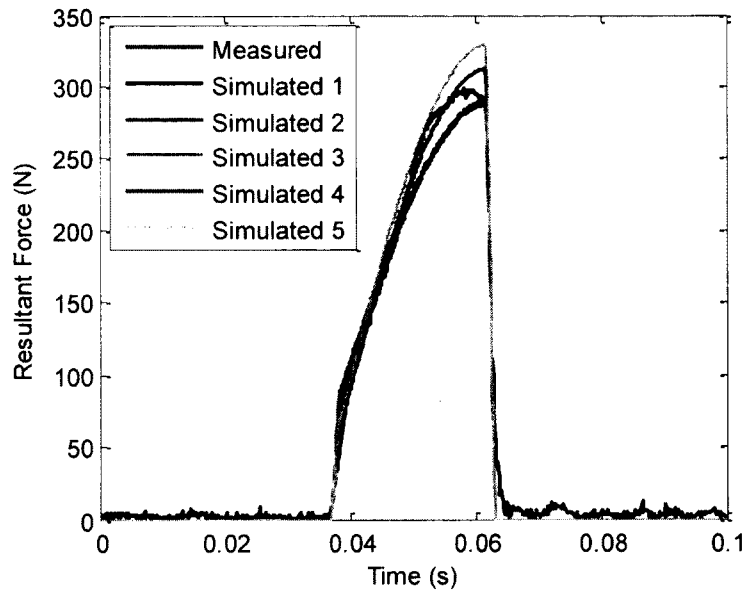


Figure 6.8 - Resultant Force Simulation for 600 rpm, Half Immersion and Feedrate 2 (T)

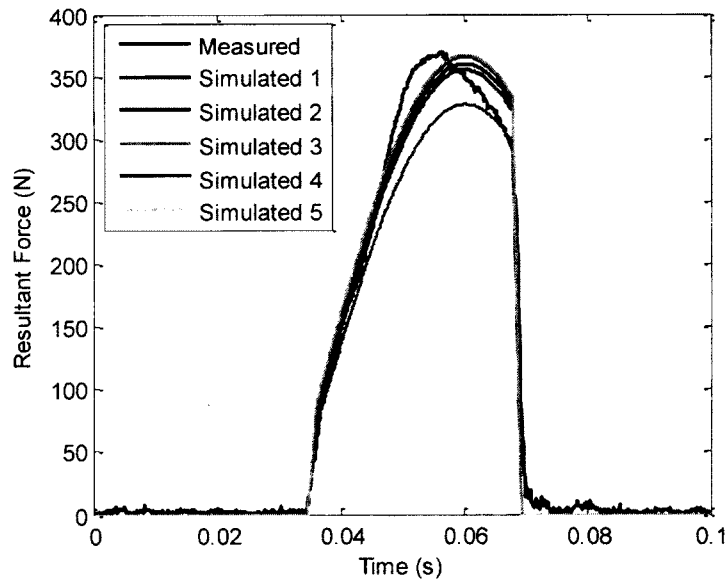


Figure 6.9 - Resultant Force Simulation for 600 rpm, Three Quarter Immersion and Feedrate 3 (T)

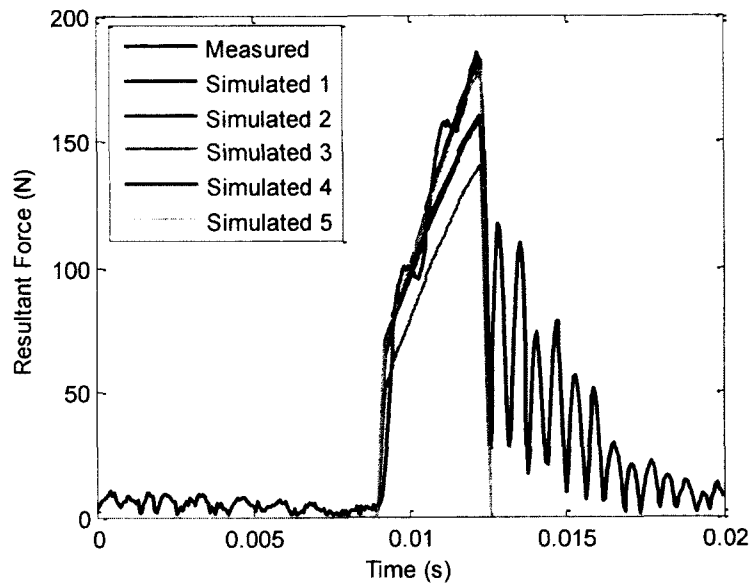


Figure 6.10 - Resultant Force Simulation for 3000 rpm, Quarter Immersion and Feedrate 1 (T)

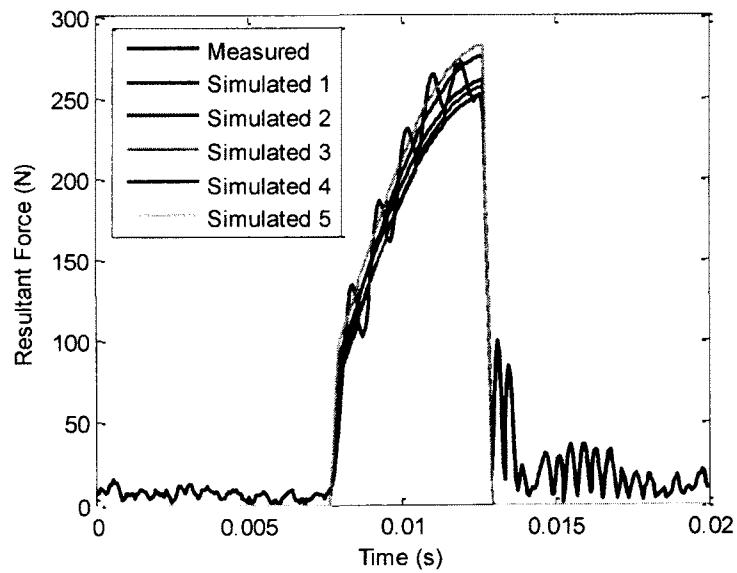


Figure 6.11 - Resultant Force Simulation for 3000 rpm, Half Immersion and Feedrate 2 (T)

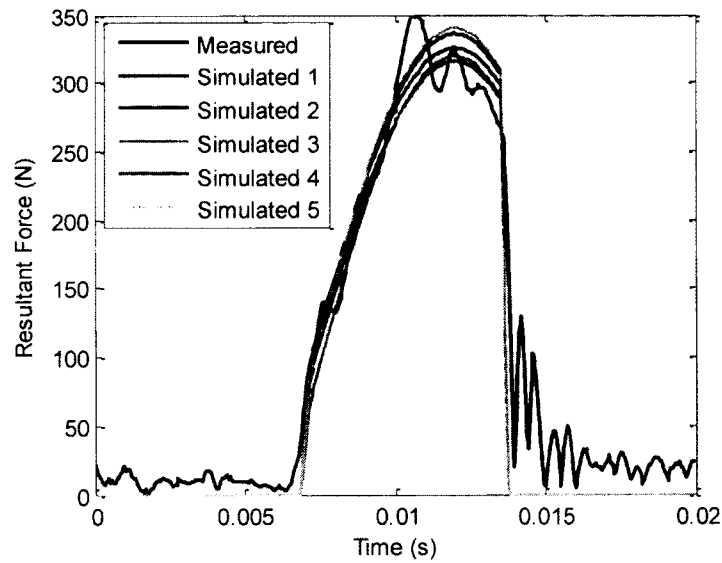


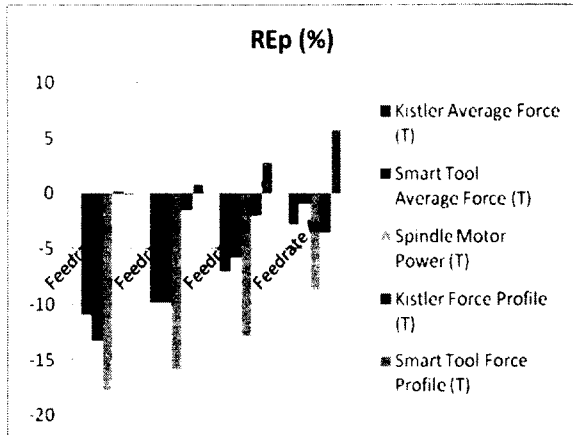
Figure 6.12 - Resultant Force Simulation for 3000 rpm, Three Quarter Immersion and Feedrate 3 (T)

The relative error of the peak force can be expressed as:

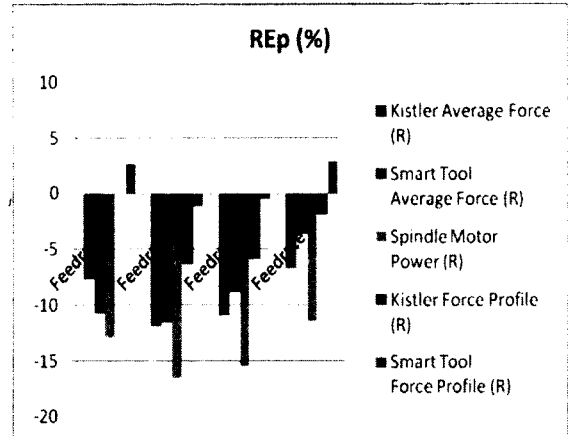
$$RE_p = \frac{F_{ps} - F_{pm}}{F_{pm}} * 100\% \quad (6.2)$$

where RE_p is the relative error between the peak of the simulated resultant force and that of the measured one, F_{ps} is the peak of the simulated resultant force and F_{pm} is the peak of the measured one.

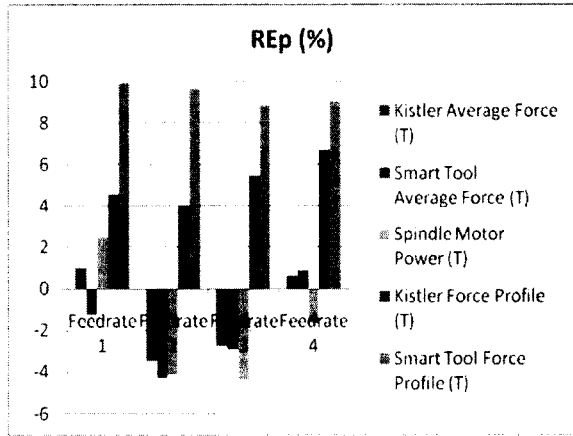
Figures 6.13 and 6.14 show the results of RE_p for all the calibration methods for the cutting tests of 600 and 3000 rpm respectively.



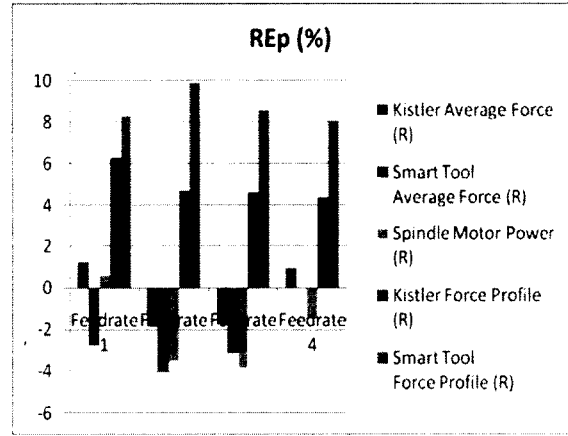
(a) Quarter Immersion (T)



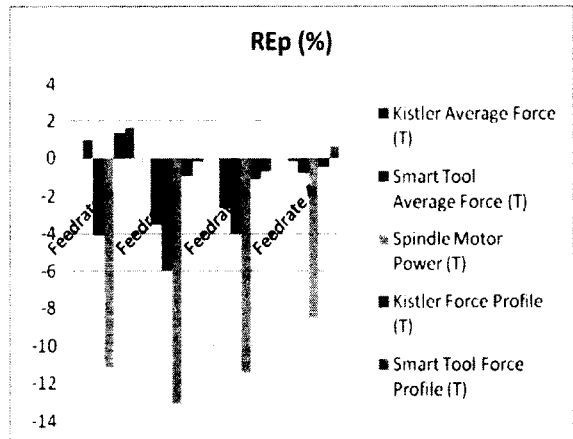
(b) Quarter Immersion (R)



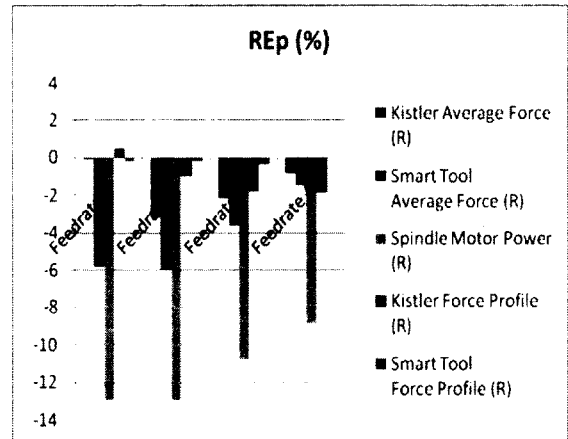
(c) Half Immersion (T)



(d) Half Immersion (R)

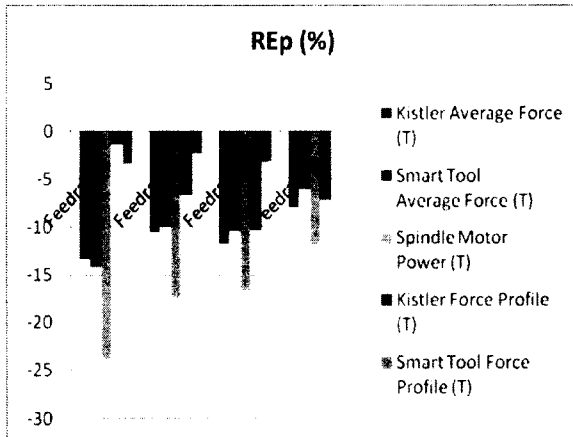


(e) Three Quarter Immersion (T)

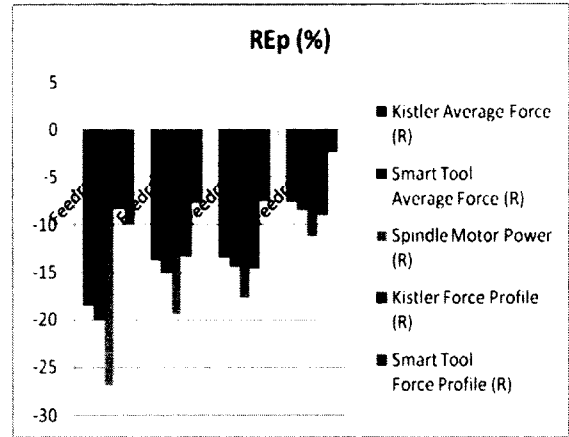


(f) Three Quarter Immersion (R)

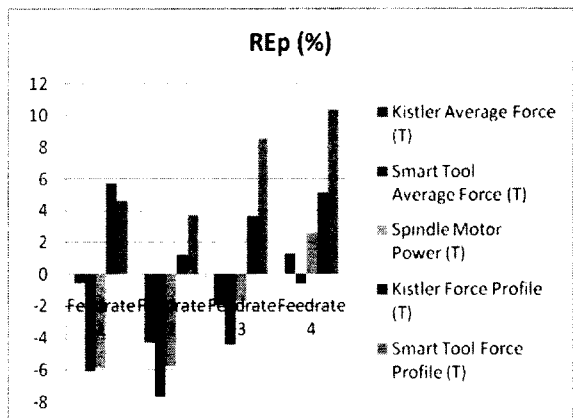
Figure 6.13 – RE_p for 600 rpm Cutting Tests



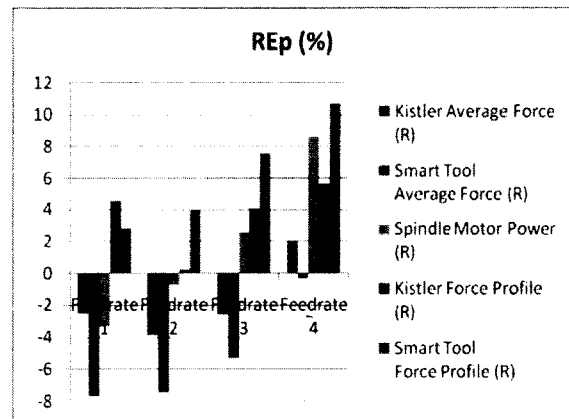
(a) Quarter Immersion (T)



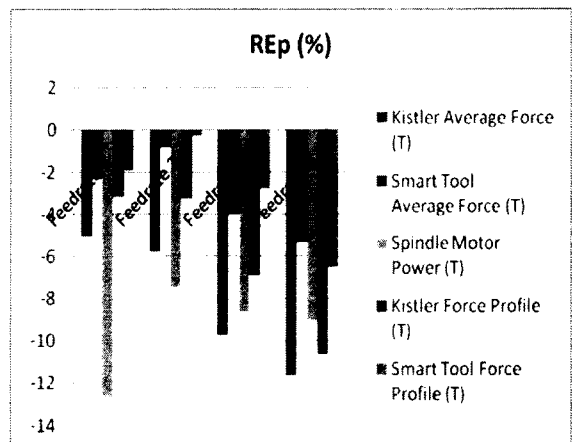
(b) Quarter Immersion (R)



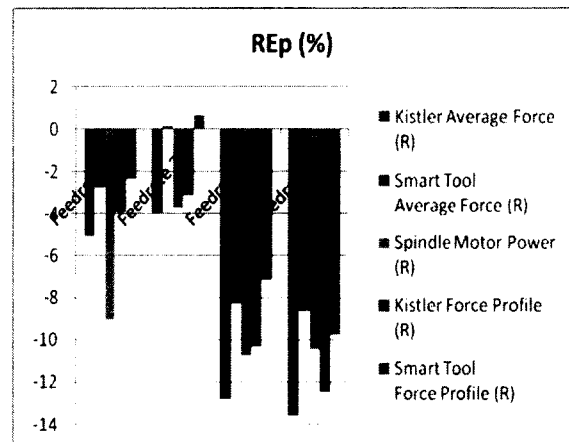
(c) Half Immersion (T)



(d) Half Immersion (R)



(e) Three Quarter Immersion (T)



(f) Three Quarter Immersion (R)

Figure 6.14 – RE_p for 3000 rpm Cutting Tests

As can be seen from Figures 6.13 and 6.14 (or all the simulation results shown in Appendix D), we can draw the following conclusions:

For quarter and three quarter immersion (for both 600 and 3000 rpm) cutting tests, almost all the simulated peak resultant forces of the five methods are less than the measured. For half immersion (for both 600 and 3000 rpm) cutting tests, the simulated peak resultant forces of the Kistler force profile and Smart Tool force profile methods are larger than the measured, while the simulated peak resultant forces of the other three methods are less than the measured.

The absolute value of the relative error between the simulated and measured peak resultant force is usually less than 10% for all the calibration methods except the spindle motor power based method. This is most evident for 600 rpm cutting tests because the low spindle speed causes less tool vibration and the Kistler dynamometer's dynamic effects can be neglected. This accuracy level would be suitable for process planning and monitoring. Since the same conditions are used for calibration and force comparison, we would expect larger errors for cuts with different spindle speeds and cut geometries.

The spindle motor power based method provides a simulation error of over 10% for almost all the quarter and three quarter immersion cutting tests, and even over 25% for some cases. Two possible sources could account for this: 1. the estimated cutting power from the measured spindle motor power used for calibration may not be accurate; 2. the assigned ratios of radial to tangential coefficients may not be accurate. The true reason is still under investigation and would be part of the future work. However, the spindle motor power based calibration method can provide good estimation for peak

resultant forces for half immersion cutting tests, with a typical error within 5% of the measured ones.

The force profile (both Kistler and Smart Tool) based calibration methods can provide better estimation of the peak resultant force than the average force (both Kistler and Smart Tool) based calibration methods for quarter immersion cutting tests while the latter ones can provide better estimation of the peak resultant force for half immersion cutting tests. They provide comparable simulation results for three quarter immersion cutting tests.

6.4 Comparison of Methods

The five different calibration methods are compared to each other in terms of the following aspects: cost, efficiency, compliance, accuracy, repeatability and applicability.

a. Cost

Table 6.2 - Cost of Different Sensors

Kistler Dynamometer	Smart Tool	LCI Power Sensor
\$35,000	\$2000 - 7000	\$650

As can be seen in Table 6.2, the LCI power sensor costs the least while the Kistler dynamometer is the most expensive. However, both the Kistler dynamometer and the LCI power sensor are commercially available products while the Smart Tool is custom-designed and not commercially available. The estimated cost of the Smart Tool includes

the strain gages, data transmission board, battery, charging circuits and other electronics, the shrouding as well as the fabricating and calibrating cost.

b. Efficiency

The Kistler and Smart Tool average force calibration methods and the spindle motor power calibration method are more efficient than the Kistler and Smart Tool force profile calibration methods if implemented on-line because the former three calibration methods don't need to find the correct edge locating angle of the cutting tool and their associated geometric matrices are much simpler and easier to handle.

c. Compliance

Although the Kistler dynamometer is really stiff, it is invasive to the CNC machine. It has a natural frequency around 1000 Hz with a workpiece attached to its top, which could affect the measurement. The LCI power sensor is non-invasive. The Smart Tool is significantly less stiff than the Kistler dynamometer, however, it does not add any additional compliance to the spindle system. The compliance does compromise its ability to obtain accurate measurement, particularly since its natural frequency is around 650 Hz which is less than the Kistler dynamometer.

d. Accuracy

The accuracy of the five different calibration methods can be assessed from the relative error of the simulation results shown in Figures 6.13 and 6.14 or in Appendix D. As can be seen, the relative error between the simulated and measured peak resultant

force is usually less than 10% for all the calibration methods except the spindle motor power based method. This is most evident for 600 rpm cutting tests because the low spindle speed causes less tool vibration and the Kistler dynamometer's dynamic effects are negligible.

The spindle motor power based method provides a simulation error of over 10% for almost all the quarter and three quarter immersion cutting tests, and even over 25% for some cases. Two possible sources could account for this: 1. the estimated cutting power from the measured spindle motor power used for calibration may not be accurate; 2. the assigned ratios of radial to tangential coefficients may not be accurate. The true reason is still under investigation and would be part of the future work. However, the spindle motor power based method can provide good estimation for peak resultant forces for half immersion cutting tests, with a typical error within 5%.

For the 3000 rpm cutting tests, although there are noticeable and significant tool vibrations and dynamic effects of the force dynamometers, all the five calibration methods can still provide good estimation of the peak resultant forces, especially for half immersion cutting tests, with a typical error within 10%.

The force profile (both Kistler and Smart Tool) based calibration methods can provide better estimation of the peak resultant force than the average force (both Kistler and Smart Tool) based calibration methods for quarter immersion cutting tests while the latter ones can provide better estimation of the peak resultant force for half immersion

cutting tests. They provide comparable simulation results for three quarter immersion cutting tests.

e. Repeatability

Repeatability means how repeatable the calibration results of a method are for the same cutting geometry. Repeatability is an important factor because a calibration method should provide the same calibration results for the same tool - workpiece pair and the same cutting geometry if tool wear is negligible. Otherwise the calibration method has little practicality. As addressed previously in Calibration Results, the Kistler average force based calibration method shows close calibration results for all four cutting coefficients for the same cutting geometry, with a typical error within 5%. We can draw the same conclusion for the Kistler force profile based and spindle motor power based calibration methods. This indicates that these three calibration methods can provide repeatable and consistent calibration results. We are not sure how repeatable the calibration results of the Smart Tool average force and force profile based calibration methods are for the same cutting condition because of the limited experiments we have conducted. This should be investigated further in future.

f. Applicability

As discussed before, due to the high cost, workpiece mounting limitations and the intrusive nature, the Kistler dynamometer is not a good choice for the shop floor environment, while the power sensor can be easily implemented and used in shop floor due to its relatively low cost and non-intrusive property. However, only tangential cutting

coefficients can be obtained from the spindle motor power based method. As for the Smart Tool, although it is inexpensive, it is custom-designed and accurate calibration is needed before its application. In addition, the Smart Tool is currently limited to one cutting tooth. More importantly, a Smart Tool is needed for each cutting tool holder whereas a Kistler dynamometer and a LCI power sensor are only one per machine.

The Kistler and Smart Tool average force methods and the spindle motor power method need at least two different cutting conditions to generate two different average chip thicknesses to realize the calibration. Thus, one cannot get the cutting coefficients from any cutting test having the same cutting condition using these three calibration methods. The Kistler and Smart Tool force profile methods can be used to calibrate cutting coefficients from any single cutting test. However, one needs to determine the correct edge locating angle of the cutting tool at each instant forces are measured for calibration, as described in Chapter 5.

6.5 Summary

Cutting coefficients calibration results of the five different methods are shown and compared in this chapter. The simulated resultant cutting force using the calibrated coefficients from each method is compared to the Kistler dynamometer measured force, due to its accurate force measurements. Discussion and comparison of the five different calibration methods in terms of cost, efficiency, compliance, accuracy, repeatability and applicability is finally presented in this chapter. As we may conclude, each calibration method has its own advantages and limitations for on-line calibration of force models.

CHAPTER 7

CONCLUSIONS AND FUTURE WORK

7.1 Introduction

This chapter summarizes the thesis work and outlines the conclusions. Suggestions for future studies are also included.

7.2 Conclusions

Five different calibration methods are introduced and compared in terms of cost, efficiency, compliance, accuracy, repeatability and applicability. They are based on spindle motor power, Kistler average force and force profile, and Smart Tool average force and force profile.

A comparison of the convenience and accuracy of the various methods leads to the following conclusions:

1. Methods based on the Kistler average force and Smart Tool average force are easy to implement on-line and can lead to reasonably good simulation results, especially for half immersion cutting tests. On average, the simulated peak resultant force is within 10% of the experimental data used for calibration.

However, there is a major limitation with these two calibration processes. Since average force is used to calibrate the cutting coefficients, there need to be at least two different cutting conditions to generate two different average chip thicknesses

in order to realize the calibration. Preferably, there should be at least four variations in the average chip thicknesses.

2. The Kistler and Smart Tool force profile calibration methods can provide consistent and reasonable calibration results and good simulation results. Typically, the simulated peak resultant force is within 10% of the experimental data used for calibration. However, they are hard to implement on-line because it is difficult to determine the correct edge locating angle of the cutting tool at each instant forces are measured. As mentioned before, we use the “tick signal” generated by a Hall effect sensor to determine the edge locating angle of the tool for the Kistler force profile calibration method. As for the Smart Tool, since the “tick signal” is not available, we can just estimate the edge locating angles from the force profiles, as shown in Chapter 5. Apparently, there would be cutting coefficients estimation errors associated with this process. However, these two calibration methods can be used to calibrate cutting coefficients for any cutting geometry as long as we can get a clean force profile and accurate estimation of the edge locating angles of the tool at each instant forces are measured.
3. Different sets of cutting coefficients could lead to similar estimation of the peak resultant force. The “see-saw effect”, which means higher (or lower) shearing coefficients (K_{tc} or K_{rc}) are offset by lower (or higher) edge coefficients (K_{te} or K_{re}), has been found consistently among almost all the calibration results. This can be verified by comparing the cutting coefficients obtained from different

methods but for the same cutting condition, or from the same force profile based method but for different feedrates. We believe the “see-saw effect” to be an artifact of the regression being applied to the cutting coefficients which are highly cross correlated [6].

4. The relative error between the simulated and measured peak resultant force is mostly less than 10% for all the calibration methods except the spindle motor power based method. This is most evident for 600 rpm cutting tests because the low spindle speed causes less tool vibration and the Kistler dynamometer’s dynamic effects can be neglected. This accuracy level would be suitable for process planning and monitoring. Since the same conditions are used for calibration and force comparison, we would expect larger errors for cuts with different spindle speeds and cut geometries.
5. The spindle motor power based method provides a simulation error of over 10% for almost all the quarter and three quarter immersion cutting tests, and even over 25% for some cases. Two possible sources could account for this: 1. the estimated cutting power from the measured spindle motor power used for calibration may not be accurate; 2. the assigned ratios of radial to tangential coefficients may not be accurate. The true reason is still under investigation and is part of the future work. However, the spindle motor power based calibration method can provide good estimation for peak resultant forces for half immersion cutting tests, with a typical error within 5% of the measured ones.

6. The force profile (both Kistler and Smart Tool) based calibration methods can provide better estimation of the peak resultant force than the average force (both Kistler and Smart Tool) based calibration methods for quarter immersion cutting tests while the latter ones can provide better estimation of the peak resultant force for half immersion cutting tests. As for three quarter immersion cutting tests, they provide comparable simulation results.
7. Each calibration method has its own advantages and limitations for on-line calibration of force models. No one method is superior.

7.3 Future Work

We have designed and conducted limited cutting tests in this research and compared the five calibration methods in terms of cost, efficiency, compliance, accuracy, repeatability and applicability. Based on what we have done so far, the future work may include:

1. More cutting tests with other cutting geometries and workpiece material such as plain steel, stainless steel and titanium, should be designed and conducted to support and verify the conclusions drawn in this research.
2. Extension to multi-tooth cutters is also essential if the force profile (both Kistler and Smart Tool) based methods are to be practical for on-line tool condition monitoring.

3. All five calibration methods presented in this research are time domain methods. While the spindle motor power based and the average force (both Kistler and Smart Tool) based calibration methods are easy to implement on-line, the force profile based calibration methods are hard to implement on-line because it is difficult to determine the correct edge locating angle of the tool during cutting. Therefore, a novel calibration method in frequency domain or a statistical force model should be investigated and developed.

REFERENCES

- [1] Xu, M., Schuyler, C. K., Fussell, B. K., and Jerard, R. B., 2006, "*Experimental Evaluation of a Smart Machining System for Feedrate Selection and Tool Condition Monitoring*", Transactions of the North American Manufacturing Research Institution/SME (NAMRC), Vol. 34, Marquette University, May 23-26.
- [2] Cui, Y., Jerard, R. B., Fussell, B. K., and Esterling, D. M., 2009, "*Tool Wear Monitoring for Milling by Tracking Cutting Force Model Coefficients*", Transactions of NAMRI/SME, Vol. 37, pp. 613-620.
- [3] Budak, E., Altintas, Y., Armarego, E., 1996, "*Prediction of Milling Force Coefficients from Orthogonal Cutting Data*", Journal of Manufacturing Science and Engineering, Transactions of the ASME, 118(2), pp. 216-224.
- [4] Lee, P., Altintas, Y., 1996, "*Prediction of Ball-end Milling Forces from Orthogonal Cutting Data*", International Journal of Machine Tools & Manufacture, 36(9), pp. 1059-1072.
- [5] Xu, M., Jerard, R. B., and Fussell, B. K., 2007, "*Energy Based Cutting Force Model Calibration for Milling*", Computer-Aided Design and Applications, 4(1-6), pp. 341-351.
- [6] Eren, F., Jerard, R. B., and Fussell, B. K., 2011, "*Force Model Uncertainty and Its Effect on Process Planning*", Proceedings of NAMRI/SME, Vol. 39.
- [7] Wan, M., Zhang, W. H., Tan, G., and Qin, G. H., 2007, "*An In-depth Analysis of the Synchronization Between the Measured and Predicted Cutting Forces for Developing Instantaneous Milling Force Model*", International Journal of Machine Tools & Manufacture, 47, pp. 2018-2030.
- [8] Yucesan, G., Altintas, Y., 1994, "*Improved Modeling of Cutting Force Coefficients in Peripheral Milling*", International Journal of Machine Tools and Manufacture, 34, pp. 473-487.
- [9] Bayoumi, A. E., Yucesan, G., Kendall, L. A., 1994, "*An Analytic Mechanistic Cutting Force Model for Milling Operations: A Theory and Methodology*", Transactions of ASME, Journal of Engineering and Industry, 116, pp. 324-330.
- [10] Zhang, Z., Zheng, L., 2005, "*A Study on Calibration of Coefficients in End Milling Forces Model*", International Journal of Advanced Manufacturing Technology, 25(7-8), pp. 652-662.

- [11] Altintas, Y., 2000, "*Manufacturing Automation: metal cutting mechanics, machine tool vibrations, and CNC design*", Cambridge University Press, ISBN 0-521-65973-6.
- [12] Yalcin, C., Fussell, B. K. and Jerard, R. B., 2007, "*Comparison of Tangential Force Models for Feedrate Selection in Milling*", Proceedings of the International Manufacturing Science and Engineering Conference, MSEC 2007, October 15-17, Atlanta, Georgia, USA.
- [13] Cui, Y., 2008, "*Tool Wear Monitoring for Milling by Tracking Cutting Force Model Coefficients*", Master's Thesis, University of New Hampshire.
- [14] Load Controls Incorporated, <http://www.loadcontrols.com/>, accessed June 10, 2011.
- [15] Xu, M., 2008, "*Smart Machining System Platform for CNC Milling with the Integration of A Power Sensor and Cutting Model*", PhD Dissertation, University of New Hampshire.
- [16] Kistler dynamometer, <http://www.kistler.com/>, accessed June 20, 2011.
- [17] Harmon, A., Fussell, B. K. and Jerard, R. B., 2012, "*Calibration and Characterization of A Low-cost Wireless Sensor for Applications in CNC End Milling*", Proceedings of the International Manufacturing Science and Engineering Conference, MSEC 2012, June 4-8, Notre Dame, Indiana, USA.
- [18] Eren, F., 2011, "*The Effect of Cutting Force Model Coefficient Variability on Process Planning in Milling*", Master's Thesis, University of New Hampshire.

APPENDIX A

EXPERIMENT PROCEDURES FOR SPINDLE MOTOR POWER SENSOR

SYSTEM CALIBRATION

- a. Before turning on the CNC machine, connect the Keithley digital multimeter to the power sensor.
- b. Turn on the CNC machine, sync it and run the spindle at 1500 rpm for 15 minutes to warm up the spindle motor.
- c. Stop the spindle and put the magnetic brake and torque sensor system on the table of the CNC machine and use two bolts and tie down clamps to fix the system on the table.
- d. Use an edge finder to find the exact center of the upper shaft of the torque sensor (if there is a coupling there, please take it off first).
- e. Mount the coupling to the upper shaft of the torque sensor, tighten down the clamping screw and install the collet with the rod to the spindle.
- f. Use the hand wheel to make the rod fall into the hub bore of the coupling gradually. In the meantime, rotate the coupling to see whether the spindle aligns with the torque sensor well. If not, adjust the position of the table of the CNC machine to make sure they are well aligned.

- g. Tighten the upper clamping screw of the coupling to make sure the coupling and the rod are strongly attached.
- h. Connect the compressed air to the magnetic brake to avoid overheating (all the operators must wear ear plugs for protection).
- i. Hook the magnetic brake to the BK power supply with the brown electrical cable (the brake is polarity-independent).
- j. Hook the power supply, the torque sensor and Keithley digital multimeter as below:

Purple to V+, Yellow to V- on 12 v power supply. White wires are 110v into power supply. Brown to High and White to Low on 1000 v side of Keithley.
- k. Turn on both Keithley and adjust their resolution to Slow 6 ½ mode (this will set the display rate on Keithley to a slow 6.5 digits readout so we can manually capture the output).
- l. Run the spindle at the desired speed.
- m. Turn on BK power supply, set the voltage output to 24 volts with current at zero.
- n. Record the readings from the power sensor and the torque sensor simultaneously for 6 times.
- o. Increase the current output from BK power supply gradually to 1 amp for low range speed and 0.6 amp for high range speed in the way mentioned in the Experiment

Setup and record the readings from the two sensors simultaneously for each current output.

- p. Reset the current output from BK to zero and record the readings.
- q. Change the spindle speed to the next one and repeat the procedures from n to p until all the spindle speeds are tested.

APPENDIX B

SPINDLE MOTOR POWER SENSOR SYSTEM CALIBRATION RESULTS

Table B.1 - Spindle Motor Power Sensor System Calibration Results

Spindle Speed (rpm)	Current Output from BK (amp)	Voltage Output From Torque Sensor (V)	Torque Measured (N*m)	Output Mechanical Power (watt)	Voltage Output from LCI Power Sensor (V)
200	0.2	0.024	0.098	2.048	0.720
200	0.4	0.080	0.320	6.702	0.750
200	0.6	0.172	0.686	14.368	0.808
200	0.8	0.298	1.191	24.937	0.878
200	1	0.427	1.707	35.758	0.953
250	0.2	0.024	0.097	2.548	0.779
250	0.4	0.082	0.326	8.535	0.819
250	0.6	0.178	0.710	18.588	0.885
250	0.8	0.305	1.218	31.887	0.976
250	1	0.434	1.737	45.483	1.076
300	0.2	0.025	0.098	3.079	0.841
300	0.4	0.084	0.337	10.577	0.890
300	0.6	0.182	0.727	22.829	0.977
300	0.8	0.311	1.242	39.019	1.092
300	1	0.443	1.773	55.711	1.208
350	0.2	0.025	0.099	3.616	0.904
350	0.4	0.084	0.337	12.364	0.963
350	0.6	0.183	0.733	26.854	1.062
350	0.8	0.316	1.263	46.304	1.196
350	1	0.452	1.808	66.267	1.335
400	0.2	0.022	0.087	3.658	0.975
400	0.4	0.081	0.323	13.544	1.041
400	0.6	0.183	0.731	30.606	1.156
400	0.8	0.321	1.283	53.728	1.316
400	1	0.463	1.852	77.576	1.479
450	0.2	0.023	0.091	4.273	1.039
450	0.4	0.084	0.335	15.802	1.114
450	0.6	0.187	0.749	35.280	1.243
450	0.8	0.327	1.306	61.544	1.420

450	1	0.470	1.881	88.656	1.603
500	0.2	0.024	0.096	5.027	1.099
500	0.4	0.086	0.344	18.012	1.184
500	0.6	0.192	0.767	40.143	1.331
500	0.8	0.333	1.332	69.743	1.530
500	1	0.481	1.924	100.740	1.738
550	0.2	0.024	0.097	5.606	1.163
550	0.4	0.087	0.347	20.005	1.259
550	0.6	0.195	0.781	44.963	1.429
550	0.8	0.341	1.363	78.484	1.656
550	1	0.491	1.962	113.003	1.895
600	0.2	0.025	0.099	6.199	1.230
600	0.4	0.089	0.355	22.284	1.337
600	0.6	0.198	0.791	49.679	1.521
600	0.8	0.346	1.383	86.917	1.771
600	1	0.501	2.005	125.957	2.046
650	0.2	0.026	0.103	6.988	1.280
650	0.4	0.091	0.365	24.822	1.397
650	0.6	0.202	0.809	55.044	1.591
650	0.8	0.355	1.420	96.656	1.879
650	1	0.515	2.061	140.311	2.166
700	0.2	0.027	0.106	7.770	1.343
700	0.4	0.092	0.369	27.074	1.470
700	0.6	0.206	0.825	60.500	1.692
700	0.8	0.361	1.445	105.948	1.996
700	1	0.522	2.089	153.156	2.320
750	0.2	0.027	0.107	8.378	1.396
750	0.4	0.095	0.379	29.740	1.534
750	0.6	0.211	0.842	66.131	1.778
750	0.8	0.367	1.469	115.401	2.109
750	1	0.534	2.135	167.709	2.468
800	0.2	0.028	0.113	9.439	1.453
800	0.4	0.096	0.383	32.114	1.603
800	0.6	0.213	0.851	71.321	1.863
800	0.8	0.372	1.488	124.658	2.215
800	1	0.536	2.145	179.727	2.593
900	0.2	0.031	0.124	11.687	1.563
900	0.4	0.101	0.402	37.888	1.724
900	0.6	0.220	0.878	82.750	2.023
900	0.8	0.383	1.530	144.199	2.453
900	1	0.556	2.225	209.670	2.892
1000	0.2	0.032	0.129	13.544	1.656

1000	0.4	0.103	0.412	43.145	1.846
1000	0.6	0.226	0.905	94.736	2.185
1000	0.8	0.395	1.581	165.597	2.646
1000	1	0.577	2.307	241.623	3.150
1100	0.2	0.034	0.135	15.512	1.732
1100	0.4	0.106	0.423	48.688	1.956
1100	0.6	0.233	0.930	107.128	2.336
1100	0.8	0.408	1.630	187.763	2.857
1100	1	0.594	2.375	273.619	3.428
1200	0.2	0.033	0.131	16.504	1.837
1200	0.4	0.107	0.426	53.533	2.069
1200	0.6	0.234	0.937	117.789	2.488
1200	0.8	0.414	1.657	208.183	3.075
1200	1	0.604	2.417	303.687	3.706
1300	0.2	0.033	0.133	18.061	1.909
1300	0.4	0.109	0.435	59.174	2.185
1300	0.6	0.240	0.961	130.872	2.635
1300	0.8	0.426	1.702	231.703	3.299
1300	1	0.623	2.491	339.159	4.022
1400	0.2	0.035	0.139	20.427	1.975
1400	0.4	0.110	0.440	64.507	2.264
1400	0.6	0.247	0.987	144.653	2.778
1400	0.8	0.445	1.779	260.766	3.538
1400	1	0.649	2.594	380.300	4.363
1500	0.2	0.035	0.140	21.991	2.057
1500	0.4	0.114	0.457	71.733	2.369
1500	0.6	0.255	1.018	159.907	2.938
1500	0.8	0.452	1.807	283.791	3.742
1500	1	0.674	2.695	423.277	4.668
1600	0.2	0.036	0.145	24.239	2.113
1600	0.4	0.117	0.467	78.302	2.451
1600	0.6	0.260	1.039	174.142	3.074
1600	0.8	0.463	1.850	309.970	3.970
1600	1	0.686	2.745	459.873	4.976
1700	0.2	0.039	0.155	27.534	2.190
1700	0.4	0.121	0.482	85.807	2.563
1700	0.6	0.268	1.073	190.960	3.253
1700	0.8	0.476	1.905	339.076	4.205
1700	1	0.712	2.848	507.011	5.360
1800	0.2	0.040	0.159	29.908	2.276
1800	0.4	0.124	0.496	93.494	2.679
1800	0.6	0.274	1.096	206.591	3.418

1800	0.8	0.489	1.955	368.572	4.477
1800	1	0.728	2.913	549.150	5.720
1900	0.2	0.043	0.171	33.957	2.183
1900	0.4	0.127	0.507	100.943	2.609
1900	0.6	0.279	1.117	222.313	3.390
1900	0.8	0.501	2.003	398.466	4.563
1900	1	0.762	3.047	606.188	5.927
2000	0.2	0.043	0.172	36.024	2.100
2000	0.4	0.130	0.519	108.769	2.568
2000	0.6	0.287	1.147	240.157	3.431
2000	0.8	0.521	2.082	436.053	4.720
2000	1	0.818	3.271	685.007	6.367
2200	0.2	0.046	0.183	42.083	2.036
2200	0.4	0.137	0.548	126.250	2.569
2200	0.6	0.304	1.215	279.993	3.579
2200	0.8	0.551	2.203	507.612	5.079
2200	1	0.849	3.397	782.689	6.947
2400	0.2	0.048	0.193	48.422	2.012
2400	0.4	0.142	0.569	142.922	2.622
2400	0.6	0.316	1.263	317.510	3.777
2400	0.8	0.571	2.285	574.199	5.561
2400	1	0.899	3.596	903.773	7.733
2500	0.2	0.049	0.195	50.964	2.032
2500	0.4	0.145	0.578	151.320	2.674
2500	0.6	0.324	1.295	338.943	3.903
2500	0.8	0.590	2.361	618.021	5.912
2500	1	0.928	3.713	971.974	8.401
2600	0.1	0.021	0.083	22.689	2.399
2600	0.2	0.042	0.169	46.105	2.563
2600	0.3	0.079	0.315	85.856	2.858
2600	0.4	0.133	0.530	144.304	3.280
2600	0.5	0.206	0.823	224.170	3.855
2600	0.6	0.300	1.199	326.363	4.581
2800	0.1	0.023	0.093	27.171	2.452
2800	0.2	0.045	0.181	52.974	2.642
2800	0.3	0.084	0.334	97.934	2.974
2800	0.4	0.138	0.550	161.268	3.412
2800	0.5	0.211	0.843	247.083	4.046
2800	0.6	0.306	1.223	358.700	4.834
3000	0.1	0.012	0.048	15.080	2.549
3000	0.2	0.034	0.136	42.726	2.758
3000	0.3	0.072	0.286	89.850	3.117

3000	0.4	0.127	0.507	159.383	3.618
3000	0.5	0.204	0.817	256.773	4.330
3000	0.6	0.302	1.207	379.295	5.215
3200	0.1	0.026	0.105	35.298	2.580
3200	0.2	0.049	0.195	65.233	2.826
3200	0.3	0.088	0.353	118.180	3.206
3200	0.4	0.145	0.581	194.807	3.749
3200	0.5	0.223	0.892	298.912	4.505
3200	0.6	0.324	1.297	434.517	5.535
3400	0.1	0.027	0.107	37.978	2.740
3400	0.2	0.051	0.204	72.634	2.941
3400	0.3	0.091	0.362	128.889	3.359
3400	0.4	0.150	0.601	214.103	3.991
3400	0.5	0.230	0.919	327.089	4.850
3400	0.6	0.334	1.335	475.442	5.995
3500	0.1	0.014	0.057	21.014	2.834
3500	0.2	0.039	0.156	57.177	3.087
3500	0.3	0.079	0.317	116.064	3.540
3500	0.4	0.139	0.557	204.273	4.191
3500	0.5	0.219	0.876	321.071	5.110
3500	0.6	0.325	1.301	476.719	6.332
3600	0.1	0.031	0.122	45.993	2.798
3600	0.2	0.053	0.213	80.425	3.080
3600	0.3	0.095	0.379	142.754	3.580
3600	0.4	0.155	0.619	233.232	4.225
3600	0.5	0.237	0.947	357.136	5.144
3600	0.6	0.342	1.368	515.724	6.380
3800	0.1	0.031	0.122	48.548	2.941
3800	0.2	0.055	0.218	86.750	3.226
3800	0.3	0.096	0.385	153.072	3.739
3800	0.4	0.159	0.635	252.556	4.475
3800	0.5	0.241	0.965	384.140	5.492
3800	0.6	0.354	1.414	562.680	6.851
4000	0.1	0.017	0.067	27.925	3.273
4000	0.2	0.042	0.167	70.092	3.652
4000	0.3	0.084	0.336	140.743	4.212
4000	0.4	0.148	0.590	247.139	5.036
4000	0.5	0.234	0.934	391.233	6.151
4000	0.6	0.350	1.399	585.872	7.645
2500R	0.2	0.040	0.159	41.539	2.119
2500R	0.4	0.125	0.498	130.376	2.672
2500R	0.6	0.279	1.117	292.343	3.737

2500R	0.8	0.516	2.063	540.005	5.389
2500R	1	0.815	3.258	852.942	7.541
3000R	0.1	0.025	0.099	31.206	2.527
3000R	0.2	0.047	0.189	59.481	2.717
3000R	0.3	0.086	0.342	107.442	3.086
3000R	0.4	0.142	0.566	177.814	3.596
3000R	0.5	0.217	0.866	272.062	4.288
3000R	0.6	0.315	1.259	395.422	5.155
3500R	0.1	0.027	0.108	39.584	2.758
3500R	0.2	0.051	0.205	75.259	3.002
3500R	0.3	0.093	0.370	135.612	3.447
3500R	0.4	0.152	0.608	222.844	4.091
3500R	0.5	0.232	0.929	340.618	5.004
3500R	0.6	0.340	1.359	498.222	6.185
4000R	0.1	0.030	0.121	50.824	3.103
4000R	0.2	0.056	0.224	93.829	3.451
4000R	0.3	0.100	0.398	166.714	3.992
4000R	0.4	0.162	0.648	271.434	4.792
4000R	0.5	0.249	0.995	416.645	5.874
4000R	0.6	0.361	1.443	604.582	7.361

R refers to the repeated tests at the specified spindle speeds.

APPENDIX C

CUTTING COEFFICIENTS CALIBRATION RESULTS

Table C.1 - Average Force and Spindle Motor Power Based Cutting Coefficients for 600 rpm Quarter Immersion (T)

	Kistler Average Force	Smart Tool Average Force	Spindle Motor Power
K_{tc} (N/mm ²)	746.1690	799.6647	707.0615
K_{te} (N/mm)	20.8209	17.5439	18.1451
K_{rc} (N/mm ²)	270.2777		260.6229
K_{re} (N/mm)	11.0708		10.2030

Table C.2 - Kistler Force Profile Based Cutting Coefficients for 600 rpm Quarter Immersion (T)

	Feedrate 1	Feedrate 2	Feedrate 3	Feedrate 4
K_{tc} (N/mm ²)	1119.3	928.4679	833.8043	777.3567
K_{te} (N/mm)	9.9	12.0608	15.5697	12.3156
K_{rc} (N/mm ²)	398.0	315.5390	281.9871	293.7649
K_{re} (N/mm)	10.3	11.5428	11.9024	10.8373

Table C.3 - Smart Tool Force Profile Based Cutting Coefficients for 600 rpm Quarter Immersion (T)

	Feedrate 1	Feedrate 2	Feedrate 3	Feedrate 4
K_{tc} (N/mm ²)	1012.4	931.7569	907.4870	870.7193
K_{te} (N/mm)	16.0	16.0682	14.3670	15.3515
K_{rc} (N/mm ²)				
K_{re} (N/mm)				

Table C.4 - Average Force and Spindle Motor Power Based Cutting Coefficients for 600 rpm Quarter Immersion (R)

	Kistler Average Force	Smart Tool Average Force	Spindle Motor Power
K_{tc} (N/mm ²)	727.7281		692.8366
K_{te} (N/mm)	22.0667		20.2278
K_{rc} (N/mm ²)	266.4187	224.7263	255.3796
K_{re} (N/mm)	11.3675	11.1968	11.3741

Table C.5 - Kistler Force Profile Based Cutting Coefficients for 600 rpm Quarter Immersion (R)

	Feedrate 1	Feedrate 2	Feedrate 3	Feedrate 4
K_{tc} (N/mm ²)	1032.7	873.3634	832.5440	817.8423
K_{te} (N/mm)	11.8	13.9909	14.5534	13.2589
K_{rc} (N/mm ²)	373.4	296.9652	284.7956	295.6732
K_{re} (N/mm)	11.1	12.3155	11.9315	10.5299

Table C.6 - Smart Tool Force Profile Based Cutting Coefficients for 600 rpm Quarter Immersion (R)

	Feedrate 1	Feedrate 2	Feedrate 3	Feedrate 4
K_{tc} (N/mm ²)				
K_{te} (N/mm)				
K_{rc} (N/mm ²)	293.9437	252.4202	243.9677	241.7016
K_{re} (N/mm)	11.3970	12.6690	12.8648	12.8214

Table C.7 - Average Force and Spindle Motor Power Based Cutting Coefficients for 600 rpm Half Immersion (T)

	Kistler Average Force	Smart Tool Average Force	Spindle Motor Power
K_{tc} (N/mm ²)	819.7100	847.2446	781.3918
K_{te} (N/mm)	19.3070	17.6526	21.4889
K_{rc} (N/mm ²)	291.0112		288.0210
K_{re} (N/mm)	11.4065		12.0832

Table C.8 - Kistler Force Profile Based Cutting Coefficients for 600 rpm Half Immersion (T)

	Feedrate 1	Feedrate 2	Feedrate 3	Feedrate 4
K_{tc} (N/mm ²)	1024.9	997.7525	1000.8	955.1660
K_{te} (N/mm)	12.5	11.4517	7.8	7.4098
K_{rc} (N/mm ²)	340.0	328.7878	325.8	306.7606
K_{re} (N/mm)	11.3	11.6809	10.6	10.7755

Table C.9 - Smart Tool Force Profile Based Cutting Coefficients for 600 rpm Half Immersion (T)

	Feedrate 1	Feedrate 2	Feedrate 3	Feedrate 4
K_{tc} (N/mm ²)	1109.6	1061.4	1017.0	958.7351
K_{te} (N/mm)	13.2	13.4	11.9	12.4380
K_{rc} (N/mm ²)				
K_{re} (N/mm)				

Table C.10 - Average Force and Spindle Motor Power Based Cutting Coefficients for 600 rpm Half Immersion (R)

	Kistler Average Force	Smart Tool Average Force	Spindle Motor Power
K_{tc} (N/mm ²)	829.2865		795.6583
K_{te} (N/mm)	20.0352		20.7882
K_{rc} (N/mm ²)	288.0796	253.0700	293.2796
K_{re} (N/mm)	11.4572	10.9745	11.6892

Table C.11 - Kistler Force Profile Based Cutting Coefficients for 600 rpm Half Immersion (R)

	Feedrate 1	Feedrate 2	Feedrate 3	Feedrate 4
K_{tc} (N/mm ²)	1109.2	1004.4	985.4192	927.4736
K_{te} (N/mm)	10.8	11.3	8.7406	9.3591
K_{rc} (N/mm ²)	384.8	330.2	328.4748	305.7325
K_{re} (N/mm)	10.4	11.7	10.4895	10.9096

Table C.12 - Smart Tool Force Profile Based Cutting Coefficients for 600 rpm Half Immersion (R)

	Feedrate 1	Feedrate 2	Feedrate 3	Feedrate 4
K_{tc} (N/mm ²)				
K_{te} (N/mm)				
K_{rc} (N/mm ²)	315.9826	286.2563	290.9590	273.5119
K_{re} (N/mm)	10.3974	11.5249	10.9380	11.3453

Table C.13 - Average Force and Spindle Motor Power Based Cutting Coefficients for 600 rpm Three Quarter Immersion (T)

	Kistler Average Force	Smart Tool Average Force	Spindle Motor Power
K_{tc} (N/mm ²)	799.1931	836.5910	754.1463
K_{te} (N/mm)	19.3823	16.1235	15.5865
K_{rc} (N/mm ²)	315.1838		277.9783
K_{re} (N/mm)	10.8860		8.7643

Table C.14 - Kistler Force Profile Based Cutting Coefficients for 600 rpm Three Quarter Immersion (T)

	Feedrate 1	Feedrate 2	Feedrate 3	Feedrate 4
K_{tc} (N/mm ²)	946.1785	864.5074	843.9186	817.7775
K_{te} (N/mm)	13.5664	16.5328	16.5556	16.7782
K_{rc} (N/mm ²)	376.2954	320.1171	308.2686	299.7482
K_{re} (N/mm)	10.4374	11.9507	11.6787	11.6541

Table C.15 - Smart Tool Force Profile Based Cutting Coefficients for 600 rpm Three Quarter Immersion (T)

	Feedrate 1	Feedrate 2	Feedrate 3	Feedrate 4
K_{tc} (N/mm ²)	919.3931	852.2999	820.6392	801.4172
K_{te} (N/mm)	15.7162	19.5255	21.1852	22.9853
K_{rc} (N/mm ²)				
K_{re} (N/mm)				

Table C.16 - Average Force and Spindle Motor Power Based Cutting Coefficients for 600 rpm Three Quarter Immersion (R)

	Kistler Average Force	Smart Tool Average Force	Spindle Motor Power
K_{tc} (N/mm ²)	798.0283		760.3425
K_{te} (N/mm)	19.5654		15.2986
K_{rc} (N/mm ²)	308.6772	259.9289	280.2622
K_{re} (N/mm)	11.7959	10.7437	8.6024

Table C.17 - Kistler Force Profile Based Cutting Coefficients for 600 rpm Three Quarter Immersion (R)

	Feedrate 1	Feedrate 2	Feedrate 3	Feedrate 4
K_{tc} (N/mm ²)	954.1917	863.5857	829.3597	791.9833
K_{te} (N/mm)	13.5895	16.4051	16.5974	19.7709
K_{rc} (N/mm ²)	396.2909	328.8271	307.6162	289.8889
K_{re} (N/mm)	10.2581	11.6738	12.0459	12.1900

Table C.18 - Smart Tool Force Profile Based Cutting Coefficients for 600 rpm Three Quarter Immersion (R)

	Feedrate 1	Feedrate 2	Feedrate 3	Feedrate 4
K_{tc} (N/mm ²)				
K_{te} (N/mm)				
K_{rc} (N/mm ²)	347.4527	287.5468	269.3323	260.1320
K_{re} (N/mm)	9.3426	10.8349	11.5118	11.7220

Table C.19 - Average Force and Spindle Motor Power Based Cutting Coefficients for 3000 rpm Quarter Immersion (T)

	Kistler Average Force	Smart Tool Average Force	Spindle Motor Power
K_{tc} (N/mm ²)	613.5699	662.7393	614.7972
K_{te} (N/mm)	17.8482	15.6311	12.5819
K_{rc} (N/mm ²)	243.8926		243.3982
K_{re} (N/mm)	11.2227		7.9279

Table C.20 - Kistler Force Profile Based Cutting Coefficients for 3000 rpm Quarter Immersion (T)

	Feedrate 1	Feedrate 2	Feedrate 3	Feedrate 4
K_{tc} (N/mm ²)	824.3090	578.2028	559.2153	551.1207
K_{te} (N/mm)	14.7075	25.3979	28.8622	32.5871
K_{rc} (N/mm ²)	309.0714	177.1644	163.5058	167.9653
K_{re} (N/mm)	11.2729	15.9450	17.7621	19.0909

Table C.21 - Smart Tool Force Profile Based Cutting Coefficients for 3000 rpm Quarter Immersion (T)

	Feedrate 1	Feedrate 2	Feedrate 3	Feedrate 4
K_{tc} (N/mm ²)	863.24	657.32	648	632.5
K_{te} (N/mm)	12.048	22.216	25.556	28.85
K_{rc} (N/mm ²)				
K_{re} (N/mm)				

Table C.22 - Average Force and Spindle Motor Power Based Cutting Coefficients for 3000 rpm Quarter Immersion (R)

	Kistler Average Force	Smart Tool Average Force	Spindle Motor Power
K_{tc} (N/mm ²)	642.9063		636.2091
K_{te} (N/mm)	17.1140		12.8368
K_{rc} (N/mm ²)	244.8721	182.8958	251.8752
K_{re} (N/mm)	11.0134	12.8150	8.0885

Table C.23 - Kistler Force Profile Based Cutting Coefficients for 3000 rpm Quarter Immersion (R)

	Feedrate 1	Feedrate 2	Feedrate 3	Feedrate 4
K_{tc} (N/mm ²)	821.7713	557.4484	552.9916	562.7009
K_{te} (N/mm)	15.0119	26.1500	29.5650	31.3897
K_{rc} (N/mm ²)	278.0837	141.5068	145.1113	170.0477
K_{re} (N/mm)	11.8852	17.8881	19.5220	19.0292

Table C.24 - Smart Tool Force Profile Based Cutting Coefficients for 3000 rpm Quarter Immersion (R)

	Feedrate 1	Feedrate 2	Feedrate 3	Feedrate 4
K_{tc} (N/mm ²)				
K_{te} (N/mm)				
K_{rc} (N/mm ²)	174.5294	120.6167	146.1970	166.7926
K_{re} (N/mm)	16.4120	21.7015	22.2501	21.6153

Table C.25 - Average Force and Spindle Motor Power Based Cutting Coefficients for 3000 rpm Half Immersion (T)

	Kistler Average Force	Smart Tool Average Force	Spindle Motor Power
K_{tc} (N/mm ²)	671.4461	689.3335	697.1742
K_{te} (N/mm)	21.8295	18.5568	18.0530
K_{rc} (N/mm ²)	232.9034		276.0113
K_{re} (N/mm)	14.0712		11.3752

Table C.26 - Kistler Force Profile Based Cutting Coefficients for 3000 rpm Half Immersion (T)

	Feedrate 1	Feedrate 2	Feedrate 3	Feedrate 4
K_{tc} (N/mm ²)	902.2263	749.2887	740.5189	720.9159
K_{te} (N/mm)	14.3096	18.9551	18.6971	18.4253
K_{rc} (N/mm ²)	385.6796	267.1295	251.1433	237.2776
K_{re} (N/mm)	12.2137	15.3964	16.0096	16.3868

Table C.27 - Smart Tool Force Profile Based Cutting Coefficients for 3000 rpm Half Immersion (T)

	Feedrate 1	Feedrate 2	Feedrate 3	Feedrate 4
K_{tc} (N/mm ²)	812.8	768.07	801.72	767.42
K_{te} (N/mm)	19.45	22.107	19.401	21.43
K_{rc} (N/mm ²)				
K_{re} (N/mm)				

Table C.28 - Average Force and Spindle Motor Power Based Cutting Coefficients for 3000 rpm Half Immersion (R)

	Kistler Average Force	Smart Tool Average Force	Spindle Motor Power
K_{tc} (N/mm ²)	676.4707		738.8071
K_{te} (N/mm)	21.5677		18.4991
K_{rc} (N/mm ²)	234.2961	192.5107	292.4937
K_{re} (N/mm)	13.8505	14.1201	11.6563

Table C.29 - Kistler Force Profile Based Cutting Coefficients for 3000 rpm Half Immersion (R)

	Feedrate 1	Feedrate 2	Feedrate 3	Feedrate 4
K_{tc} (N/mm ²)	920.8222	731.6559	768.0431	723.2580
K_{te} (N/mm)	13.9447	19.0729	16.4577	18.5387
K_{rc} (N/mm ²)	400.3115	267.9117	275.2306	238.0865
K_{re} (N/mm)	11.6614	15.5432	14.4955	15.6561

Table C.30 - Smart Tool Force Profile Based Cutting Coefficients for 3000 rpm Half Immersion (R)

	Feedrate 1	Feedrate 2	Feedrate 3	Feedrate 4
K_{tc} (N/mm ²)				
K_{te} (N/mm)				
K_{rc} (N/mm ²)	205.9839	154.3716	184.5939	159.8609
K_{re} (N/mm)	14.7884	18.8047	18.5888	21.0035

Table C.31 - Average Force and Spindle Motor Power Based Cutting Coefficients for 3000 rpm Three Quarter Immersion (T)

	Kistler Average Force	Smart Tool Average Force	Spindle Motor Power
K_{tc} (N/mm ²)	656.8417	761.5866	738.6378
K_{te} (N/mm)	19.6580	17.8042	13.8394
K_{rc} (N/mm ²)	301.1310		292.4267
K_{re} (N/mm)	11.2332		8.7202

Table C.32 - Kistler Force Profile Based Cutting Coefficients for 3000 rpm Three Quarter Immersion (T)

	Feedrate 1	Feedrate 2	Feedrate 3	Feedrate 4
K_{tc} (N/mm ²)	773.7842	673.9103	676.4758	672.9911
K_{te} (N/mm)	15.1519	20.0383	21.4392	20.5569
K_{rc} (N/mm ²)	377.9153	275.9240	250.4006	240.0820
K_{re} (N/mm)	11.1882	14.2210	15.7230	16.3100

Table C.33 - Smart Tool Force Profile Based Cutting Coefficients for 3000 rpm Three Quarter Immersion (T)

	Feedrate 1	Feedrate 2	Feedrate 3	Feedrate 4
K_{tc} (N/mm ²)	883.7097	768.9125	776.8609	781.4713
K_{te} (N/mm)	13.9690	18.0664	17.2415	13.4155
K_{rc} (N/mm ²)				
K_{re} (N/mm)				

Table C.34 - Average Force and Spindle Motor Power Based Cutting Coefficients for 3000 rpm Three Quarter Immersion (R)

	Kistler Average Force	Smart Tool Average Force	Spindle Motor Power
K_{tc} (N/mm ²)	672.8909		742.7247
K_{te} (N/mm)	18.8466		15.4482
K_{rc} (N/mm ²)	299.3752	233.5516	294.0447
K_{re} (N/mm)	12.2490	13.0211	9.7339

Table C.35 - Kistler Force Profile Based Cutting Coefficients for 3000 rpm Three Quarter Immersion (R)

	Feedrate 1	Feedrate 2	Feedrate 3	Feedrate 4
K_{tc} (N/mm ²)	713.8636	677.4449	697.1114	674.3120
K_{te} (N/mm)	17.2368	19.1035	19.8320	22.3713
K_{rc} (N/mm ²)	334.1894	276.5013	268.7876	238.0956
K_{re} (N/mm)	12.4858	14.1964	14.6687	16.6682

Table C.36 - Smart Tool Force Profile Based Cutting Coefficients for 3000 rpm Three Quarter Immersion (R)

	Feedrate 1	Feedrate 2	Feedrate 3	Feedrate 4
K_{tc} (N/mm ²)				
K_{te} (N/mm)				
K_{rc} (N/mm ²)	133.7280	149.3496	213.0565	201.1375
K_{re} (N/mm)	15.9564	18.1526	16.0614	17.0142

APPENDIX D

SIMULATION RESULTS

Table D.1 - REp for 600 rpm Quarter Immersion (T)

	Kistler Average Force	Smart Tool Average Force	Spindle Motor Power	Kistler Force Profile	Smart Tool Force Profile
Feedrate 1	-10.88	-13.21	-17.8	0.19	-0.15
Feedrate 2	-9.84	-9.82	-15.92	-1.51	0.76
Feedrate 3	-7.01	-5.83	-12.85	-2.03	2.81
Feedrate 4	-2.9	-0.97	-8.74	-3.61	5.75

Table D.2 - REp for 600 rpm Quarter Immersion (R)

	Kistler Average Force	Smart Tool Average Force	Spindle Motor Power	Kistler Force Profile	Smart Tool Force Profile
Feedrate 1	-7.69	-10.75	-12.83	0.04	2.68
Feedrate 2	-11.92	-11.53	-16.57	-6.3	-1.15
Feedrate 3	-10.86	-8.87	-15.44	-5.86	-0.51
Feedrate 4	-6.72	-3.67	-11.43	-1.91	2.87

Table D.3 - REp for 600 rpm Half Immersion (T)

	Kistler Average Force	Smart Tool Average Force	Spindle Motor Power	Kistler Force Profile	Smart Tool Force Profile
Feedrate 1	1.01	-1.25	2.48	4.58	9.92
Feedrate 2	-3.47	-4.25	-4.14	4.04	9.62
Feedrate 3	-2.75	-2.9	-4.38	5.48	8.84
Feedrate 4	0.6	0.84	-1.64	6.69	9.01

Table D.4 - REp for 600 rpm Half Immersion (R)

	Kistler Average Force	Smart Tool Average Force	Spindle Motor Power	Kistler Force Profile	Smart Tool Force Profile
Feedrate 1	1.22	-2.74	0.59	6.29	8.26
Feedrate 2	-1.86	-4.04	-3.49	4.7	9.87
Feedrate 3	-1.74	-3.14	-3.83	4.62	8.56
Feedrate 4	0.96	-0.02	-1.47	4.35	8.09

Table D.5 - REp for 600 rpm Three Quarter Immersion (T)

	Kistler Average Force	Smart Tool Average Force	Spindle Motor Power	Kistler Force Profile	Smart Tool Force Profile
Feedrate 1	0.94	-4.1	-11.22	1.33	1.66
Feedrate 2	-3.53	-5.98	-13.17	-0.97	-0.23
Feedrate 3	-2.67	-4	-11.47	-1.13	-0.76
Feedrate 4	-0.14	-0.81	-8.62	-0.5	0.65

Table D.6 - REp for 600 rpm Three Quarter Immersion (R)

	Kistler Average Force	Smart Tool Average Force	Spindle Motor Power	Kistler Force Profile	Smart Tool Force Profile
Feedrate 1	-0.09	-5.83	-12.99	0.48	-0.17
Feedrate 2	-3.18	-5.95	-12.98	-0.98	-0.19
Feedrate 3	-2.15	-3.6	-10.78	-1.81	-0.35
Feedrate 4	-0.82	-1.49	-8.83	-1.83	-0.04

Table D.7 - REp for 3000 rpm Quarter Immersion (T)

	Kistler Average Force	Smart Tool Average Force	Spindle Motor Power	Kistler Force Profile	Smart Tool Force Profile
Feedrate 1	-13.36	-14.22	-23.89	-1.39	-3.48
Feedrate 2	-10.62	-10.05	-17.4	-6.7	-2.36
Feedrate 3	-11.82	-10.5	-16.66	-10.37	-3.26
Feedrate 4	-7.97	-6.11	-11.92	-7.22	0.05

Table D.8 - REp for 3000 rpm Quarter Immersion (R)

	Kistler Average Force	Smart Tool Average Force	Spindle Motor Power	Kistler Force Profile	Smart Tool Force Profile
Feedrate 1	-18.49	-20.02	-26.9	-8.32	-10
Feedrate 2	-13.73	-14.96	-19.42	-13.37	-7.69
Feedrate 3	-13.44	-14.42	-17.7	-14.59	-7.5
Feedrate 4	-7.59	-8.45	-11.26	-8.93	-2.45

Table D.9 - REp for 3000 rpm Half Immersion (T)

	Kistler Average Force	Smart Tool Average Force	Spindle Motor Power	Kistler Force Profile	Smart Tool Force Profile
Feedrate 1	-0.6	-6.1	-5.95	5.72	4.57
Feedrate 2	-4.3	-7.71	-5.79	1.18	3.67
Feedrate 3	-1.96	-4.44	-1.68	3.66	8.56
Feedrate 4	1.26	-0.66	2.65	5.12	10.34

Table D.10 - REp for 3000 rpm Half Immersion (R)

	Kistler Average Force	Smart Tool Average Force	Spindle Motor Power	Kistler Force Profile	Smart Tool Force Profile
Feedrate 1	-2.5	-7.67	-3.35	4.57	2.82
Feedrate 2	-3.91	-7.43	-0.72	0.23	3.98
Feedrate 3	-2.58	-5.3	2.6	4.05	7.58
Feedrate 4	2.01	-0.29	8.64	5.68	10.75

Table D.11 - REp for 3000 rpm Three Quarter Immersion (T)

	Kistler Average Force	Smart Tool Average Force	Spindle Motor Power	Kistler Force Profile	Smart Tool Force Profile
Feedrate 1	-5.06	-2.3	-12.67	-3.16	-1.92
Feedrate 2	-5.75	-0.84	-7.46	-3.25	-0.31
Feedrate 3	-9.74	-3.94	-8.66	-6.9	-2.76
Feedrate 4	-11.66	-5.33	-9.02	-10.66	-6.51

Table D.12 - REp for 3000 rpm Three Quarter Immersion (R)

	Kistler Average Force	Smart Tool Average Force	Spindle Motor Power	Kistler Force Profile	Smart Tool Force Profile
Feedrate 1	-5.06	-2.76	-9.08	-3.94	-2.39
Feedrate 2	-3.97	0.1	-3.76	-3.11	0.63
Feedrate 3	-12.82	-8.29	-10.76	-10.34	-7.17
Feedrate 4	-13.61	-8.62	-10.49	-12.5	-9.77

APPENDIX E

MATLAB PROGRAMS

Force Model Calibration Using Kistler Average Force and Spindle Motor Power

```
%  
%  
% Calibrate the cutting coefficients using average force from the  
% Kistler force dynamometer and the average power from the LCI sensor  
% for standard cutting test  
% Program can be used in down milling and up milling  
  
% Input: cutting geometry and measured data file for Kistler and LCI  
power sensor  
% Output: cutting coefficients calibrated from the Kistler average  
force and the spindle motor power methods  
  
% By Yong Zhao  
% Revised on February 09 2012  
% Design and Manufacturing Lab, University of New Hampshire  
  
clc;  
close all;  
clear all;  
  
%  
rpm=600;  
fs=7200; % Sampling frequency  
numpercycle=60*fs/rpm;  
cycles=20; % number of cycles of force to be used  
% degree=0.5; % data sampling at every 3 degree of tool rotation  
N=1; % number of tooth  
AD=0.125; % axial depth unit:inch  
D=0.75; % diameter of the tool unit: inch  
  
% % motor coefficient for 600 rpm  
motor_efficiency=0.982;  
Ptare=174; % measured data from a recent 600 rpm cutting test unit:  
watt  
  
% % motor coefficient for 3000 rpm  
% motor_efficiency=0.918;  
% Ptare=365;  
  
% % motor coefficient for 3600 rpm  
% motor_efficiency=0.883;
```

```

% Ptare=400;

% motor coefficient for 4000 rpm
% motor_efficiency=0.865;
% Ptare=450;

j=6; % i=1,2 and 3 means down milling 1/4 immersion, 1/2 immersion and
3/4
    % immersion; i=4,5 and 6 means up milling 1/4 immersion, 1/2
immersion
    % and 3/4 immersion.
if j==1
    disp('Quarter Immersion Down Milling');
    enter=2/3*pi;
    exit=pi;
    Theta=1/3*pi;
    RD=1/4*D; % radial depth quarter immersion unit: inch
    Feed=[5.445 10.891 16.336 21.782]'; % feedrate unit:inch/min
elseif j==2
    disp('Half Immersion Down Milling');
    enter=1/2*pi;
    exit=pi;
    Theta=1/2*pi;
    RD=1/2*D; % radial depth half immersion unit: inch
    Feed=[4.084 8.168 12.252 16.336]'; % feedrate unit:inch/min
elseif j==3
    disp('Three Quarter Immersion Down Milling');
    enter=1/3*pi;
    exit=pi;
    Theta=2/3*pi;
    RD=3/4*D; % radial depth three quarter immersion unit: inch
    Feed=[3.63 7.261 10.891 14.521]'; % feedrate unit:inch/min
elseif j==4
    disp('Quarter Immersion Up Milling');
    enter=0;
    exit=1/3*pi;
    Theta=1/3*pi;
    RD=1/4*D; % radial depth quarter immersion unit: inch
    Feed=[1.257 2.513 3.770 5.027]'; % feedrate for 600 rpm
unit:inch/min
    %Feed=[6.283 12.566 18.850 25.133]'; % feedrate for 3000 rpm
    %Feed=[7.540 15.080 22.619 30.159]'; % feedrate for 3600 rpm
    %Feed=[8.378 16.755 25.133 33.510]'; % feedrate for 4000 rpm
elseif j==5
    disp('Half Immersion Up Milling');
    enter=0;
    exit=1/2*pi;
    Theta=1/2*pi;
    RD=1/2*D; % radial depth half immersion unit: inch
    Feed=[0.942 1.885 2.827 3.770]'; % feedrate for 600 rpm
unit:inch/min
    %Feed=[4.712 9.425 14.137 18.850]'; % feedrate for 3000 rpm
    %Feed=[5.655 11.310 16.965 22.619]'; % feedrate for 3600 rpm

```

```

    %Feed=[6.283 12.566 18.850 25.133]'; % feedrate for 4000 rpm
elseif j==6
    disp('Three Quarter Immersion Up Milling');
    enter=0;
    exit=2/3*pi;
    Theta=2/3*pi;
    RD=3/4*D; % radial depth three quarter immersion unit: inch
    Feed=[0.838 1.676 2.513 3.351]'; % feedrate for 600 rpm
unit:inch/min
    %Feed=[4.189 8.378 12.566 16.755]'; % feedrate for 3000 rpm
    %Feed=[5.027 10.053 15.080 20.106]'; % feedrate for 3600 rpm
    %Feed=[5.585 11.170 16.755 22.340]'; % feedrate for 4000 rpm
end

Fx=zeros(4,1);
Fy=zeros(4,1);

%% Read the data file
[fileName,PathName,FilterIndex] = uigetfile('*.csv', 'Please choose an
excel file to calibrate the cutting coefficients');
if( fileName == 0 )
    return;
end;
fname = sprintf('%s%s', PathName, fileName)
[a b c]=xlsread(fname);

% Nfiles=2;
% filename='Aluminum3k36k4kQuarterUpRadial';
% a=[];
% for n = 1:Nfiles
%
%     % Name of sub-file to read
%     namespace = strcat(filename,int2str(n-1),'.csv');
%
%     % Read xls data
%     [newdata, headertext] = xlsread(namespace);
%
%     % Concatenate data
%     a = vertcat(a,newdata);
%
% end

%%
% Plot raw Fx and Fy from Kistler
a(:,2)=-a(:,2);
a(:,3)=-a(:,3);

%%
figure
subplot(2,1,1)
plot(a(:,1),a(:,2));
title('Raw Force Data from Kistler in X Direction');
xlabel('Time (s)');

```

```

ylabel('Fx (volt)');

subplot(2,1,2)
plot(a(:,1),a(:,3));
title('Raw Force Data from Kistler in Y Direction');
xlabel('Time (s)');
ylabel('Fy (volt)');

figure
subplot(2,1,1)
plot(a(:,1),a(:,2));
title('Raw Force Data from Kistler in X Direction');
xlabel('Time (s)');
ylabel('Fx (volt)');

subplot(2,1,2)
plot(a(:,1),a(:,5));
title('Raw Power Data from LCI');
xlabel('Time (s)');
ylabel('Power (volt)');

%%
% plot raw Fx
num1=cursor_info_0.DataIndex;
num2=cursor_info_00.DataIndex;

disp('Kistler zero offset at X and Y direction in the end');
Fx_zero_offset=mean(a(num1:num2,2))
Fy_zero_offset=mean(a(num1:num2,3))

a(:,2)=a(:,2)-Fx_zero_offset;
a(:,3)=a(:,3)-Fy_zero_offset;

figure;
plot(a(:,1),a(:,2));
title('Raw Force Data from Kistler in X Direction');
xlabel('Time (s)');
ylabel('Fx (volt)');

%%
% plot raw force data in X direction for the first feedrate and
calculate
% the mean of the raw force and cutting power
cycles=20;
figure
startnum=cursor_info_1.DataIndex;
endnum=startnum+numpercycle*cycles-1;
time=a(startnum:endnum,1);
Fx_raw=500*a(startnum:endnum,2);
Fy_raw=500*a(startnum:endnum,3);
Pe=a(startnum:endnum,5)/10*2.006*746; % unit:watt
plot(time,Fx_raw);

```

```

Fx(1,1)=mean(Fx_raw);
Fy(1,1)=mean(Fy_raw);
Pcut(1,1)=(mean(Pe)-Ptare)*motor_efficiency;

%%
% plot raw force data in X direction for the second feedrate calculate
% the mean of the raw force and cutting power
figure
startnum=cursor_info_2.DataIndex;
endnum=startnum+numpercycle*cycles-1;
time=a(startnum:endnum,1);
Fx_raw=500*a(startnum:endnum,2);
Fy_raw=500*a(startnum:endnum,3);
Pe=a(startnum:endnum,5)/10*2.006*746;
plot(time,Fx_raw);

Fx(2,1)=mean(Fx_raw);
Fy(2,1)=mean(Fy_raw);
Pcut(2,1)=(mean(Pe)-Ptare)*motor_efficiency;

%%
% plot raw force data in X direction for the third feedrate and
calculate
% the mean of the raw force and cutting power
figure
startnum=cursor_info_3.DataIndex;
endnum=startnum+numpercycle*cycles-1;
time=a(startnum:endnum,1);
Fx_raw=500*a(startnum:endnum,2);
Fy_raw=500*a(startnum:endnum,3);
Pe=a(startnum:endnum,5)/10*2.006*746;
plot(time,Fx_raw);

Fx(3,1)=mean(Fx_raw);
Fy(3,1)=mean(Fy_raw);
Pcut(3,1)=(mean(Pe)-Ptare)*motor_efficiency;

%%
% plot raw force data in X direction for the fourth feedrate and
calculate
% the mean of the raw force and cutting power
figure
startnum=cursor_info_4.DataIndex;
endnum=startnum+numpercycle*cycles-1;
time=a(startnum:endnum,1);
Fx_raw=500*a(startnum:endnum,2);
Fy_raw=500*a(startnum:endnum,3);
Pe=a(startnum:endnum,5)/10*2.006*746;
plot(time,Fx_raw);

Fx(4,1)=mean(Fx_raw);

```



```

Fy(4,1)=mean(Fy_raw);
Pcut(4,1)=(mean(Pe)-Ptare)*motor_efficiency;

%%
% Using the averaged force and power to calibrate the cutting
coefficients

Q_dot=AD*RD*Feed/60*25.4^3; % material removal rate unit:mm^3/s
Ac_dot=D/2*Theta*rpm*AD/60*25.4^2; % contact area rate unit:mm^2/s
Ac_dot=[Ac_dot Ac_dot Ac_dot Ac_dot]';
G=[Q_dot Ac_dot];
Kt=inv(G'*G)*G'*(Pcut)*1000;

if j<4
    for i=1:4
        fp(i)=Feed(i)/(N*rpm);
        A1x(i)= 25.4^2*N*AD*fp(i)/(8*pi)*(cos(2*exit) - cos(2*enter));
        A2x(i)= -25.4*N*AD/(2*pi)*(sin(exit) - sin(enter));
        A3x(i)=-25.4^2*N*AD*fp(i)/(8*pi)*(2*exit-2*enter-
sin(2*exit)+sin(2*enter));
        A4x(i)=25.4*N*AD/(2*pi)*(cos(exit)-cos(enter));

        A1y(i)=25.4^2*N*AD*fp(i)/(8*pi)*(2*exit-2*enter-
sin(2*exit)+sin(2*enter));
        A2y(i)=-25.4*N*AD/(2*pi)*(cos(exit)-cos(enter));
        A3y(i)=25.4^2*N*AD*fp(i)/(8*pi)*(cos(2*exit)-cos(2*enter));
        A4y(i)=-25.4*N*AD/(2*pi)*(sin(exit)-sin(enter));
    end
else
    for i=1:4
        fp(i)=Feed(i)/(N*rpm);
        A1x(i)= 25.4^2*N*AD*fp(i)/(8*pi)*(cos(2*exit) - cos(2*enter));
        A2x(i)= -25.4*N*AD/(2*pi)*(sin(exit) - sin(enter));
        A3x(i)=-25.4^2*N*AD*fp(i)/(8*pi)*(2*exit-2*enter-
sin(2*exit)+sin(2*enter));
        A4x(i)=25.4*N*AD/(2*pi)*(cos(exit)-cos(enter));

        A1y(i)=25.4^2*N*AD*fp(i)/(8*pi)*(2*exit-2*enter-
sin(2*exit)+sin(2*enter));
        A2y(i)=-25.4*N*AD/(2*pi)*(cos(exit)-cos(enter));
        A3y(i)=25.4^2*N*AD*fp(i)/(8*pi)*(cos(2*exit)-cos(2*enter));
        A4y(i)=-25.4*N*AD/(2*pi)*(sin(exit)-sin(enter));
    end
end

M=[A1x(1) A2x(1) A3x(1) A4x(1);A1y(1) A2y(1) A3y(1) A4y(1);
A1x(2) A2x(2) A3x(2) A4x(2);A1y(2) A2y(2) A3y(2) A4y(2);
A1x(3) A2x(3) A3x(3) A4x(3);A1y(3) A2y(3) A3y(3) A4y(3);
A1x(4) A2x(4) A3x(4) A4x(4);A1y(4) A2y(4) A3y(4) A4y(4)];

F=[Fx(1);Fy(1);Fx(2);Fy(2);Fx(3);Fy(3);Fx(4);Fy(4)];

```

```
K=inv(M'*M)*M'*F;
```

```
%%  
% display the cutting coefficients
```

```
disp('Using the averaged force Fx and Fy');  
K  
disp('Using the averaged power');  
Kt
```

Force Model Calibration Using Smart Tool Average Force

```
%%  
% Calibrate the cutting coefficients using average force from Smart  
Tool  
% for standard cutting test  
% Program can be used in down milling and up milling  
  
% Input: cutting geometry and measured data file for Smart Tool  
% Output: cutting coefficients calibrated from the Smart Tool average  
force methods
```

```
% By Yong Zhao  
% Revised on February 13 2012  
% Design and Manufacturing Lab, University of New Hampshire
```

```
clc;  
close all;  
clear all;
```

```
%%  
rpm=600;  
fs=10240;  
N=1; % number of tooth  
AD=0.125; % axial depth unit:inch  
D=0.75; % diameter of the tool unit: inch
```

```
k=1; % k=1 tangential coefficients calibration; k=2 radial coefficients  
calibration
```

```
j=6; % j=1,2 and 3 means down milling 1/4 immersion, 1/2 immersion and  
3/4
```

```
    % immersion; j=4,5 and 6 means up milling 1/4 immersion, 1/2  
immersion
```

```
    % and 3/4 immersion.
```

```
if j==1
```

```
    disp('Quarter Immersion Down Milling');
```

```
    enter=2/3*pi;
```

```
    exit=pi;
```

```
    Theta=1/3*pi;
```

```
    RD=1/4*D; % radial depth quarter immersion unit: inch
```

```
    Feed=[5.445 10.891 16.336 21.782]'; % feedrate unit:inch/min
```

```

elseif j==2
    disp('Half Immersion Down Milling');
    enter=1/2*pi;
    exit=pi;
    Theta=1/2*pi;
    RD=1/2*D; % radial depth half immersion unit: inch
    Feed=[4.084 8.168 12.252 16.336]'; % feedrate unit:inch/min
elseif j==3
    disp('Three Quarter Immersion Down Milling');
    enter=1/3*pi;
    exit=pi;
    Theta=2/3*pi;
    RD=3/4*D; % radial depth three quarter immersion unit: inch
    Feed=[3.63 7.261 10.891 14.521]'; % feedrate unit:inch/min
elseif j==4
    disp('Quarter Immersion Up Milling');
    enter=0;
    exit=1/3*pi;
    Theta=1/3*pi;
    RD=1/4*D; % radial depth quarter immersion unit: inch
    Feed=[1.257 2.513 3.770 5.027]'; % feedrate for 600 rpm
unit:inch/min
    %Feed=[6.283 12.566 18.850 25.133]'; % feedrate for 3000 rpm
    %Feed=[7.540 15.080 22.619 30.159]'; % feedrate for 3600 rpm
    %Feed=[8.378 16.755 25.133 33.510]'; % feedrate for 4000 rpm
elseif j==5
    disp('Half Immersion Up Milling');
    enter=0;
    exit=1/2*pi;
    Theta=1/2*pi;
    RD=1/2*D; % radial depth half immersion unit: inch
    Feed=[0.942 1.885 2.827 3.770]'; % feedrate for 600 rpm
unit:inch/min
    %Feed=[4.712 9.425 14.137 18.850]'; % feedrate for 3000 rpm
    %Feed=[5.655 11.310 16.965 22.619]'; % feedrate for 3600 rpm
    %Feed=[6.283 12.566 18.850 25.133]'; % feedrate for 4000 rpm
elseif j==6
    disp('Three Quarter Immersion Up Milling');
    enter=0;
    exit=2/3*pi;
    Theta=2/3*pi;
    RD=3/4*D; % radial depth three quarter immersion unit: inch
    Feed=[0.838 1.676 2.513 3.351]'; % feedrate for 600 rpm
unit:inch/min
    %Feed=[4.189 8.378 12.566 16.755]'; % feedrate for 3000 rpm
    %Feed=[5.027 10.053 15.080 20.106]'; % feedrate for 3600 rpm
    %Feed=[5.585 11.170 16.755 22.340]'; % feedrate for 4000 rpm
end

%%
figure
strain_data=[s(i:end),s(1:i-1)];
plot(strain_time,strain_data);

```

```

title('Strain Data from Smart Tool');
xlabel('Time (s)');
ylabel('Strain (bit)');

%%
% calculate the zero offset of smart tool
num1=cursor_info_0.DataIndex;
num2=cursor_info_00.DataIndex;
zerobit=mean(strain_data(num1:num2))
strain=strain_data-zerobit;
Ft_data=strain/1.64*4.448222; % unit:N
figure
plot(strain_time,Ft_data);
title('Raw Force from Smart Tool');
xlabel('Time (s)');
ylabel('Ft (N)');

%%
% Find the tangential force for the first feedrate used for calibration
cycles=20; % use 20 cycles of data to get the average
number=floor(60/rpm*fs); % how many samples collected in one cycle
startnum=cursor_info_1.DataIndex;
endnum=startnum+number*cycles-1;
time=strain_time(startnum:endnum);
Ft_raw=Ft_data(startnum:endnum);
figure
plot(time,Ft_raw);
Ft(1)=mean(Ft_raw);

%%
% Find the tangential force for the second feedrate used for
calibration
startnum=cursor_info_2.DataIndex;
endnum=startnum+number*cycles-1;
time=strain_time(startnum:endnum);
Ft_raw=Ft_data(startnum:endnum);
figure
plot(time,Ft_raw);
Ft(2)=mean(Ft_raw);

%%
% Find the tangential force for the third feedrate used for calibration
startnum=cursor_info_3.DataIndex;
endnum=startnum+number*cycles-1;
time=strain_time(startnum:endnum);
Ft_raw=Ft_data(startnum:endnum);
figure
plot(time,Ft_raw);
Ft(3)=mean(Ft_raw);

%%
% Find the tangential force for the fourth feedrate used for
calibration

```

```

startnum=cursor_info_4.DataIndex;
endnum=startnum+number*cycles-1;
time=strain_time(startnum:endnum);
Ft_raw=Ft_data(startnum:endnum);
figure
plot(time,Ft_raw);
Ft(4)=mean(Ft_raw);

%%
% Tangential coefficients calibration
if j<4
    for i=1:4
        fp(i)=Feed(i)/(N*rpm);
        Gtc(i)= -25.4^2*N*AD*fp(i)/(2*pi)*(cos(exit) - cos(enter));
        Gte(i)= 25.4*N*AD/(2*pi)*(exit - enter);
    end
else
    for i=1:4
        %fp(i)=Feed(i)/(N*rpm_avg);
        fp(i)=Feed(i)/(N*rpm);
        Gtc(i)= -25.4^2*N*AD*fp(i)/(2*pi)*(cos(exit) - cos(enter));
        Gte(i)= 25.4*N*AD/(2*pi)*(exit - enter);
    end
end

G=[Gtc(1) Gte(1);Gtc(2) Gte(2);Gtc(3) Gte(3);Gtc(4) Gte(4)];

if k==1
    Ft=[Ft(1);Ft(2);Ft(3);Ft(4)];
    disp('Tangential coefficients: Ktc and Kte');
    Kt=inv(G'*G)*G'*Ft
else
    Fr=[Ft(1);Ft(2);Ft(3);Ft(4)];
    disp('Radial coefficients: Krc and Kre');
    Kr=inv(G'*G)*G'*Fr
end

```

Force Model Calibration Using Kistler Force Profile

```

% This program can only be used in up milling
% Using the cutting force profile measured from Kistler to calibrate
the cutting coefficients
% Considering the helix angle but ignoring tool dynamics effect while
% calculating instantaneous chip thickness
% Using the integration idea and least squares to get the cutting
% coefficients
% Coordinates have been changed to make the radial immersion angle
starting
% from 0, thus the final equations should be the same as the equations
% shown on Page 44 of Altintas's book.

```

```
% Input: cutting geometry and measured data file for Kistler
% Output: cutting coefficients calibrated from the Kistler force
profile method
```

```
% By Yong Zhao
% Revised on April 06 2012
% Design and Manufacturing Lab, University of New Hampshire
```

```
clc;
close all;
clear all;
```

```
%%
rpm=3000;
fs=18000; % Sampling frequency
% fs=7200;
numpercycle=floor(60*fs/rpm);
cycles=20; % number of cycles of force to be used
```

```
%%
% Input related parameters
```

```
N=1; % number of tooth
AD=0.125*25.4; % axial depth : mm
D=0.75*25.4; % diameter of the tool : mm
beta=14.73/180*pi; % helix angle in radians
```

```
i=4; % i=4,5,6 means quarter, half and three quarter immersion in up
milling;
```

```
if i==4
```

```
enter=0;
exit=1/3*pi;
%Feed=[1.257 2.513 3.770 5.027]'; % feedrate for 600 rpm
```

```
unit:inch/min
```

```
Feed=[6.283 12.566 18.850 25.133]'; % feedrate for 3000 rpm
%Feed=[7.540 15.080 22.619 30.159]'; % feedrate for 3600 rpm
%Feed=[8.378 16.755 25.133 33.510]'; % feedrate for 4000 rpm
```

```
elseif i==5
```

```
enter=0;
exit=1/2*pi;
Feed=[0.942 1.885 2.827 3.770]'; % feedrate for 600 rpm
```

```
unit:inch/min
```

```
%Feed=[4.712 9.425 14.137 18.850]'; % feedrate for 3000 rpm
%Feed=[5.655 11.310 16.965 22.619]'; % feedrate for 3600 rpm
%Feed=[6.283 12.566 18.850 25.133]'; % feedrate for 4000 rpm
```

```
elseif i==6
```

```
enter=0;
exit=2/3*pi;
Feed=[0.838 1.676 2.513 3.351]'; % feedrate for 600 rpm
```

```
unit:inch/min
```

```
%Feed=[4.189 8.378 12.566 16.755]'; % feedrate for 3000 rpm
%Feed=[5.027 10.053 15.080 20.106]'; % feedrate for 3600 rpm
```

```

    %Feed=[5.585 11.170 16.755 22.340]'; % feedrate for 4000 rpm
end

clear Fx_new Fy_new tick_new;

%% Get the correct data file
% Single data file
% [fileName,PathName,FilterIndex] = uigetfile('*.csv', 'Please choose
an excel file');
% if( fileName == 0 )
%     return;
% end;
% fname = sprintf('%s%s', PathName, fileName)
% [a b c]=xlsread(fname);

% Multiple data files
a=[];
Nfiles=2;
filename='Aluminum3k36k4kQuarterUpTangential';
for n = 1:Nfiles

    % Name of sub-file to read
    namespace = strcat(filename,int2str(n-1),'.csv');

    % Read xls data
    [newdata, headertext] = xlsread(namespace);

    % Concatenate data
    a = vertcat(a,newdata);

end

%%
% Plot raw Fx and Fy from Kistler
figure
subplot(2,1,1)
plot(a(:,1),-a(:,2));
title('Raw Force Data from Kistler in X Direction');
xlabel('Time (s)');
ylabel('Fx (volt)');

subplot(2,1,2)
plot(a(:,1),-a(:,3));
title('Raw Force Data from Kistler in Y Direction');
xlabel('Time (s)');
ylabel('Fy (volt)');

%%
% plot raw Fx
num1=cursor_info_0.DataIndex;
num2=cursor_info_00.DataIndex;

```

```

disp('Kistler zero offset at X and Y direction in the end');
Fx_zero_offset=mean(a(num1:num2,2))
Fy_zero_offset=mean(a(num1:num2,3))

a(:,2)=a(:,2)-Fx_zero_offset;
a(:,3)=a(:,3)-Fy_zero_offset;
Fx_all=-500*a(:,2);
Fy_all=-500*a(:,3);
tick_all=100*a(:,6);
figure
% plot(a(:,1),Fx_all,a(:,1),tick_all);
plot(a(:,1),Fy_all)
title('Raw Force Data from Kistler in Y Direction');
xlabel('Time (s)');
ylabel('Fy (N)');

%%
% Get 20 cycles of force data for the selected feedrate

startnum=cursor_info_1.DataIndex;
endnum=startnum+numpercycle*cycles-1;

time=(linspace(0,60/(rpm*numpercycle)*(numpercycle*cycles-1),numpercycle*cycles));
time_one=(linspace(0,60/(rpm*numpercycle)*(numpercycle-1),numpercycle)');

Fx=Fx_all(startnum:endnum);
Fy=Fy_all(startnum:endnum);
tick=tick_all(startnum:endnum);

figure;
plot(time,Fx,time,tick)

%%
% find the first trigger point of each cycle of tick signal to
calculate
% the actual spindle speed and be as the reference position for later
% calibration
for i=1:cycles
    tickout=tick(1+numpercycle*(i-1):numpercycle*i);
    tickoutnum=find(tickout<10);
    ticknum(i)=min(tickoutnum)+numpercycle*(i-1);
end
    hold on;
    plot(time(ticknum),tick(ticknum),'ro');
for i=1:cycles-1
    rpm_ins(i)=60*fs/(ticknum(i+1)-ticknum(i));
end
rpm_avg=19*60*fs/(ticknum(cycles)-ticknum(1))

```



```

%%
% Align the 20 cycles of raw force data and average them to get one
cycle of
% raw force data

for i=1:cycles
    Fx_new(i,:)=Fx(1+numpercycle*(i-1):numpercycle*i);
    Fy_new(i,:)=Fy(1+numpercycle*(i-1):numpercycle*i);
    tick_new(i,:)=tick(1+numpercycle*(i-1):numpercycle*i);
end

figure
subplot(2,2,1);
plot(time_one,Fx_new);
title('Unshifted Fx');
xlabel('Time (s)');
ylabel('Fx (N)');
%ylim([-250 50])

subplot(2,2,2);
% figure;
plot(time_one,Fy_new);
title('Unshifted Fy');
xlabel('Time (s)');
ylabel('Fy (N)');
%ylim([-100 150])

%%
% Shift and align the 20 cycles of the raw force data

for i=1:cycles
    [magx idx] = max(xcorr(Fx_new(1,:),Fx_new(i,:),numpercycle));
    Fx_new(i,:) = circshift(Fx_new(i,:),[0,idx-numpercycle-1]);
    Fy_new(i,:) = circshift(Fy_new(i,:),[0,idx-numpercycle-1]);
end

% Plot the shifted raw data
hold on;
subplot(2,2,3);
% figure;
plot(time_one,Fx_new);
title('Shifted Fx');
xlabel('Time (s)');
ylabel('Fx (N)');
%ylim([-250 50]);

subplot(2,2,4);
% figure;
plot(time_one,Fy_new);
title('Shifted Fy');
xlabel('Time (s)');
ylabel('Fy (N)');

```

```

%ylim([-100 150]);

% Average to get one cycle of raw force data
Fx_one=mean(Fx_new);
Fy_one=mean(Fy_new);
Fres=sqrt(Fx_one.^2+Fy_one.^2); % Calculate the raw resultant force

%%
% figure
% plot(time_one,Fx_one);
% xlabel('Time (s)');
% ylabel('Fx (N)');
% %ylim([-250 50]);
% figure
% plot(time_one,Fy_one);
% xlabel('Time (s)');
% ylabel('Fy (N)');
% %ylim([-100 150]);

%%
figure;
[AX,H1,H2] =
plotyy(time_one,Fx_one,time_one,tick(1:numpercycle)/100,'plot');
set(get(AX(1),'Ylabel'),'String','Force (N)')
set(get(AX(2),'Ylabel'),'String','Tick Signal (Volts)')
set(AX(1),'ylim',[-500 500]);
set(AX(2),'ylim',[-5 5]);
xlabel('Time (s)')

%%
hold on;
plot(time_one,Fy_one,'g')
legend('Averaged Fx','Averaged Fy','Tick Signal');
set(AX,{'ycolor'},{'k';'r'})

%%
clear Fxc Fyc A1x A2x A3x A4x A1y A2y A3y A4y;
%%
ft=Feed(4)*25.4/rpm/N; % feed per tooth : mm/tooth
degree=1/fs*rpm*360/60;
alpha=-94/180*pi;
startnum=ticknum(1);
endnum=numpercycle;
delta=10/180*pi; % angle used to subtract from the enter-exit range to
% narrow the range to do calibration
lag=2*AD*tan(beta)/D;
n=1;
for j=1:endnum-startnum+1
    index=j+startnum-1;
    theta=alpha+degree*(j-1)/180*pi;
    if (theta<=exit-delta) && (theta>=enter+delta)

```

```

        thetal=theta;
        theta2=theta-lag;

        Fxc(n)=Fx_one(index);
        Fyc(n)=Fy_one(index);

        A1x(n)=-1/4*ft*(cos(2*theta2)-cos(2*thetal));
        A2x(n)=sin(theta2)-sin(thetal);
        A3x(n)=1/4*ft*(2*(theta2-thetal)-(sin(2*theta2)-
sin(2*thetal)));
        A4x(n)=- (cos(theta2)-cos(thetal));

        A1y(n)=-1/4*ft*(2*(theta2-thetal)-(sin(2*theta2)-
sin(2*thetal)));
        A2y(n)=cos(theta2)-cos(thetal);
        A3y(n)=-1/4*ft*(cos(2*theta2)-cos(2*thetal));
        A4y(n)=sin(theta2)-sin(thetal);

        n=n+1;
    end
end

%%
Mx=[A1x' A2x' A3x' A4x'];
My=[A1y' A2y' A3y' A4y'];
Fx_cali=Fxc';
Fy_cali=Fyc';
Mxy=cat(1,Mx,My);
Fxy=cat(1,Fx_cali,Fy_cali);

%%
disp('Using Kistler Force Profile')
Kxy=2*tan(beta)/D*inv(Mxy'*Mxy)*Mxy'*Fxy

```

Force Model Calibration Using Smart Tool Force Profile

```

% This program can only be used in up milling
% Using the cutting force profile measured from Smart Tool to calibrate
the
% cutting coefficients
% Coordinates have been changed to make the radial immersion angle
starting from 0

% Input: cutting geometry and measured data file for Smart Tool
% Output: cutting coefficients calibrated from the Smart Tool force
profile method

% By Yong Zhao
% February 20 2012
% Design and Manufacturing Lab, University of New Hampshire

```

```

clc;
close all;
clear all;

%%
figure
strain_data=[s(i:end),s(1:i-1)];
plot(strain_time,strain_data);
title('Strain Data from Smart Tool');
xlabel('Time (s)');
ylabel('Strain (bit)');

%%
rpm=3000;
fs=10240;
numpercycle=floor(60*fs/rpm);
cycles=20; % number of cycles of force to be used

N=1; % number of tooth
AD=0.125; % axial depth unit:inch
D=0.75; % diameter of the tool unit: inch
beta=14.73/180*pi;
lag=2*AD*tan(beta)/D;

k=1; % k=1 tangential coefficients calibration; k=2 radial coefficients
calibration
j=4; % j=1,2 and 3 means down milling 1/4 immersion, 1/2 immersion and
3/4
% immersion; j=4,5 and 6 means up milling 1/4 immersion, 1/2
immersion
% and 3/4 immersion.
if j==1
disp('Quarter Immersion Down Milling');
enter=2/3*pi;
exit=pi;
Theta=1/3*pi;
RD=1/4*D; % radial depth quarter immersion unit: inch
Feed=[5.445 10.891 16.336 21.782]'; % feedrate unit:inch/min
elseif j==2
disp('Half Immersion Down Milling');
enter=1/2*pi;
exit=pi;
Theta=1/2*pi;
RD=1/2*D; % radial depth half immersion unit: inch
Feed=[4.084 8.168 12.252 16.336]'; % feedrate unit:inch/min
elseif j==3
disp('Three Quarter Immersion Down Milling');
enter=1/3*pi;
exit=pi;
Theta=2/3*pi;
RD=3/4*D; % radial depth three quarter immersion unit: inch
Feed=[3.63 7.261 10.891 14.521]'; % feedrate unit:inch/min

```

```

elseif j==4
    disp('Quarter Immersion Up Milling');
    enter=0;
    exit=1/3*pi;
    Theta=1/3*pi;
    RD=1/4*D; % radial depth quarter immersion unit: inch
    %Feed=[1.257 2.513 3.770 5.027]'; % feedrate for 600 rpm
unit:inch/min
    Feed=[6.283 12.566 18.850 25.133]'; % feedrate for 3000 rpm
    %Feed=[7.540 15.080 22.619 30.159]'; % feedrate for 3600 rpm
    %Feed=[8.378 16.755 25.133 33.510]'; % feedrate for 4000 rpm
elseif j==5
    disp('Half Immersion Up Milling');
    enter=0;
    exit=1/2*pi;
    Theta=1/2*pi;
    RD=1/2*D; % radial depth half immersion unit: inch
    Feed=[0.942 1.885 2.827 3.770]'; % feedrate for 600 rpm
unit:inch/min
    %Feed=[4.712 9.425 14.137 18.850]'; % feedrate for 3000 rpm
    %Feed=[5.655 11.310 16.965 22.619]'; % feedrate for 3600 rpm
    %Feed=[6.283 12.566 18.850 25.133]'; % feedrate for 4000 rpm
elseif j==6
    disp('Three Quarter Immersion Up Milling');
    enter=0;
    exit=2/3*pi;
    Theta=2/3*pi;
    RD=3/4*D; % radial depth three quarter immersion unit: inch
    Feed=[0.838 1.676 2.513 3.351]'; % feedrate for 600 rpm
unit:inch/min
    %Feed=[4.189 8.378 12.566 16.755]'; % feedrate for 3000 rpm
    %Feed=[5.027 10.053 15.080 20.106]'; % feedrate for 3600 rpm
    %Feed=[5.585 11.170 16.755 22.340]'; % feedrate for 4000 rpm
end

%%
clear Ft_new Ft_one Ft_cal h;
%%
% calculate the zero offset of smart tool
num1=cursor_info_0.DataIndex;
num2=cursor_info_00.DataIndex;
zerobit=mean(strain_data(num1:num2))
strain=strain_data-zerobit;
Ft_data=strain/1.64*4.448222; % unit:N
figure
plot(strain_time,Ft_data);
title('Raw Force from Smart Tool');
xlabel('Time (s)');
ylabel('Ft (N)');

%%
% Find the tangential force for the first feedrate used for calibration
startnum=cursor_info_1.DataIndex;

```

```

endnum=startnum+numpercycle*cycles-1;

% time=strain_time(startnum:endnum);
time=(linspace(0,60/(rpm*numpercycle)*(numpercycle*cycles-
1),numpercycle*cycles));

time_one=(linspace(0,60/(rpm*numpercycle)*(numpercycle-
1),numpercycle));
Ft_raw=Ft_data(startnum:endnum);
figure
plot(time,Ft_raw);
xlabel('Time (s)');
ylabel('Ft (N)');
% ylim([-20 90]);

%% FFT of the chose 20 cycles of tangential or radial force
NFFT=numpercycle*cycles;
n=floor(NFFT/2+1);
for i=1:n
    f(i)=(i-1)*fs/NFFT;
end

w = hann(NFFT);
g1 = (Ft_raw-mean(Ft_raw))';
Ft_fft = fft(g1.*w,NFFT)/NFFT;

figure
stem(f,2*abs(Ft_fft(1:n)), '*');
% title('Single-Sided Amplitude Spectrum of Ft')
xlim([0 2000])
xlabel('Frequency (Hz)')
ylabel('|Fr| (N)')

%%
for i=1:cycles
    Ft_raw_new(i,:)=Ft_raw(1+numpercycle*(i-1):numpercycle*i);
end

figure
plot(time_one,Ft_raw_new);
% title('Unshifted Ft');
xlabel('Time (s)');
ylabel('Fr (N)')
% Shift and align the 20 cycles of the raw force data

for i=1:cycles
    [magFt idFt] =
max(xcorr(Ft_raw_new(1,:),Ft_raw_new(i,:),numpercycle));
    Ft_raw_new(i,:) = circshift(Ft_raw_new(i,:),[0,idFt-
numpercycle-1]);
end

```

```

% Plot the shifted raw data
figure;
plot(time_one,Ft_raw_new);
% title('Shifted Fdraw');
xlabel('Time (s)');
ylabel('Fr (N)');
% ylim([-20 90]);
% Average to get one cycle of raw force data
Ft_raw_one=mean(Ft_raw_new);

%%
figure
plot(time_one,Ft_raw_one);
xlabel('Time (s)');
ylabel('Fr (N)');

%%
startnum=cursor_info_a.DataIndex;

%%
% Cutting coefficients calibration
ft=Feed(4)*25.4/rpm/N; % feed per tooth : mm/tooth
alpha=0;
degree=1/fs*rpm*360/60;
delta=10/180*pi; % angle used to subtract from the enter-exit range to
% narrow the range to do calibration

n=1;
for j=1:floor((Theta+lag)*numpercycle/2/pi)
    index=j+startnum-1;
    theta=(alpha+degree*(j-1))/180*pi;
    if (theta<=exit-delta) && (theta>=enter+delta)
        Ft_cali(n)=Ft_raw_one(index);
        h(n)=ft*sin(theta-1/2*lag);
        n=n+1;
    end
end

%%
if k==1
    disp('Tangential coefficients: Ktc and Kte');
    Kt=polyfit(h,Ft_cali/(AD*25.4),1)
else
    disp('Radial coefficients: Krc and Kre');
    Kr=polyfit(h,Ft_cali/(AD*25.4),1)
end

%%
figure;
plot(h,Ft_cali/(AD*25.4),'*');
xlabel('Instantaneous Chip Thickness h: mm');
ylabel('Ft/a: N/mm')

```

Resultant Force Simulation and Comparison

```
% Simulate resultant cutting force by using coefficients obtained from
% each calibration method
% This program can only be used in up milling
% Considering the helix angle but ignoring tool dynamics effect while
% calculating instantaneous chip thickness
% Coordinates have been changed to make the radial immersion angle
starting from 0
```

```
% Input: cutting geometry, obtained cutting coefficients from each
calibration method and measured data file for Kistler
% Output: Fx, Fy and resultant force simulated based on the input and
the relative error of the peak resultant force between the simulated
and the Kistler measured
```

```
% By Yong Zhao
% Revised on April 08 2012
% Design and Manufacturing Lab, University of New Hampshire
```

```
clc;
close all;
clear all;
```

```
%%
rpm=3000;
fs=18000; % Sampling frequency for 3000 RPM
% fs=7200; % Sampling frequency for 600 RPM
numpercycle=floor(60*fs/rpm);
cycles=20; % number of cycles of force to be used
```

```
% the following ratios have been checked and confirmed
% ratio1=[0.3686 0.5623]; % ratio from 600 RPM cutting tests
ratio1=[0.3959 0.6301]; % ratio from 3000 RPM cutting tests
% ratio2=[0.3822 0.5962]; % ratio from the combined data
```

```
%%
% Input related parameters
```

```
N=1; % number of tooth
AD=0.125*25.4; % axial depth : mm
D=0.75*25.4; % diameter of the tool : mm
beta=14.73/180*pi; % helix angle in radians
```

```
i=6; % i=4,5,6 means quarter, half and three quarter immersion in up
milling;
if i==4
    enter=0;
    exit=1/3*pi;
    %Feed=[1.257 2.513 3.770 5.027]'; % feedrate for 600 rpm
unit:inch/min
```



```

        Feed=[6.283 12.566 18.850 25.133]'; % feedrate for 3000 rpm
        %Feed=[7.540 15.080 22.619 30.159]'; % feedrate for 3600 rpm
        %Feed=[8.378 16.755 25.133 33.510]'; % feedrate for 4000 rpm
elseif i==5
    enter=0;
    exit=1/2*pi;
    %Feed=[0.942 1.885 2.827 3.770]'; % feedrate for 600 rpm
unit:inch/min
    Feed=[4.712 9.425 14.137 18.850]'; % feedrate for 3000 rpm
    %Feed=[5.655 11.310 16.965 22.619]'; % feedrate for 3600 rpm
    %Feed=[6.283 12.566 18.850 25.133]'; % feedrate for 4000 rpm
elseif i==6
    enter=0;
    exit=2/3*pi;
    %Feed=[0.838 1.676 2.513 3.351]'; % feedrate for 600 rpm
unit:inch/min
    Feed=[4.189 8.378 12.566 16.755]'; % feedrate for 3000 rpm
    %Feed=[5.027 10.053 15.080 20.106]'; % feedrate for 3600 rpm
    %Feed=[5.585 11.170 16.755 22.340]'; % feedrate for 4000 rpm
end

clear Fx_new Fy_new tick_new;

%% Get the correct data file
% Single data file
% [fileName,PathName,FilterIndex] = uigetfile('*.csv', 'Please choose
an excel file');
% if( fileName == 0 )
%     return;
% end;
% fname = sprintf('%s%s', PathName, fileName)
% [a b c]=xlsread(fname);

% Multiple data files
a=[];
Nfiles=2;
filename='Aluminum3k36k4kThreeQuarterUpTangential';
for n = 1:Nfiles

    % Name of sub-file to read
    namespace = strcat(filename,int2str(n-1),'.csv');

    % Read xls data
    [newdata, headertext] = xlsread(namespace);

    % Concatenate data
    a = vertcat(a,newdata);

end

%%
% Plot raw Fx and Fy from Kistler

```

```

figure
subplot(2,1,1)
plot(a(:,1),-a(:,2));
title('Raw Force Data from Kistler in X Direction');
xlabel('Time (s)');
ylabel('Fx (volt)');

subplot(2,1,2)
plot(a(:,1),-a(:,3));
title('Raw Force Data from Kistler in Y Direction');
xlabel('Time (s)');
ylabel('Fy (volt)');

%%
% plot raw Fx
num1=cursor_info_0.DataIndex;
num2=cursor_info_00.DataIndex;

disp('Kistler zero offset at X and Y direction in the end');
Fx_zero_offset=mean(a(num1:num2,2))
Fy_zero_offset=mean(a(num1:num2,3))

a(:,2)=a(:,2)-Fx_zero_offset;
a(:,3)=a(:,3)-Fy_zero_offset;
Fx_all=-500*a(:,2);
Fy_all=-500*a(:,3);
tick_all=100*a(:,6);
figure
% plot(a(:,1),Fx_all,a(:,1),tick_all);
plot(a(:,1),Fy_all)
title('Raw Force Data from Kistler in Y Direction');
xlabel('Time (s)');
ylabel('Fy (N)');

%%
% Get 20 cycles of force data for the selected feedrate

startnum=cursor_info_3.DataIndex;
endnum=startnum+numpercycle*cycles-1;

time=(linspace(0,60/(rpm*numpercycle)*(numpercycle*cycles-1),numpercycle*cycles));
time_one=(linspace(0,60/(rpm*numpercycle)*(numpercycle-1),numpercycle))';

Fx=Fx_all(startnum:endnum);
Fy=Fy_all(startnum:endnum);
tick=tick_all(startnum:endnum);

figure;
plot(time,Fx,time,tick)

```

```

%%
% find the first trigger point of each cycle of tick signal to
calculate the actual spindle speed and be as the reference position

for i=1:cycles
    tickout=tick(1+numpercycle*(i-1):numpercycle*i);
    tickoutnum=find(tickout<10);
    ticknum(i)=min(tickoutnum)+numpercycle*(i-1);
end
    hold on;
    plot(time(ticknum),tick(ticknum),'ro');
for i=1:cycles-1
    rpm_ins(i)=60*fs/(ticknum(i+1)-ticknum(i));
end
rpm_avg=19*60*fs/(ticknum(cycles)-ticknum(1))

%%
% Align the 20 cycles of raw force data and average them to get one
cycle of
% raw force data

for i=1:cycles
    Fx_new(i,:)=Fx(1+numpercycle*(i-1):numpercycle*i);
    Fy_new(i,:)=Fy(1+numpercycle*(i-1):numpercycle*i);
    tick_new(i,:)=tick(1+numpercycle*(i-1):numpercycle*i);
end

figure
subplot(2,2,1);
plot(time_one,Fx_new);
title('Unshifted Fx');
xlabel('Time (s)');
ylabel('Fx (N)');
%ylim([-250 50])

subplot(2,2,2);
% figure;
plot(time_one,Fy_new);
title('Unshifted Fy');
xlabel('Time (s)');
ylabel('Fy (N)');
%ylim([-100 150])

%%
% Shift and align the 20 cycles of the raw force data

for i=1:cycles
    [magx idx] = max(xcorr(Fx_new(1,:),Fx_new(i,:),numpercycle));
    Fx_new(i,:) = circshift(Fx_new(i,:),[0,idx-numpercycle-1]);
    Fy_new(i,:) = circshift(Fy_new(i,:),[0,idx-numpercycle-1]);
end

```

```

% Plot the shifted raw data
hold on;
subplot(2,2,3);
% figure;
plot(time_one,Fx_new);
title('Shifted Fx');
xlabel('Time (s)');
ylabel('Fx (N)');
%ylim([-250 50]);

subplot(2,2,4);
% figure;
plot(time_one,Fy_new);
title('Shifted Fy');
xlabel('Time (s)');
ylabel('Fy (N)');
%ylim([-100 150]);

% Average to get one cycle of raw force data
Fx_one=mean(Fx_new);
Fy_one=mean(Fy_new);
Fres=sqrt(Fx_one.^2+Fy_one.^2); % Calculate the raw resultant force

%%
ft=Feed(3)*25.4/rpm/N; % feed per tooth : mm/tooth
degree=1/fs*rpm*360/60;
startnum=ticknum(1);

%%
clear Fx_est Fy_est;

%%
% Using the Kistler Average Force Based Cutting Coefficients to
% simulate the Instantaneous Cutting Force
L=100;

Ktc=656.8417; % unit: N/mm^2
Kte=19.6580; % unit: N/mm
Krc=301.1310; % unit: N/mm^2
Kre=11.2332; % unit: N/mm

alpha=-94-(startnum-1)*degree; .
for j=1:numpercycle
    theta=(alpha+degree*(j-1))/180*pi;
    if (theta>enter) && ((theta-2*AD*tan(beta)/D)<=enter)
        Fx_est(j)=0;
        Fy_est(j)=0;
        for k=1:L
            theta2=theta-2*tan(beta)/D*AD/L*k;
            if (theta2>=enter)
                dFt=(Ktc*ft*sin(theta2)+Kte)*AD/L;
                dFr=(Krc*ft*sin(theta2)+Kre)*AD/L;
            end
        end
    end
end

```

```

        dFx=-dFt*cos(theta2)-dFr*sin(theta2);
        dFy=dFt*sin(theta2)-dFr*cos(theta2);
        Fx_est(j)=Fx_est(j)+dFx;
        Fy_est(j)=Fy_est(j)+dFy;
    else
        break;
    end
end
elseif (theta<=exit) && ((theta-2*AD*tan(beta)/D)>=enter)
    Fx_est(j)=0;
    Fy_est(j)=0;
    for k=1:L
        theta2=theta-2*tan(beta)/D*AD/L*k;
        dFt=(Ktc*ft*sin(theta2)+Kte)*AD/L;
        dFr=(Krc*ft*sin(theta2)+Kre)*AD/L;
        dFx=-dFt*cos(theta2)-dFr*sin(theta2);
        dFy=dFt*sin(theta2)-dFr*cos(theta2);
        Fx_est(j)=Fx_est(j)+dFx;
        Fy_est(j)=Fy_est(j)+dFy;
    end
elseif (theta>exit) && ((theta-2*AD*tan(beta)/D)<exit)
    Fx_est(j)=0;
    Fy_est(j)=0;
    for k=1:L
        theta2=theta-2*tan(beta)/D*AD/L*k;
        if (theta2<=exit)
            dFt=(Ktc*ft*sin(theta2)+Kte)*AD/L;
            dFr=(Krc*ft*sin(theta2)+Kre)*AD/L;
            dFx=-dFt*cos(theta2)-dFr*sin(theta2);
            dFy=dFt*sin(theta2)-dFr*cos(theta2);
            Fx_est(j)=Fx_est(j)+dFx;
            Fy_est(j)=Fy_est(j)+dFy;
        else
            theta1=theta2;
        end
    end
end
else
    Fx_est(j)=0;
    Fy_est(j)=0;
end
end

```

```

Fx_kistler_avg=Fx_est;
Fy_kistler_avg=Fy_est;
Fres_kistler_avg=sqrt(Fx_kistler_avg.^2+Fy_kistler_avg.^2);

```

```

%%
% Using the Smart Tool Average Force Based Cutting Coefficients to
% simulate the Instantaneous Cutting Force

```

```

Ktc=761.5866; % unit: N/mm^2
Kte=17.8042; % unit: N/mm
Krc=233.5516; % unit: N/mm^2

```

```

Kre=13.0211; % unit: N/mm

for j=1:numpercycle
    theta=(alpha+degree*(j-1))/180*pi;
    if (theta>enter) && ((theta-2*AD*tan(beta)/D)<=enter)
        Fx_est(j)=0;
        Fy_est(j)=0;
        for k=1:L
            theta2=theta-2*tan(beta)/D*AD/L*k;
            if (theta2>=enter)
                dFt=(Ktc*ft*sin(theta2)+Kte)*AD/L;
                dFr=(Krc*ft*sin(theta2)+Kre)*AD/L;
                dFx=-dFt*cos(theta2)-dFr*sin(theta2);
                dFy=dFt*sin(theta2)-dFr*cos(theta2);
                Fx_est(j)=Fx_est(j)+dFx;
                Fy_est(j)=Fy_est(j)+dFy;
            else
                break;
            end
        end
    elseif (theta<=exit) && ((theta-2*AD*tan(beta)/D)>=enter)
        Fx_est(j)=0;
        Fy_est(j)=0;
        for k=1:L
            theta2=theta-2*tan(beta)/D*AD/L*k;
            dFt=(Ktc*ft*sin(theta2)+Kte)*AD/L;
            dFr=(Krc*ft*sin(theta2)+Kre)*AD/L;
            dFx=-dFt*cos(theta2)-dFr*sin(theta2);
            dFy=dFt*sin(theta2)-dFr*cos(theta2);
            Fx_est(j)=Fx_est(j)+dFx;
            Fy_est(j)=Fy_est(j)+dFy;
        end
    elseif (theta>exit) && ((theta-2*AD*tan(beta)/D)<exit)
        Fx_est(j)=0;
        Fy_est(j)=0;
        for k=1:L
            theta2=theta-2*tan(beta)/D*AD/L*k;
            if (theta2<=exit)
                dFt=(Ktc*ft*sin(theta2)+Kte)*AD/L;
                dFr=(Krc*ft*sin(theta2)+Kre)*AD/L;
                dFx=-dFt*cos(theta2)-dFr*sin(theta2);
                dFy=dFt*sin(theta2)-dFr*cos(theta2);
                Fx_est(j)=Fx_est(j)+dFx;
                Fy_est(j)=Fy_est(j)+dFy;
            else
                theta1=theta2;
            end
        end
    else
        Fx_est(j)=0;
        Fy_est(j)=0;
    end
end
end

```

```

Fx_ST_avg=Fx_est;
Fy_ST_avg=Fy_est;
Fres_ST_avg=sqrt(Fx_ST_avg.^2+Fy_ST_avg.^2);

%%
% Using ratiol to simulate the Instantaneous Cutting Force

Ktc=738.6378 % unit: N/mm^2
Kte=13.8394 % unit: N/mm

disp('Radial Cutting Coefficients obtained from Ratio 1');
Krc=Ktc*ratiol(1) % unit: N/mm^2
Kre=Kte*ratiol(2) % unit: N/mm

for j=1:numpercycle
    theta=(alpha+degree*(j-1))/180*pi;
    if (theta>enter) && ((theta-2*AD*tan(beta)/D)<=enter)
        Fx_est(j)=0;
        Fy_est(j)=0;
        for k=1:L
            theta2=theta-2*tan(beta)/D*AD/L*k;
            if (theta2>=enter)
                dFt=(Ktc*ft*sin(theta2)+Kte)*AD/L;
                dFr=(Krc*ft*sin(theta2)+Kre)*AD/L;
                dFx=-dFt*cos(theta2)-dFr*sin(theta2);
                dFy=dFt*sin(theta2)-dFr*cos(theta2);
                Fx_est(j)=Fx_est(j)+dFx;
                Fy_est(j)=Fy_est(j)+dFy;
            else
                break;
            end
        end
    elseif (theta<=exit) && ((theta-2*AD*tan(beta)/D)>=enter)
        Fx_est(j)=0;
        Fy_est(j)=0;
        for k=1:L
            theta2=theta-2*tan(beta)/D*AD/L*k;
            dFt=(Ktc*ft*sin(theta2)+Kte)*AD/L;
            dFr=(Krc*ft*sin(theta2)+Kre)*AD/L;
            dFx=-dFt*cos(theta2)-dFr*sin(theta2);
            dFy=dFt*sin(theta2)-dFr*cos(theta2);
            Fx_est(j)=Fx_est(j)+dFx;
            Fy_est(j)=Fy_est(j)+dFy;
        end
    elseif (theta>exit) && ((theta-2*AD*tan(beta)/D)<exit)
        Fx_est(j)=0;
        Fy_est(j)=0;
        for k=1:L
            theta2=theta-2*tan(beta)/D*AD/L*k;
            if (theta2<=exit)
                dFt=(Ktc*ft*sin(theta2)+Kte)*AD/L;
                dFr=(Krc*ft*sin(theta2)+Kre)*AD/L;

```

```

        dFx=-dFt*cos(theta2)-dFr*sin(theta2);
        dFy=dFt*sin(theta2)-dFr*cos(theta2);
        Fx_est(j)=Fx_est(j)+dFx;
        Fy_est(j)=Fy_est(j)+dFy;
    else
        theta1=theta2;
    end
end
else
    Fx_est(j)=0;
    Fy_est(j)=0;
end
end

Fx_ratiol=Fx_est;
Fy_ratiol=Fy_est;
Fres_ratiol=sqrt(Fx_ratiol.^2+Fy_ratiol.^2);

%%
% Using the Kistler Force Profile Based Cutting Coefficients to
simulate the Instantaneous Cutting Force

Ktc=676.4758; % unit: N/mm^2
Kte=21.4392; % unit: N/mm
Krc=250.4006; % unit: N/mm^2
Kre=15.7230; % unit: N/mm

for j=1:numpercycle
    theta=(alpha+degree*(j-1))/180*pi;
    if (theta>enter) && ((theta-2*AD*tan(beta)/D)<=enter)
        Fx_est(j)=0;
        Fy_est(j)=0;
        for k=1:L
            theta2=theta-2*tan(beta)/D*AD/L*k;
            if (theta2>=enter)
                dFt=(Ktc*ft*sin(theta2)+Kte)*AD/L;
                dFr=(Krc*ft*sin(theta2)+Kre)*AD/L;
                dFx=-dFt*cos(theta2)-dFr*sin(theta2);
                dFy=dFt*sin(theta2)-dFr*cos(theta2);
                Fx_est(j)=Fx_est(j)+dFx;
                Fy_est(j)=Fy_est(j)+dFy;
            else
                break;
            end
        end
    elseif (theta<=exit) && ((theta-2*AD*tan(beta)/D)>=enter)
        Fx_est(j)=0;
        Fy_est(j)=0;
        for k=1:L
            theta2=theta-2*tan(beta)/D*AD/L*k;
            dFt=(Ktc*ft*sin(theta2)+Kte)*AD/L;
            dFr=(Krc*ft*sin(theta2)+Kre)*AD/L;

```



```

        dFx=-dFt*cos(theta2)-dFr*sin(theta2);
        dFy=dFt*sin(theta2)-dFr*cos(theta2);
        Fx_est(j)=Fx_est(j)+dFx;
        Fy_est(j)=Fy_est(j)+dFy;
    end
elseif (theta>exit) && ((theta-2*AD*tan(beta)/D)<exit)
    Fx_est(j)=0;
    Fy_est(j)=0;
    for k=1:L
        theta2=theta-2*tan(beta)/D*AD/L*k;
        if (theta2<=exit)
            dFt=(Ktc*ft*sin(theta2)+Kte)*AD/L;
            dFr=(Krc*ft*sin(theta2)+Kre)*AD/L;
            dFx=-dFt*cos(theta2)-dFr*sin(theta2);
            dFy=dFt*sin(theta2)-dFr*cos(theta2);
            Fx_est(j)=Fx_est(j)+dFx;
            Fy_est(j)=Fy_est(j)+dFy;
        else
            theta1=theta2;
        end
    end
else
    Fx_est(j)=0;
    Fy_est(j)=0;
end
end

Fx_kistler_ins=Fx_est;
Fy_kistler_ins=Fy_est;
Fres_kistler_ins=sqrt(Fx_kistler_ins.^2+Fy_kistler_ins.^2);

%%
% Using the Smart Tool Force Profile Based Cutting Coefficients to
simulate the Instantaneous Cutting Force

Ktc=776.8609; % unit: N/mm^2
Kte=17.2415; % unit: N/mm
Krc=213.0565; % unit: N/mm^2
Kre=16.0614; % unit: N/mm

for j=1:numpercycle
    theta=(alpha+degree*(j-1))/180*pi;
    if (theta>enter) && ((theta-2*AD*tan(beta)/D)<=enter)
        Fx_est(j)=0;
        Fy_est(j)=0;
        for k=1:L
            theta2=theta-2*tan(beta)/D*AD/L*k;
            if (theta2>=enter)
                dFt=(Ktc*ft*sin(theta2)+Kte)*AD/L;
                dFr=(Krc*ft*sin(theta2)+Kre)*AD/L;
                dFx=-dFt*cos(theta2)-dFr*sin(theta2);
                dFy=dFt*sin(theta2)-dFr*cos(theta2);
                Fx_est(j)=Fx_est(j)+dFx;
            end
        end
    end
end

```

```

        Fy_est(j)=Fy_est(j)+dFy;
    else
        break;
    end
end
elseif (theta<=exit) && ((theta-2*AD*tan(beta)/D)>=enter)
    Fx_est(j)=0;
    Fy_est(j)=0;
    for k=1:L
        theta2=theta-2*tan(beta)/D*AD/L*k;
        dFt=(Ktc*ft*sin(theta2)+Kte)*AD/L;
        dFr=(Krc*ft*sin(theta2)+Kre)*AD/L;
        dFx=-dFt*cos(theta2)-dFr*sin(theta2);
        dFy=dFt*sin(theta2)-dFr*cos(theta2);
        Fx_est(j)=Fx_est(j)+dFx;
        Fy_est(j)=Fy_est(j)+dFy;
    end
elseif (theta>exit) && ((theta-2*AD*tan(beta)/D)<exit)
    Fx_est(j)=0;
    Fy_est(j)=0;
    for k=1:L
        theta2=theta-2*tan(beta)/D*AD/L*k;
        if (theta2<=exit)
            dFt=(Ktc*ft*sin(theta2)+Kte)*AD/L;
            dFr=(Krc*ft*sin(theta2)+Kre)*AD/L;
            dFx=-dFt*cos(theta2)-dFr*sin(theta2);
            dFy=dFt*sin(theta2)-dFr*cos(theta2);
            Fx_est(j)=Fx_est(j)+dFx;
            Fy_est(j)=Fy_est(j)+dFy;
        else
            theta1=theta2;
        end
    end
else
    Fx_est(j)=0;
    Fy_est(j)=0;
end
end

Fx_ST_ins=Fx_est;
Fy_ST_ins=Fy_est;
Fres_ST_ins=sqrt(Fx_ST_ins.^2+Fy_ST_ins.^2);

%%
figure;
plot(time_one,Fres,time_one,Fres_kistler_avg,time_one,Fres_ST_avg,time_
one,Fres_ratiol,time_one,Fres_kistler_ins,time_one,Fres_ST_ins,'LineWid
th',2);
xlabel('Time (s)');
ylabel('Resultant Force (N)');
legend('Measured','Simulated 1','Simulated 2','Simulated 3','Simulated
4','Simulated 5');

```

*/

```
RE_kistler_avg=abs(max(Fres)-max(Fres_kistler_avg))/max(Fres)
RE_ST_avg=abs(max(Fres)-max(Fres_ST_avg))/max(Fres)
RE_ratiol=abs(max(Fres)-max(Fres_ratiol))/max(Fres)
RE_kistler_ins=abs(max(Fres)-max(Fres_kistler_ins))/max(Fres)
RE_ST_ins=abs(max(Fres)-max(Fres_ST_ins))/max(Fres)
```